Technische Universität München
TUM School of Engineering and Design

Thermal Behavior of Wet Clutches in Industrial Applications

Daniel Grötsch

Vollständiger Abdruck der von der TUM School of Engineering and Design der Technischen Universität München zur Erlangung eines

Doktors der Ingenieurwissenschaften (Dr.-Ing.)

genehmigten Dissertation.

Vorsitz: Prof. Dr.-Ing. Klaus Drechsler

Prüfer der Dissertation:

1. Prof. Dr.-Ing. Karsten Stahl
2. Prof. Pär Marklund, Ph.D.

Die Dissertation wurde am 27.03.2023 bei der Technischen Universität München eingereicht und durch die TUM School of Engineering and Design am 17.07.2023 angenommen.

Danksagung

Die vorliegende Dissertation entstand während meiner Tätigkeit als wissenschaftlicher Mitarbeiter am Lehrstuhl für Maschinenelemente, Forschungsstelle für Zahnräder und Getriebebau (FZG) der Technischen Universität München.

Ich möchte an dieser Stelle allen Personen herzlich danken, die mich unterstützt haben. Gleichzeitig bitte ich diejenigen um Verzeihung die hier vergessen wurden.

Ich bedanke mich bei …

... meinem Doktorvater Prof. Dr.-Ing. Karsten Stahl für den großen Vertrauensvorschuss und für die Rahmenbedingungen, die er am Lehrstuhl geschaffen hat.

... meinem Zweitprüfer Prof. Pär Marklund, Ph.D., der eine Inspiration während meiner eigenen Forschungstätigkeit war und den ich als fairen Prüfer kennenlernen durfte.

... dem Prüfungsvorsitzenden Prof. Dr.-Ing. Klaus Drechsler, der durch seine freundliche und wohlgesonnene Art eine angenehme Prüfungsatmosphäre geschaffen hat.

... meinem Abteilungsleiter im Ruhestand Dr.-Ing. Hermann Pflaum für die stets kompetente Hilfestellung in allen Belangen und die vielen Freiräume, in denen ich meinen Forschungsdrang ausleben konnte.

... meiner Wegbereiterin an die FZG, geschätzten Kollegin, Teamleiterin und am Ende auch Abteilungsleiterin Dr.-Ing. Katharina Völkel, die immer an mich geglaubt und meine Arbeiten unterstützt hat. Ich denke gerne zurück an die vielen Jahre, die wir gemeinsam im Kupplungsgeschäft und der thermischen Simulation, sowie darüber hinaus, miteinander verbracht haben.

... allen KollegInnen an der FZG, die mir über die Jahre ans Herz gewachsen sind und die mir oft weiterhalfen. Insbesondere erwähnen möchte ich meine hochgeschätzten KollegInnen und Freunde aus der Kupplungsabteilung: Patrick, Lukas, Uli, Thomas, Stefan und Marco.

... den Teilnehmenden an zahlreichen FZG-Kaffeerunden, weil es einfach immer schön war sich hier fachlich und überfachlich auszutauschen.

... den fleißigen studentischen und wissenschaftlichen HelferInnen. Insbesondere möchte ich hier erwähnen: Elias, Felix, Medard, Markus und Rudi. Ihr wart mir eine große Stütze und es war mir eine Freude mit Euch zusammenzuarbeiten.

... den MitarbeiterInnen aus Sekretariat, Labor, Prüffeld und mechanischer Werkstatt des Lehrstuhls, die unzählige Male ihre große Hilfsbereitschaft unter Beweis gestellt haben. Insbesondere geht mein Dank hier an Konny und Andrea: Ihr seid das Herz des Lehrstuhls und es ist einfach schön, dass es Euch gibt!

... den Forschungspartnern der Fa. Simerics Dirk und Rudi, die große CFD-Experten sind und mich über einen langen Zeitraum tatkräftig unterstützt haben. Unsere Projekte waren für mich eine große Bereicherung.

... dem projektbegleitenden Ausschuss „Schaltbare Kupplungen und Bremsen“, ohne dessen wertvolle Hinweise und die (auch finanzielle) Unterstützung meine Forschungsarbeiten nicht möglich gewesen wären.

... meinen KollegInnen bei INFODAS, die mich herzlich aufgenommen haben und die beeindruckende IT-Security-Ninjas sind.

... meiner Schwiegerfamilie Christine, Alois und Florian für die große Unterstützung und Freundschaft.

... meiner Familie Christa und Angelika für das Vertrauen, die Rückendeckung und den Zusammenhalt während meines ganzen Lebens.

Besonders bedanke ich mich bei meinen liebsten Verena und Luisa, die in all den Jahren die Belastungen dieser Arbeit mitgetragen haben und mir immer die größte Stütze sind. Ihr seid mein Glück.

Garching, im Dezember 2023

Kurzfassung

Nasslaufende Lamellenkupplungen realisieren in Getrieben von Schiffen und Fahrzeugen fast ausnahmslos sicherheitskritische Anwendungen, da ein Ausfall der Kupplung zur Manövrierunfähigkeit des Schiffes führt oder mit einem Drehmomentverlust verbunden ist. Die Auswertung des aktuellen Stands der Forschung zeigt eine Forschungslücke bezüglich des thermischen Verhaltens von nassen Kupplungen in industriellen Anwendungen, insbesondere hinsichtlich der Ölverteilung und des Einflusses einer druckbehafteten Zwangsbeölung durch den Innenmitnehmer. Der Fokus dieser Arbeit liegt auf der Erweiterung des Wissens über das thermische Verhalten von nassen Industriekupplungen mit einem ganzheitlichen Ansatz, der simulative und experimentelle Ansätze in effizienter Weise kombiniert. Die Untersuchungen werden größtenteils mit Serienbauteilen durchgeführt. Zu den theoretischen Ansätzen gehört die Entwicklung eines effizienten, echtzeitfähigen Temperaturmodells für Temperaturberechnungen und Vorhersagen. Darüber hinaus wird ein 3D-CFD-Modell zur Analyse von Öl- und Druckverteilungen an den Reibflächen erstellt. Zur Validierung werden experimentelle Untersuchungen zur Bestimmung des Reibungs- und thermischen Verhalten durchgeführt. Zusätzlich wird die Ölverteilung experimentell durch Hochgeschwindigkeitskameraaufnahmen auf dem Prüfstand unter Verwendung von transparenten Teilen, die mit 3D-Druck und Laserschneiden hergestellt wurden, visualisiert. Ein wichtiges Ergebnis ist, dass der Öldruck an der Reibfläche die Drehmomentübertragungsfähigkeit der Kupplung deutlich reduziert. Die vielfältigen weiteren Ergebnisse und Einflussfaktoren in Bezug auf das thermische Verhalten nasser Industriekupplungen können zudem zur optimierten Auslegung von zukünftigen Kupplungen verwendet werden.

Abstract

Applications of wet clutches in the gearboxes of ships and vehicles are almost without exception safety-critical applications, since a clutch failure results in an inability to maneuver the vessel or is associated with a loss of torque. Evaluation of current research shows a lack of knowledge concerning the thermal behavior of wet clutches in industrial applications, in particular regarding oil distribution and the influences of pressurized oil supply through the inner carrier. The focus of this work is about enhancing knowledge on the thermal behavior of wet industrial clutches by a holistic approach that combines simulative and experimental investigations in an efficient manner. The investigations are mainly performed with parts from serial production. The theoretical approaches include the development of an efficient real-time capable temperature model for temperature calculations and predictions. Furthermore, a 3D-CFD model is established to analyze oil and pressure distributions at the friction interfaces. Experimental investigations are performed to determine friction and thermal behavior for validation purposes. Additionally, the oil distribution is experimentally visualized by high-speed camera recordings on the test rig using transparent parts manufactured with 3D printing and laser cutting. One important finding is that the oil pressure at the friction interface significantly reduces the torque transfer capability of the clutch. Additionally, the results and identified influencing factors relating to the thermal behavior of wet industrial clutches can be used to optimize the design of future clutches.

Contents

Nomenclature

Symbol	Unit	Name
A	m²	surface
α	W/m²K	conjugate heat transfer coefficient
$\overline{\beta}$	1e-6/K	coefficient of linear thermal expansion
C	J/K	thermal capacity
c	m	contour
c	J/kgK	specific heat
Δ	-	differential
d	m	diameter
η	Pas	dynamic viscosity
$f_{x,y,z}$	N/m³	volume force component in cartesian x,y,z direction
F	N	force
J	kgm²	inertia
λ	W/mK	heat conduction coefficient
μ	-	CoF
n	rpm	differential speed
ν	m²/s	kinematic viscosity
ω	1/s	angular velocity
P	W	thermal power
p	N/mm²	surface pressure
$\dot{Q}$	W	thermal (friction) power
$\dot{q}$	W/m³	internal heat source
Q	J	(friction) work
r_m	m	mean radius
R	K/W	thermal resistance
Re	-	Reynolds number
ρ	kg/m³	density
T_f	Nm	friction torque
T	K	temperature
t	s	time
ϑ	°C	temperature
u	m/s	flow velocity component in x-direction
$\dot{V}_{oil}$	mm³/s	absolute oil flow rate
$\dot{v}_{oil}$	mm³/mm²s	specific oil flow rate
v_s	m/s	sliding velocity
v	m/s	flow velocity component in y-direction

Symbol	Unit	Name
w	m/s	flow velocity component in z-direction
x		cartesian x-direction
y		cartesian y-direction
z		cartesian z-direction
z	-	number of friction interfaces

Indices

ax	axial	m	mean
conv	convection	nom	nominal
d	drag torque	o	outer
eff	effective	red	reduced
f	friction	s	sliding
fp	friction plate	sp	steel plate
g	groove	syn	synchronized
hc	heat conduction	therm	thermal
i	inner		

Glossary

AI	artificial intelligence
ATF	automatic transmission fluid
CFD	computational fluid dynamics
CHT	conjugate heat transfer
CoF	coefficient of friction
DIN	Deutsches Institut für Normung e. V.
EHL	elastohydrodynamic lubrication
FEM	finite element
FVA	Forschungsvereinigung Antriebstechnik e.V.
GUM	Guide to the Expression of Uncertainty in Measurement
LIF	Laser Induced Fluorescence
LL	load level
LS	load stage
MP	multi-purpose
neutrography	dynamic neutron radiography
PIV	Particle Image Velocimetry
RZ	refinement zone

SLA	Stereolithography Apparatus
ST	static loads
vof	volume of fluid

1 Introduction

In industrial applications (e.g. marine), wet multi-plate clutches are frequently used for the connection of auxiliary units, e.g. for connecting and disconnecting compressors, fans, (fire-fighting) pumps and as slipping clutches. Applications as slipping clutches are for example the trolling mode and the so-called fire-fighting mode. Trolling mode is a variation of the propeller speed at constant engine speed to realize propeller speeds below idle speed for harbor and canal cruising as well as positioning tasks. In fire-fighting mode, the drive motor runs constantly at the rated speed to drive a fire pump. At the same time, the drive speed of the propeller is controlled by a slipping clutch. This results in great thermal loads on the clutch depending on the speed of the motor.

The applications in the gearboxes of ships and vehicles are almost without exception safety-critical applications, since a clutch failure results in an inability to maneuver the vessel or is associated with a loss of torque. To prevent this condition, the clutch is designed with a high degree of safety in mind. Thermal overloading of the clutch during operation must be avoided. In this context, the steadily increasing requirements in terms of power density are in competition with the demand for high operational reliability. As a result, clutches are either over-dimensioned (focus on safety) or there is a possibility of failure due to thermal overload during operation.

The loads on the clutch can be quantified by mechanical and thermal load spectrums. Previous investigations have shown that the thermal behavior of multi-plate clutches mainly influences their damage behavior and service life. Knowledge of thermal behavior is therefore indispensable for quantified estimation of the service life.

Investigations of the thermal behavior are typically carried out by means of time-intensive test series. The tests require extensive test rig capacities that are often not available to this extent in the industrial environment. In the case of industrial clutches (e.g. marine), the size of the clutches and transmitted torques are very large, which is why tests can often only be carried out with reduced reference systems. For example, the diameter or the number of friction interfaces is reduced compared to the practical application to be able to use existing test rigs. Regardless of size, the challenge is to set up representative test conditions to simulate operating conditions that are close to the application. The deviations of the load conditions between test and practice make it difficult to transfer the test rig results to the application in the gearbox.

Simulative investigations of thermal behavior of clutches offer an important step towards reducing effort and designing operating conditions more freely. In this context, a degree of detail of modeling adapted to the respective problem should be implemented to optimize the computational and modeling effort. Established programs, such as for example the KUPSIM simulation program, already allow virtual thermal investigations of clutches. KUPSIM makes it possible to estimate the thermal behavior of the clutch under changing loads.

During the development of KUPSIM, the focus was on lubrication situations and geometries of inner carriers typical for applications in the automotive sector. However, in industrial applications, different inner carrier designs are typically used. The lubrications of these so-called industrial inner carriers differ from that of clutches used in the automotive sector. Industrial inner carriers have a bore system (oil distributor pattern) by which the oil is supplied to the clutch package in axial and radial directions in a volume-flow- or pressure-controlled manner.

The need for further research on the thermal behavior of clutches in industrial applications is therefore identified in the following sections after presenting the current state of research, and the results of the performed investigations are presented.

2 Literature Review

2.1 Wet Multi-Plate Clutches in Industrial Applications

2.1.1 Setup and Operating Principle

Wet multi-plate clutches are categorized as shiftable clutches with external actuation [Ver71]. They allow shifting with differential speed and enable stepless adjustment of the transmitted torque. Clutches can operate as a clutch to synchronize two rotating shafts, or as a brake to brake a shaft against a stationary housing.

The plate pack consists of various clutch plates, among which power is transmitted by frictional torque. The plates have alternating internal or external teeth, whereby they are connected to the corresponding inner and outer carriers. This connection is rotationally fixed, but axially displaceable. Thus, an axial force can press the plates together and establish frictional contact [Nie83].

In addition to the classification into inner and outer plates, plates can be categorized as steel and friction plates depending on their function. A conventionally designed plate pack of a clutch consists of steel and friction plates arranged in alternating sequence. A steel plate corresponds to a steel ring with teeth and two flat contact surfaces. A lining plate consists of a toothed carrier plate to which a friction lining is applied on both sides to establish frictional contact with the two adjacent steel plates. The lining can be made of paper, carbon or sintered metal and has grooves to improve oil cooling [Fis16, Nie03].

Figure 1 shows a typical structure of a multi-plate clutch. The sectional view on the left shows a plate pack containing four externally toothed steel plates and three internally toothed friction plates, resulting in six friction interfaces. The outer and inner diameters d_o and d_i refer to the friction lining between the steel and friction plate. The top view on the right shows a partial segment of a friction lining and the mean friction radius r_m.

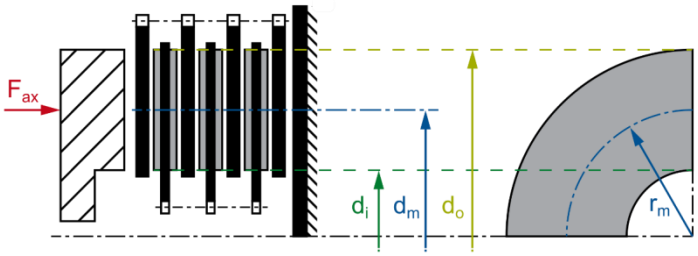

Figure 1: Sectional view of a multi-plate clutch with friction lining diameters (left) and partial segment of a friction surface with mean friction radius (right) according to [Mei17] from [Sch22a]

When the plates are separated with a thin gap, the clutch is in the open state, where no torque can be transmitted. Applying the axial force F_{ax} to the clutch leads to contact between the plates, and the clutch is in the closed state. The coefficient of friction (CoF) μ and the applied axial force at the interface together with the number of friction interfaces z and the mean friction radius r_m define the transmittable friction torque [Mei17, Win85].

$$T_f = F_{ax} \cdot \mu \cdot r_m \cdot z \tag{2.1}$$

According to Winkelmann [Win85], the mean friction radius can be determined as the arithmetic mean of the friction surface diameters d_o and d_i:

$$r_m = \frac{d_o + d_i}{4} \tag{2.2}$$

The contact area between a steel and friction plate in the closed state is called the gross friction area. Groove patterns are not considered in the definition of the gross friction area [Hen14, Mei17]. The gross friction area is calculated from the inner and outer diameters of the friction lining.

$$A = \frac{\pi \cdot (d_o^2 - d_i^2)}{4} \tag{2.3}$$

To compare the loads on clutches of different sizes, the characteristic values of the clutch pressure and sliding speed are widely used. According to [Nie03], the nominal clutch pressure sets the axial force in relation to the gross friction area.

$$p = \frac{F_{ax}}{A} \tag{2.4}$$

The sliding velocity v_s can be calculated from the relative angular velocity $\Delta\omega$ or differential speed Δn of the plates. Their relationship can be described by the following equation:

$$v_s = \Delta\omega \cdot r_m = \frac{2\pi}{60} \cdot \Delta n \cdot r_m \tag{2.5}$$

2.1.2 Tribological System and Friction Behavior

Tribology examines mechanical systems in terms of friction, lubrication and wear. In the optimization of tribological systems, the minimization of energy and material losses can be seen as the main objective. Crucial for this is the knowledge of the CoF during operation [Czi20].

Friction and wear are influenced by many parameters. The current operating conditions, external influences and complex interactions between the friction partners affect the behavior of the friction system. The tribological system (tribosystem) of a wet multi-plate clutch consists of the friction pairing of the steel and lining plates and the lubricant. The tribological system is influenced by the geometry and material properties of the plates, the loads, as well as the physical properties of the lubricant and other surrounding fluids as sketched on the left side of Figure 3.

To be able to assess these complex mechanisms, the behavior of the tribological system can be described by the current CoF. Figure 2 provides an overview of the influencing variables obtained from various sources [Mei17, Nau19, Rao12, Wei12, Zou13] that can affect the CoF.

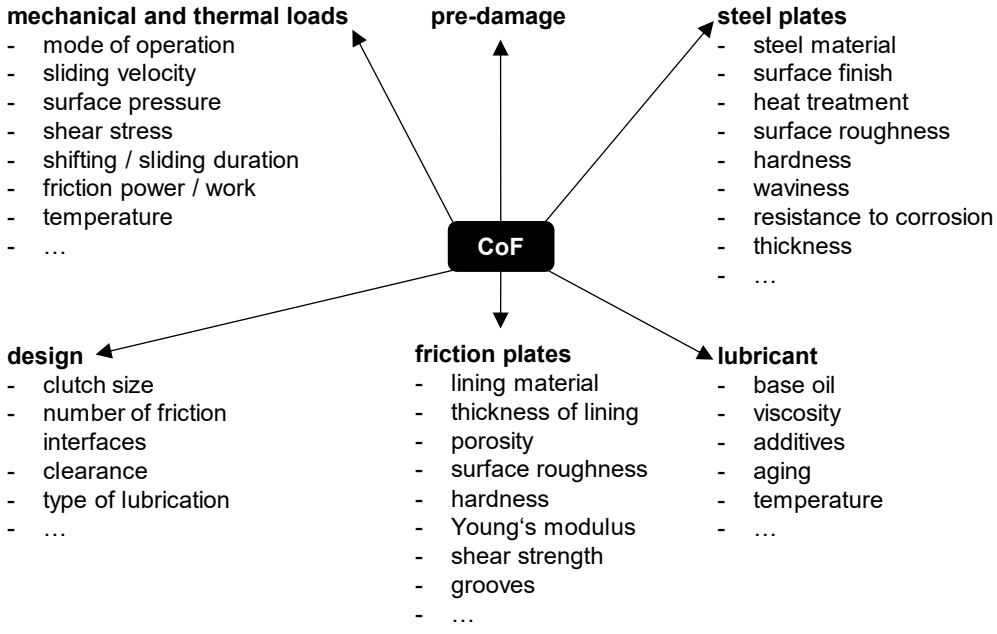

Figure 2: Overview of the influencing variables on the CoF of a wet multi-plate clutch translated from [Mei17]

From this multitude of influencing variables, the sliding velocity v_s should be emphasized for wet clutch systems as it influences e.g. interfacial lubricant film thickness. Based on this, the Stribeck-Curve can be used to classify different friction states. The Stribeck-Curve as shown in Figure 3 on the right is a graphical representation of the CoF as a function of the interfacial lubricant film thickness [Wäs14].

Herein, the lubricated friction states are defined as fluid friction, mixed friction and boundary friction. During the engagement process of a wet multi plate clutch all three states are present whereas the boundary friction is the most important friction state [Czi20, Lay11, Pfl88]. According to Voelkel [Voe20] the surface topography of the friction lining is designed such that the formation of hydrodynamic load-bearing components is avoided as far as possible. While the clutch is disengaged (open) drag torque is transferred due to shear stresses of the fluid (fluid friction). As these are parasitic losses the objective during clutch development is to avoid them.

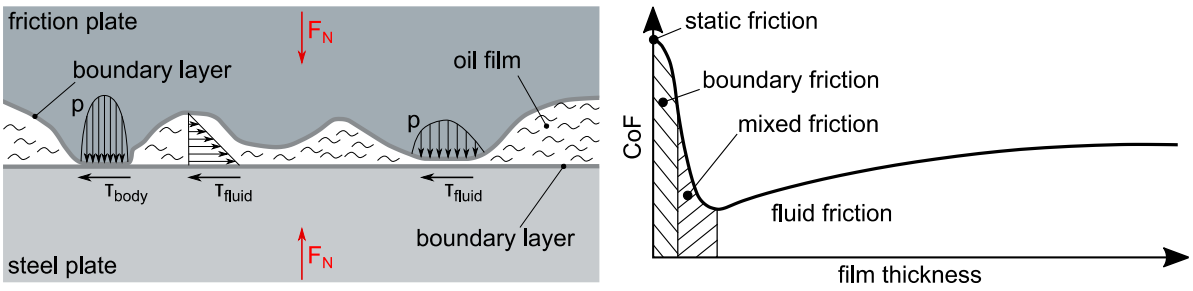

Figure 3: Sketch of tribological system at the friction interface (left) and Stribeck-Curve showing influence of film thickness on CoF (right) translated from [Zör17]

Further insight in terms of a model for the inner and outer friction boundary layer is developed by Winkler [Win08] for the use case of synchronizers. According to literature [Egu01, Ing10a, Voe20] this model is also fully applicable to wet clutch applications.

Figure 4 schematically shows the structure of the outer boundary layer consisting of a base layer which carries the adsorption layer consisting of polar groups and attached alkyl chains. According to the summary description of Voelkel [Voe20] this adsorption layer interacts with lubricant molecules.

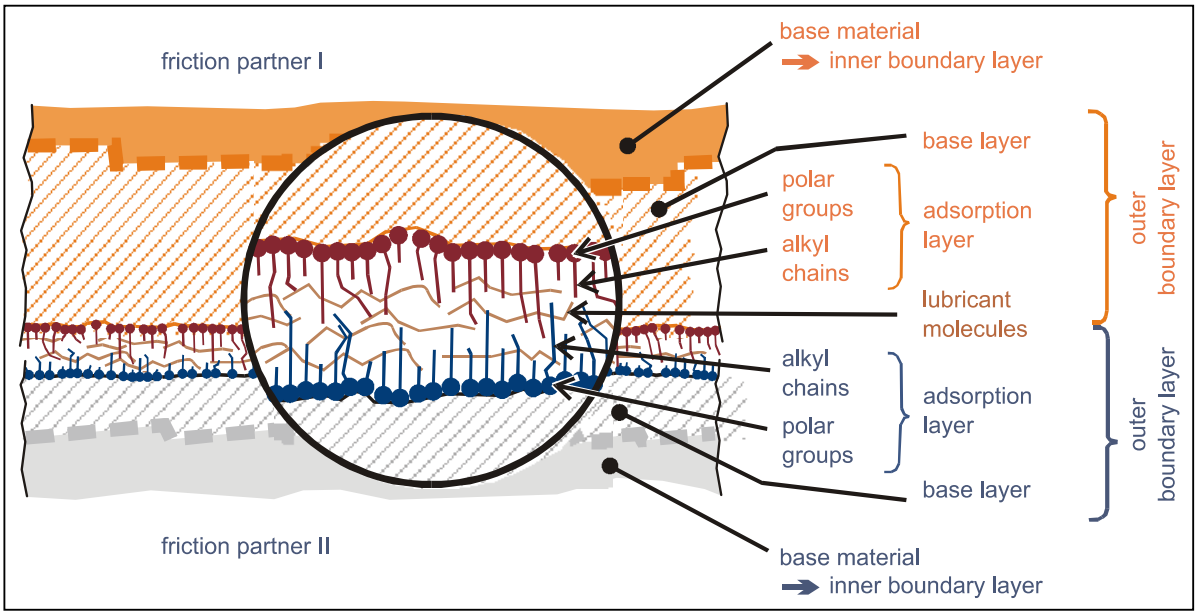

Figure 4: Schematic structure of the outer boundary layer translated from [Win08]

The outer boundary layer determines the friction behavior of the clutch. To minimize free energy, the surfaces react with the surrounding materials. Even during production, the free surface generated due to machining reacts with the surrounding substances such as coolant/lubricant or atmospheric oxygen. In the gearbox, locally occurring mechanical stresses during the friction process, which are greater than the bonding forces of the boundary layer components, lead to new free surfaces. These react immediately with the surrounding substances, i.e. with components of the lubricant, the material of the friction partner or other substances added to the contact, such as removed boundary layer components from other areas. These reactions show a strong dependence on temperature. [Win08]

2.1.3 Characterization of Friction Behavior

Rearranging of equation (2.1) enables the calculation of the CoF from measurements of the axial force and friction torque. Thereby courses of CoF over time and CoF over sliding velocity are obtained (μ-v-curves). Since the CoF depends on many influencing variables, it is suitable to introduce characteristic values of CoF to enable systematic characterization of the friction behavior of different friction systems.

The reasonable application of characteristic values depends on operating conditions. Typically, according to sliding speed ranges different characteristic values are used to characterize the friction behavior. According to Meingassner [Mei17] three speed ranges are distinguished as micro slip (or no slip as static friction, $v_{s,m}$ = 0 … 0.0001 m/s), low speed slip ($v_{s,m}$ = 0.0001 … 0.5 m/s) and brake shift ($v_{s,m}$ > 0.5 m/s) as pictured in Figure 5.

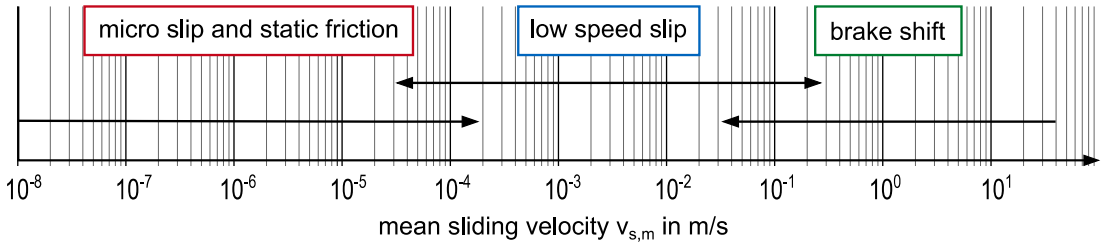

Figure 5: Classification of the operating modes of wet multi-plate clutches according to sliding velocity from [Mei17]

Using the data of the μ-v-curve the average CoF (μ_{avg}) is calculated by averaging in the interval of 0…60 % of maximum differential sliding velocity, as visualized in Figure 6. The average CoF indicates the torque transfer capability of the clutch [Acu14, Sto19, Sto18a, Voe19].

Furthermore, the value μ_2/μ_5 is calculated by division of the CoF at 50 % of max. sliding velocity (μ_2) and the maximum of the CoF in the interval from 0 … 10 % of max. sliding velocity (μ_5). The characteristic value μ_2/μ_5 is a measure for the gradient of the μ-v-curve (dμ/dv). Near the end of engagement, the CoF should decrease as sliding velocity decreases to achieve good control and comfort from the clutch package and to avoid self-excited vibrations (shudder) [Acu14, Mäk05b, Oht94, Ran04].

Shudder can occur when dμ/dv in the μ-v-curve is negative [Mäk05b] which is equal to μ_2/μ_5 < 1.0 [Acu14]. The friction behavior is stable with values of μ_2/μ_5 > 1.0 [Acu14, Sta13, Sto18a].

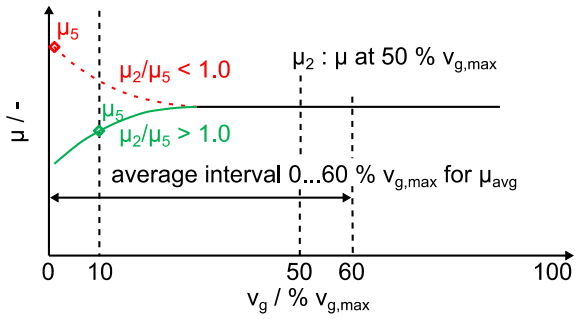

Figure 6: Specific values friction behavior according to [Hen14, Sta13] from [Sto21]

According to Meingassner [Mei17] and Voelkel [Voe20], μ_{top} is a good characteristic value to describe the friction in unsteady low speed slip. It represents the value of the CoF at maximum differential speed. Figure 7 shows an explanation for the measured value for two types of μ-v-curves leading to equivalent values of μ_{top} according to Strobl [Str22].

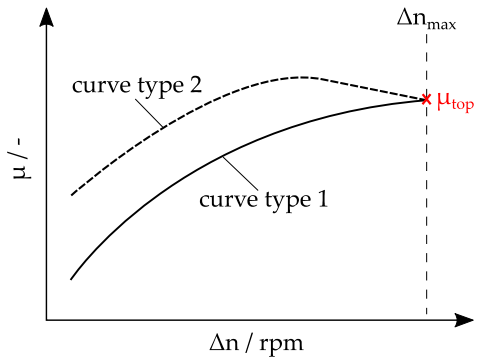

Figure 7: Explanation of μ_{top} for two types of μ-v-curves with equivalent values of μ_{top} from [Str22]

2.1.4 Fundamentals of Lubrication and Drag Torque

The transmittable torque and the endurable friction power of a multi-plate clutch are to a large extent limited by the thermal behavior of the clutch. To reduce the thermal load, multi-plate clutches are operated wet in many applications. In this case, the clutch plates operate in a lubricated environment that primarily serves to dissipate heat. Lubrication can be carried out centrally via the inner carrier and can also be implemented as pressure lubrication by means of appropriate seals. Alternatively, a multi-plate clutch can be operated with sump lubrication, whereby the plates rotate in an oil sump with a defined oil level.

To allow oil to flow between the plates even in the closed state, the friction lining often has a groove pattern. In addition to the cross-section and the arrangement of the grooves, heat dissipation to the cooling oil and the surrounding components is influenced by many other factors. Important factors are the supplied oil flow, the oil distribution within the interfaces, and the air intake into the cooling oil. To be able to compare the volume flow between different sizes, the characteristic value of the specific oil flow rate is used,

$$\dot{v}_{oil} = \frac{\dot{V}_{oil}}{A \cdot z} \tag{2.6}$$

which relates the total oil flow rate $\dot{V}_{oil}$ to the gross friction area A of the clutch [Nie03, Wit13].

However, the improved cooling due to wet operation simultaneously increases the power losses of the clutch. The losses of a wet multi-plate clutch are referred to as drag torque. These occur in the open state and are therefore load independent. The drag torque is generated by fluid shear in the air gap between the plates, which is filled with cooling oil [Nie03]. Especially when several wet multi-plate clutches are applied in an application, the drag torque can account for a significant proportion of the power loss of the overall system [Plo17].

The drag torque depends on many factors that can be considered to reduce these losses. These include the grooving of the friction lining, the clearance between the plates, the oil flow rate supplied and the temperature or viscosity of the cooling oil. The number of friction interfaces and their mean diameter also influence the drag torque. Nevertheless, these parameters are largely responsible for the maximum transmittable torque and are therefore defined by the application. In addition, the drag torque is strongly dependent on the differential speed, which is also mostly defined by the application [Drä13, Drä16, Drä15, Oer00, Poi22].

Analysis of drag torque is usually performed on the drag torque over the differential speed curve. This curve can be separated in three phases depending on differential speed and drag torque behavior. The rise and fall to the maximum drag torque occurs in phase one. Initially the gap between the plates is approximately fully filled with oil and the drag torque increases almost linearly until reaching a peak value. After reaching the peak the drag torque decreases indicating that the gap is now filled with an oil-air mixture. The drag torque continuously decreases until it reaches a plateau with an approximately constant value indicating the beginning of phase 2. The air input into the cooling oil can be explained by

the fact that the centrifugal force of the rotating clutch promotes a larger volume flow than supplied. In phase 3, a renewed increase in drag torque can be observed due to wobbling plates [Drä16, Poi22].

2.1.5 Industrial Operating Conditions and Requirements

Typical use cases for wet multi-plate clutches include the acceleration of large propeller and generator masses in a secure manner in the marine industry, or comparable heavy-duty applications in other industrial and agricultural powertrains. These applications require clutches with high torque and high heat capacity [Gro22, Lin18].

The shifting cycles involve transitions between open and closed modes. However, non-stationary and continuous slip under high clutch pressures are also typical modes of operation in industrial / marine clutches [Gro22]. The application as shifting element enables synchronization of rotational speeds and transmission of torque. The clutches face high differential speeds and clutch pressures, but compared to continuous slip, this is usually for a limited period of time [Sch19].

Production batch sizes of large clutches used in maritime and industrial environments are small and often do not allow extensive functional and durability tests on prototype parts. Further limitations of the experimental validation can be found in the clutch sizes, with diameters in the range of more than one meter, and the large torques that are transmitted. Due to the high security and durability demands, designs based on assumptions of worst-case scenarios are used. This leads to over-dimensioning of the clutches and increases costs as well as weight, fuel consumption and CO2 emissions [Gro21b].

2.1.6 Materials and Oil

Materials and oils are key parameters that define the performance of wet friction systems such as high CoF, good friction characteristics (e.g. decreasing CoF at the end of the engagement), high temperature resistance and durability, minimal run in period, minimal wear, and a low influence of oils and their additives [Kea97, Lam06, Ran04, Sto21]. According to [Bac10] the selection of the best friction lining always depends on multiple functional and economical requirements. Nevertheless, proven materials for industrial applications are combinations of steel plates with sinter-based friction linings and high viscosity oils [Hoe01].

Sintered friction linings based on bronze and iron represent the largest group of metallic friction linings [Ber17]. Depending on the manufacturing process used, sintered friction linings can be divided into scatter sintered and foil sintered friction linings. In the case of scatter sintered friction linings, the sintered friction lining and the bonding layer are scattered directly as powder onto the steel plate and then sintered in the furnace. This produces a uniform, non-detachable bond with the carrier plate. A plane-parallel surface and the desired grooving of the friction lining is achieved by pressing. In the foil process, on the other hand, the friction lining is first prepressed and then bonded onto a previously copper-plated carrier plate. After application of the friction lining, the friction plate must be ground to achieve thickness tolerances and the required parallelism. The grinding process can deteriorate the friction behavior by clogging the pores. [Hoe01]

Besides the sinter and steel material, the friction behavior of multi-plate clutches is significantly influenced by the composition of the oil, its additives and viscosity as well as the ageing condition [Hau07, Lay11, Müh18]. The oil considerably influences the friction behavior of the clutch and the shifting comfort. Furthermore, the oil supply ensures cooling and lubrication of the shifting elements. The additives play a key role in ensuring that the wide range of requirements placed on the oil are met. The oils typical temperature resistance is within the range of about -40°C to 150°C [Lay11]. Thermal ageing of the oil should be avoided, due to the high thermal resistance of the oil. Foam formation must be avoided, and deposits and corrosion must be prevented. Compatibility with the materials that meet the oil must be achieved. Finally, the additives contained in the oil ensure that there is a high static CoF and - for reasons of comfort, good friction characteristics.

2.2 Thermal Behavior of Wet Multi-Plate Clutches

The thermal behavior of wet multi-plate clutches mainly influences their service life and damaging effects. Especially peak temperatures and the temperature profiles over time influence spontaneous and permanent damages of the clutch [Hen14, Lin17].

The temperature in the clutch plates rises through heat input during the slip phase. The relative movements of the plates at the friction interfaces of the closed clutch lead to friction losses that occur in the form of thermal power. Under the assumption that there are no further power losses, the thermal power $\dot{Q}$ is defined as the difference between input and output power.

$$\dot{Q}=P_{in}(t)-P_{out}(t)=T_f(t)\cdot(\omega_{in}(t)-\omega_{out}(t)) \tag{2.7}$$

Integrating the thermal power over the duration of one synchronization process results in the friction work that defines the thermal load.

$$Q=\int_0^{t_{syn}} P_{in}(t)-P_{out}(t)\,dt \tag{2.8}$$

The thermal load of a clutch increases with the frequency of shift cycles and the height of specific loads. The sum of friction work of the shifting cycles per hour is the value of the friction work per hour. The limit value from the manufacturer for the maximum permissible friction work per hour must not be exceeded during operation [Zör17].

Basically, heat transfer can be described by different phenomena: by heat conduction between components, by convection as well as by heat radiation. The latter is negligible regarding wet multi-plate clutches.

The advantage of a wet multi-plate clutch compared to a dry clutch is the ability to transfer the heat introduced by friction to the fluid by forced convection on the cooling oil. This process can be described by Newton's cooling law.

The heat distribution within a wet clutch is shown qualitatively in Figure 8. In the case of a steel/paper friction interface, the heat input occurs almost exclusively in the steel plates. This is due to the different thermal conductivity of the materials. The paper lining behaves like a heat conductor, which is why the carrier plate can hardly absorb any energy. This different distribution of heat results in very high peak temperatures in the steel plates. At the steel/sinter interface, on the other hand, heat is distributed evenly over all components, which results in a balanced temperature distribution with comparatively lower peak temperatures [Voe18, Woh12].

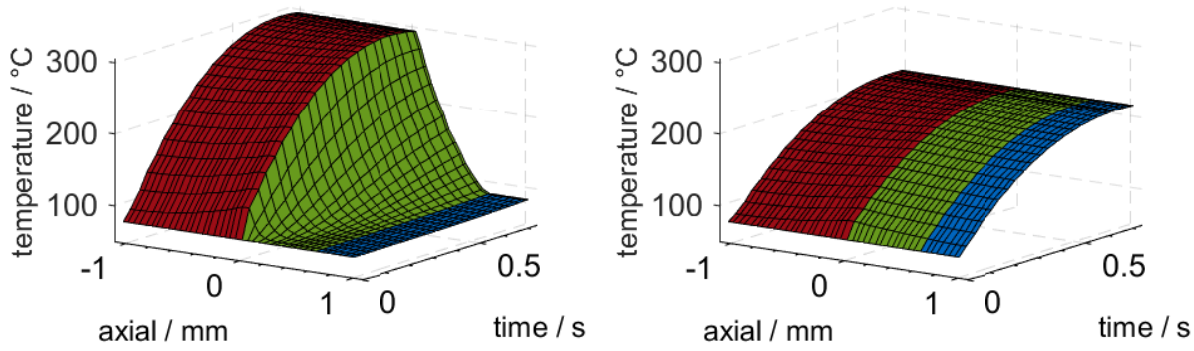

Figure 8: Comparison of temperature distributions (red: steel plate, green: friction lining, blue: carrier plate) of two friction interfaces with paper (left) / sinter (right) friction linings at the same specific loads according to [Woh12]

Heat is also transferred to the surrounding components, such as shafts and housings. This occurs via the contact surface of the plates with the shafts in the splines [Gro21b, Voe18].

2.2.1 Governing Equations for CFD and Temperature

The basic equations of hydrodynamics are used to calculate the oil flow and solid temperatures in wet multi-plate clutches in this thesis. These equations are based on the continuum mechanical conservation laws for mass, momentum and energy (a.o. [Bar10, Dur06, Pol09, Sch06]).

Depending on the kind of observation, the properties in a moving fluid are either determined on a fixed point in space (Eulerian approach) or by following the fluid parts along their streamlines (Lagrangian approach). In the context of this work, the Eulerian approach is used, in which the changes of the flow variables at a fixed fluid element (balance volume) are considered. The equations consist of the local derivative at the balance volume and a convective derivative of the quantity, which results from the change of the quantity flowing in and out of the balance volume.

Flows can be further categorized into compressible and incompressible flows. Compressible fluids react to pressure changes with a change in density and volume. Incompressible fluids do not show any density changes due to pressure. Furthermore, laminar and turbulent flows can be distinguished from each other. Laminar flows are characterized by flows flowing in smooth paths with layers, whereas turbulent flow is fluid motion characterized by chaotic changes in pressure and flow velocity.

With computational fluid dynamics (CFD), quantities such as density, pressure, velocity, temperature and friction of a flow can be calculated. For this purpose, the fluid is divided into fluid elements, to which volumes with continuum properties are assigned. Corresponding balance considerations are then carried out on these volume elements. A sufficiently fine subdivision of the balance volumes should be considered to resolve the flow well. Furthermore, a lower limit results from the compliance with the continuum assumption on which the derivation is based. Recommendations for a lower limit of the volume element size with the same side length are approx. 0.215 µm to 1 µm [Bar10].

In the following, the equations for conservation of mass, momentum and energy are given in dependence of cartesian coordinates (x, y, z) and time t. A detailed derivation and description of the equation components can be found, for example, in [Bar10] and [Pol09].

The mass conservation equation at a volume element describes that the temporal change of the mass in the volume element is equal to the difference between incoming and outgoing mass flows at the volume element. Mathematically, this can be represented for a compressible flow as follows.

$$\frac{\partial \mathrm{u}}{\partial \mathrm{x}}+\frac{\partial \mathrm{v}}{\partial \mathrm{y}}+\frac{\partial \mathrm{w}}{\partial \mathrm{z}}=0 \tag{2.9}$$

Here u,v,w are the velocity components belonging to the corresponding coordinate direction.

The balance of momentum conservation at the volume element is established by considering the change in time of the momentum within this volume. The momentum change is calculated as the difference of the momentum currents entering and leaving the volume element, the surface forces acting on the volume element and the mass forces acting on the mass of the volume element. The momentum of a fluid element is the product of its mass and velocity. The resulting system of equations is also known as the Navier-Stokes equations. The Navier-Stokes equations for an incompressible flow with Newtonian fluid behavior and constant viscosity are.

$$\rho\cdot\left(\frac{\partial \mathrm{u}}{\partial \mathrm{t}}+\mathrm{u}\cdot\frac{\partial \mathrm{u}}{\partial \mathrm{x}}+\mathrm{v}\cdot\frac{\partial \mathrm{u}}{\partial \mathrm{y}}+\mathrm{w}\cdot\frac{\partial \mathrm{u}}{\partial \mathrm{z}}\right)=\mathrm{f_x}-\frac{\partial \mathrm{p}}{\partial \mathrm{x}}+\eta\cdot\left(\frac{\partial^2 \mathrm{u}}{\partial \mathrm{x}^2}+\frac{\partial^2 \mathrm{u}}{\partial \mathrm{y}^2}+\frac{\partial^2 \mathrm{u}}{\partial \mathrm{z}^2}\right) \tag{2.10}$$

$$\rho\cdot\left(\frac{\partial \mathrm{v}}{\partial \mathrm{t}}+\mathrm{u}\cdot\frac{\partial \mathrm{v}}{\partial \mathrm{x}}+\mathrm{v}\cdot\frac{\partial \mathrm{v}}{\partial \mathrm{y}}+\mathrm{w}\cdot\frac{\partial \mathrm{v}}{\partial \mathrm{z}}\right)=\mathrm{f_y}-\frac{\partial \mathrm{p}}{\partial \mathrm{y}}+\eta\cdot\left(\frac{\partial^2 \mathrm{v}}{\partial \mathrm{x}^2}+\frac{\partial^2 \mathrm{v}}{\partial \mathrm{y}^2}+\frac{\partial^2 \mathrm{v}}{\partial \mathrm{z}^2}\right) \tag{2.11}$$

$$\rho\cdot\left(\frac{\partial \mathrm{w}}{\partial \mathrm{t}}+\mathrm{u}\cdot\frac{\partial \mathrm{w}}{\partial \mathrm{x}}+\mathrm{v}\cdot\frac{\partial \mathrm{w}}{\partial \mathrm{y}}+\mathrm{w}\cdot\frac{\partial \mathrm{w}}{\partial \mathrm{z}}\right)=\mathrm{f_z}-\frac{\partial \mathrm{p}}{\partial \mathrm{z}}+\eta\cdot\left(\frac{\partial^2 \mathrm{w}}{\partial \mathrm{x}^2}+\frac{\partial^2 \mathrm{w}}{\partial \mathrm{y}^2}+\frac{\partial^2 \mathrm{w}}{\partial \mathrm{z}^2}\right) \tag{2.12}$$

Here ρ corresponds to the density of the fluid element, f describes an applied volume force, p corresponds to the pressure and η is the dynamic viscosity

The basis of temperature calculations within the solids of a wet multi-plate clutch is derived from the three-dimensional fundamental heat transfer equation (2.13). The equation can be derived by applying

the principle of conservation of energy to the balance of the thermal energy of a volume element inside a heat-conducting body. In sum, energy can neither be dissipated nor generated, so the addition of heat during a time interval must lead to a corresponding increase in the internal energy. This is consistent with the First Law of Thermodynamics for an open system without work and without consideration of kinetic or potential energy. Details on derivation and further explanations can be found in [Pol09].

$$\rho c \frac{\partial T}{\partial t} = \frac{\partial}{\partial x}\left(\lambda \frac{\partial T}{\partial x}\right) + \frac{\partial}{\partial y}\left(\lambda \frac{\partial T}{\partial y}\right) + \frac{\partial}{\partial z}\left(\lambda \frac{\partial T}{\partial z}\right) + \dot{q} \tag{2.13}$$

Here c is the specific heat, T is the temperature, λ is the heat conduction coefficient and q̇ is an internal heat source.

2.2.2 Modeling of Energy Input by Friction

The energy input on the friction surface corresponds to the friction work performed per unit of time. Therefore, modeling of energy input during the slip phase assumes that the friction work is completely dissipated as heat [Gei37]. According to equation (2.7) the energy input is defined as the product of differential speed and friction torque. Thus, the modeling of energy input by friction corresponds to the question of an accurate friction torque or CoF model [Voe17]. The results presented below have been published by Strobl, Schermer, Grötsch, Pointner-Gabriel, Voelkel, Pflaum and Stahl [Str22]. Modeling the friction behavior of wet multi-plate clutches is difficult whereas the friction behavior is the key parameter defining thermal loads and comfort characteristics [Göp21] at the same time. Experimental research on the friction behavior of wet clutches shows various influencing factors e.g. oil, material and applied load (a.o. [Acu14, Ing10b, Kat19, Mäk05b]). Due to lack of hands-on applicable friction models, energy input is often modeled with constant CoF, friction maps (e.g. [Gro21b]) or models lacking any possible physical interpretation (e.g. [Ma19]). The development of state-of-the-art friction models is based on physical modeling or curve fitting methods. Sophisticated physical modeling approaches exist in the case of elastohydrodynamic lubrication (EHL) based on Reynolds linear elasticity and load balance equations [Bjö13]. For low entrainment speeds during ball on disc tests, the deviations between numerical predictions and experiments of CoF are in general less than 10 % [Bjö13]. However, the large gap and the porosity of the friction lining prohibit application of EHL methods to wet clutches [Ing10a]. Nevertheless, there are physical models from application of dynamic pressure lubrication theory and Hertz contact theory enabling the estimation of CoF in wet clutches and helping to understand the friction mechanisms [Wan18, Yos19]. However, their practical relevance is limited which is caused by the assumptions and simplifications during model derivation. Besides these physical approaches, many empirical models exist that are parameterized by curve fitting with measurement data. The models consist of linear/quadratic (a.o. [Yan98]), logarithmic (a.o. [Gao02, Yan98]), exponential (a.o. [Dav00]) or hyperbolic (a.o. [Mar07]) terms or combinations of these mathematical terms (a.o. [Häg16, Yan98]). Another approach is the fitting of the Stribeck-curve to measurement data (a.o. [Bar15, Zha09, Zha18]. All of these models have sliding velocity (respectively rotational speed) in common as an input parameter, sometimes extended by clutch pressure and contact temperature [Häg16, Yos19, Zha18]. Logarithmic approaches are motivated by the logarithmic dependence of shear stress of organic friction modifier boundary films [Ing10a], but need special assumptions for zero sliding velocity. Stribeck-curve models distinguish between the friction behavior with the constant static friction coefficient and kinetic friction coefficient and try to combine curve fitting methods with the possibility of physical interpretation. Most of these empirical models concentrate on reproducing the friction behavior of a single tribological system. Furthermore, sliding velocity is often considered to be the only variable model input parameter. As a result, it is not possible to identify the main influencing parameters on the friction behavior, and evaluation of applicability across different tribological systems is impossible.

Recent research also applies data mining [Wu21] and machine learning [Shu21] techniques on the torque transfer behavior of wet clutches. The data mining approach analyses friction behavior and states the main influences on the CoF of the studied tribological system in descending order as clutch pressure, friction surface temperature, feeding oil temperature and differential speed. The authors state that their

approach is superior to the classical one factor at a time and designed experiment approaches, but do not rate the high effort of experiments to apply their method. The machine learning approach focuses on a non-linear torque transfer function representing the whole clutch system, and therefore is not a contribution for modeling the CoF.

2.2.3 CFD Approaches and Modeling of Oil Flow

The oil flow defines cooling conditions within the clutch and is therefore an important part of thermal models. The flow situation, which has a major influence on cooling, differs significantly for closed (friction and closed cooling phase) and open (open cooling phase) clutches. Excerpts of the text presented below have been published by Grötsch, Niedenthal, Völkel, Pflaum and Stahl [Gro22, Gro20].

Most CFD publications focus on the open phase and the calculation of cooling performance and drag torque (a.o. [Bin18, Gro20, Neu19]). Computational methods for the calculation of lubrication in open clutches are current topics of research [Gro19a, Neu19, Pan19, Par19, Pen19]. The approaches can be categorized into analytical or reduced 2D CFD models and 3D approaches [Cui14a, Hu09, Iqb13, Iqb14, Mah15a, Pah14, Pah16a, Pah16b, Pah17, Pen19, Sun14, Yua11, Yua10, Yua07]. Due to the limited options of the consideration of the various influencing factors of the complex flow conditions, especially in the grooves, 2D models usually only give acceptable results for non-grooved clutch designs.

The state of the art is therefore the development of 3D numerical fluid simulation models. At higher speeds, it is necessary to consider a multiphase (oil-air-mixture) flow [Yua03]. Most common is the volume of fluid (vof) method [Asa18, Jam11, Mah15b, Mah16, Mah17, Neu17, Ter18a, Ter18b, Wu15]. Results from these models show a good match between calculation and test rig measurements. Due to the high computational costs and calculation times of this method, strong simplifications of the clutch geometry are often applied. Groove designs with symmetries or periodicity are preferred to reduce model sizes. Transient and stationary solutions can be obtained with the vof method.

Other approaches for the calculation of open clutch lubrication are mixture models [Tak11] and cavitation [Gro19a, Rud11, Sin02] models. These solve the multiphase flow region by considering a viscosity of the oil-air-mixture. One advantage of these is short computational time. Furthermore, Dümeland [Düm84] describes the flow state in the gap with an analytical solution of basic hydrodynamic equations. This solution can be used to calculate the possible oil flow rate when the gap is filled, as well as the pressure and velocity distribution in radial direction.

Besides open clutch modeling, few models consider the closed state that can be solved stationary (a.o. [Beh18, Mar09, Ter18a]) or transient (a.o. [Cui14b]), often with constant sliding velocity. Solving the two-phase-flow of oil-air mixtures at the friction interfaces is also computationally expensive (a.o. [Bas16, Beh18, Ter18a]). Nevertheless, recent publications show that CFD simulations enable the estimation of the oil distribution at each friction interface depending on loads and oil distributor patterns [Bas16, Gro22, Ter18a] of a closed clutch. The influence of the pattern of oil distributors at the inner carrier for automotive / motorcycle clutches shows nonlinear effects on oil distribution at each friction interface. Even six evenly distributed oil inlets lead to non-uniform oil distributions [Ter18a], which corresponds to the experimental investigations of [Grü13]. The authors state that the design of the inner carrier dominates oil distribution at the friction interfaces [Grü13]. On the other hand, clutches with pressurized oil-supply, which is typical in industrial applications, show uniform oil distribution if sufficient oil is supplied to ensure single-phase flow conditions. The design of the oil supply in the inner carrier has no influence on the stationary oil distribution in the sealed clutch [Gro22].

Another approach is to simplify the oil flow by means of the homogenized Reynolds equation [Mar09] or by solving a simplified 1D flow model [Häm95, Voe18]. This significantly reduces computational costs but prohibits oil distribution analysis and introduces new input parameters that have to be gathered by preliminary simulations [Mar09] or measurements [Häm95, Mar09, Voe18].

The calculation of shifting cycles [Voe16b] with long durations involves transitions between open and closed modes, and could be important for designing clutches that are operated in both regimes.

2.2.4 Conjugate Heat Transfer Coefficients

The convective heat dissipation through the cooling oil ensures that the temperature increase is quickly reduced after a shifting cycle. The cooling situation is very complex due to the underlying physics and the interconnection with the oil flow in the grooves and interface gaps. To be able to take the main effects into account in a calculation model, suitable model assumptions must be made.

On the basis of analytical models [Alb10], it is possible to calculate a conjugate heat transfer (CHT) coefficient of the open and closed clutch by measurements of the steel plate temperature and the oil temperatures entering and leaving the grooves [Häm95]. By applying empirical knowledge from a lot of test rig results and further physical ideas, the CHT coefficients are also applicable during multiphase conditions [Häm95, Voe18]. However, there is a wide variety in the numerical results, since not all physical effects are captured.

Besides the analytical methods, it is also possible to define an empirical based lumped CHT coefficient through experiments [Kim18, Le 17, Rao12] or a Nusselt correlation [Che11]. The lumped CHT coefficients work as calibration factors for the thermal model, and they unite all unknown heat transfer phenomena, such that the calculated temperatures correspond to the measured ones. The disadvantages of this approach are the lack of direct physical interpretability and the need for extensive measurements. Furthermore, the results usually show great variability depending on operating conditions.

However the calculation of CHT coefficients between oil flow and solid regions depending on groove patterns and applied loads is also possible [Beh18, Kar11, Par16, Yas18]. The possibilities of application seem to be only limited by the available computational power. Most authors limit their models to one friction interface [Beh18, Yas18], whereas others even take the whole surrounding and the calculation of its CHT coefficients into account, and show very good agreement to the measurements [Kar11]. The advantages of the simulative approaches are deep insights into the complex physics that influence the CHT coefficients and the possibility to assess influencing factors precisely. E.g. according to [Beh18], the right choice of rotational direction and an appropriate choice of groove angle can increase CHT coefficients in a disengaged automotive clutch by five times. Furthermore, [Yas18] investigate three different groove designs and show differences in CHT coefficients of each design.

2.2.5 Thermal Calculation Models and Results from Numerical Studies

First works, which form the basis of today's thermal calculation models, had already been published at the beginning of the last century. Geiger [Gei37], for example, calculated the temperature of a clutch with a simple one-dimensional model, which is probably real-time capable with today's hardware. He already considered the heat conduction in connecting components and stated that the friction interface temperature is a damage criterion. Furthermore, he defined the coupling condition during the friction power input at the friction interface.

Other works that can be regarded as an important basis for thermal calculation of wet clutches are the experimental and theoretical investigations of Steinhilper [Ste62, Ste63a, Ste63b, Ste63c, Ste64]. Based on the laws of heat conduction, he developed one- and two-dimensional equations for calculating the temperature in multi-plate clutches. Furthermore, he transferred these systems of equations into thermal networks, in which, however, oil cooling cannot be considered. The thermal networks are converted into electrical circuit diagrams to carry out experimental investigations. The accuracy of the calculation results is confirmed by comparison with experiments. Furthermore, he found that for practical purposes, a one-dimensional approach to thermal design is usually sufficient. Due to the strongly deviating operating conditions and friction materials (e.g. asbestos), more current literature is summarized in the further course.

The importance of thermal modeling results, among other things, from the goal of preventing overloads and adapting control strategies to the temperature-dependent friction behavior. Depending on the objective, models of various complexities have proven themselves, ranging from the simplest estimation formulas [AT303] to multiphysics [Cho12] or coupled CFD and finite element (FEM) simulation

approaches [Kar11]. Besides self-developed research codes in C [Yan95] and Fortran [Häm95], models were also built in Matlab/Simulink [Gro21b, Liu12, Roh04, Zha09] as well as in Ansys [Lei12, Sch22b], SimericsMP+ [Gro22] or other commercial programs.

Most computations are performed in the research or pre-development area on appropriate desktop hardware. E.g. the FVA (Forschungsvereinigung Antriebstechnik e.V.) program KUPSIM enables thermal design and recalculation in order to estimate thermal loads on the clutch under changing operational loads. The calculation models and the results are validated with good agreement by comparison with test rig results [Häm95, Voe18, Woh12].

However, especially for the online monitoring of clutches in operation, real-time capable simulation models have been developed that work as virtual temperature sensors. There are publications for rear axle gearboxes [Seo15, Seo11], automotive transmissions [Cho12], double clutch applications [Wu19] as well as parametric modeling for multiple use cases (automotive, marine, industry) [Gro21b]. Online monitoring by means of real-time capable calculation models allows the control strategy to be adapted to the thermal behavior of the clutch. This can, for example, improve the shifting quality in the case of strongly temperature-dependent friction behavior [Cho12, Mar07, Wu19]. Furthermore, the pressure in the clutch, which leads to shorter shifting durations but higher temperatures, can be optimally adjusted [Zhi16]. In addition to these comfort optimizations, overload protection is also possible by means of real-time capable calculation models. For this purpose, the clutch pressure should be automatically reduced if a certain clutch temperature is reached [AT303, Gro21b, Wu19]. [Wu19] propose a clutch temperature limit of 250°C. According to [Cho12], a counter could also document the exceeding of critical temperatures and thus be used for lifetime predictions.

However, 2D or 3D simulation models are required to evaluate and analyze the temperature distribution in the clutch components. If the thermo-mechanical stresses are also considered in the calculations, damage can be made accessible to the calculation. [Xie10] determined with his model that the temperature rise at hot spots generates thermal stresses in the plates that exceed the yield strength and can thus cause deformation and thus also severe wear up to failure. Further thermo-mechanical investigations can be found in [Sch22b, Xie10, Yan95], which confirm an uneven contact of the friction partners.

Calculations by [Zha09] predict the maximum of the calculated temperatures in radial direction in the region of the mean friction radius, which decreases slightly towards both edges. However, more recent publications see the temperature maximum rather in the region of the outer diameter [Lei12, Sch22b]. Schneider also confirms that in axial direction, the middle plate is thermally most severely loaded, which is implicitly used as a model assumption in many other models [Gro21b, Woh12]. However, this seems to depend strongly on the installation and lubrication situation, since [Cui14b], for example, see the highest temperatures in the area of the second friction interface in their installation with 12 friction interfaces.

Advanced computational models also take into account the influence of heat dissipation via the gears to the connected carriers, since these make a significant contribution to the cooling of the clutch [Cho12, Gro21b, Kar11, Voe18].

The influence of grooves in the lining materials on the thermal behavior can be investigated with the aid of complex modeling. [Miy09] show that a combination of radial and circumferential grooves causes significant reductions in the maximum temperatures, with the influence of the circumferential grooves dominating. [Lei12] assume that the heat can be dissipated best by radial grooves. This is confirmed by the results of [Jan11]. However, the authors' statement that the use of waffle-shaped grooves does not provide any advantages over non-grooved plates regarding thermal behavior must be critically questioned.

Calculation models that also include the diffusion of cooling oil into the friction lining as well as the compressibility of the linings show that both variables lead to a reduction in peak temperatures [Yan95, Zhi16]. Furthermore, permeability and the deformations of the lining influence the occurrence of thermal instabilities [Jan99].

The thermal conductivity of the friction partners significantly influences the distribution of heat [Jen08]. Furthermore, depending on the lining material, the thermal conductivity in radial direction is more pronounced than in axial direction [Xie15]. A change in the thickness of the friction partners as well as the thermal conductivity can strongly change the temperatures [Sch22b]. In contrast, variation of the elastic modulus shows very little effect on temperatures [Jan99, Sch22b].

2.3 Experiments

2.3.1 Plate and Oil Temperature Measurements

The high dynamics of temperature changes in a wet multi-plate clutch, especially during the friction phase, requires a fast temperature measurement technology. Thermocouples (mostly NiCr-Ni class 1) are well established for this purpose [Beh18, Gro21b, Hen14, Mar09, Pay91, Voe18]. Their function is based on the thermoelectric effect due to which charge carriers are arranged in a conductor along the temperature gradient. In metals, the electrons shift to areas of low temperature. This results in a voltage that depends on the temperature at the measuring point [Mai06]. Thermocouples are contact thermometers, which means that they must be in contact with the body to be measured. To measure temperatures within a component, holes are drilled or eroded to the desired depth. Thermal resistance in the contact can be reduced by using thermal paste [Sch19]. A further application is possible by gluing, but deviations in the measurements are to be expected due to the contact resistance of the adhesive, which must be compensated by suitable calibration [Ost01]. When applied to rotating components, telematics is required for data transmission [Czé09, Hen14]. Thermocouples are usually used to determine the mass temperature of the plates to draw conclusions about the friction interface temperature. For this purpose, the thermocouple is positioned axially in the center of the plate [Gro21a, Par16]. This type of installation is mainly selected for thin steel plates, since here, in conjunction with the high thermal conductivity, a very low axial temperature gradient occurs within the plate [Iva09].

[Fis94] measures the friction interface temperature directly by welding the thermocouple to the plate at the level of the friction interface. The weld spot is ground to minimize the influence on the friction system. This complex application of the thermocouple does not allow the plate to be dismantled for further investigations between tests. A compromise between effort and proximity to the friction contact is the placement of the thermocouple just below the friction interface. E.g. [Mar08, Mat93] choose this position, whereby [Mar08] takes the temperature 0.3 mm below the friction interface as the friction interface temperature. He justifies this with good thermal conductivity, since the temperature signal reacts to changes in the differential speed without relevant delay.

The choice of the radial position of the thermocouple often falls on the mean friction radius to map the mass temperature. Since the sliding velocity increases with the radius, a higher energy input is expected in the outer region of the friction lining compared to the interior. To capture these differences, [Czé09] chose different radii for their thermocouples, but the same axial distance to the friction contact.

[Hol99] does without thermocouples and determines the friction interface temperature with the aid of an infrared thermometer. However, this option is only possible for special test rig setups.

Another very complex alternative to thermocouples is the use of fiber-optic temperature sensors. [Alb18] achieves a very high spatial resolution with up to 700 measuring points in a clutch pressure plate. Since the measuring points are distributed around the circumference as well as lying at different depths below the friction surface, this method enables a comprehensive analysis of the temperature distribution and heat flow in the component. However, there is a very high effort in the context of application, test execution and the later data analysis. The method is to be classified as a niche application for special use cases.

2.3.2 Investigations for Optical Validation of Oil Flow

The validation of CFD simulations, which often represent very complex processes and depend on many influencing variables, is usually carried out using test rig experiments or measurements from field

operations. For example, values from measurements can be compared with the simulated values to check the transferability of the simulation results [Sch22a].

For many CFD simulations, an optical validation of the flow is chosen. With a suitable test rig setup, details such as air entrainment in the grooves as well as global flow conditions in the entire clutch can be investigated. However, due to the complex geometric conditions and operating modes of multi-plate clutches, optical validation methods of the lubrication situation often prove to be very elaborate and costly.

[Alb12] use the particle image velocimetry (PIV) method for optical validation. With this, particles are added to the oil and a reduced clutch with a single lining plate is mounted in a transparent test environment. A high-speed camera records the particles that are made visible by a laser. In the evaluation, a mapping of the particles is performed in successive images, resulting in the generation of a velocity vector field of the oil flow. [Web10] use the laser induced fluorescence (LIF) method, in which a fluorescent dye is added to the oil. By irradiating the oil with UV light, a very high-contrast image of the oil can be obtained. This method enables examination of details such as the topography of seals and the oil film. [Grü13] use dynamic neutron radiography (neutrography) to ensure that the clutch operates as close to the application as possible during optical validation. This procedure is like an examination with X-rays. If the components are made of aluminum, the neutron radiation can visualize the oil distribution in the plate grooves and in the rotating clutch.

A less complex approach can be found in [Kit03], who replace the foremost steel plate in a multi-plate clutch by a fixed acrylic glass pane in order to enable a view on the plate. [Neu19, Neu21, Ter18a] validate their CFD simulations with high-speed cameras. [Ter18a] uses 3D-printed plates and transparent components in the area of the oil supply. [Neu19, Neu21], on the other hand, use a special test rig setup, in which a single lining plate with a defined air gap rotates in front of a transparent disc and is lubricated from the inside. Similar approaches with transparent plexiglass discs have already been used at FZG to investigate the lubrication of gears with sump lubrication. [Liu18] investigates the effect of oil level on efficiency, while [Hil22] evaluates the effect of oil baffle plates. Both papers involve CFD simulations validated by high-speed camera imaging.

According to [Sch22a], an optical validation is suitable when the objective of a CFD simulation is not only about measuring characteristic values, such as temperature, pressure or drag torque, but the flow behavior of the oil. The complex methods of PIV, LIF or neutrography are suitable to make very specific details visible that could not be observed otherwise. These are sometimes associated with great effort and expense. Simpler methods, such as the use of transparent components or operation behind a plexiglass pane, are suitable for validating more general statements about flow behavior that can be observed with the eyes or a camera. The use of a high-speed camera extends the scope to very short events, such as air bubble formation, but also increases the costs.

2.3.3 Investigations of Friction Behavior

[Acu14] indicate in their publication that the friction behavior of wet multi-plate clutches is not predictable, and that therefore experimental investigations must be carried out. This applies in particular to new friction and oil combinations. It is therefore not surprising that many new publications with new test methods for characterizing the frictional behavior of wet multi-plate clutches are still being published. Overview studies comparing different test methods have also been published [Lin98, Mur00].

Internationally, modified SAE2 machines are usually used for the tests. A description of the setup can be found in [Mäk05a]. German institutes usually operate their own test rig setups [Bis21, Mei17, Str21].

A large part of the tests carried out deals with automatic transmission fluid (ATFs) releases or tractor applications [Mäk05a]. In the field of research, however, the influencing parameters and effect variables are also investigated. [Ing10b] shows with ball on disc tests that friction behavior is significantly influenced by additives in the oil. He himself speaks of a transferability of his tests to the system of wet multi-plate clutches. Investigations by [Müh18] indirectly confirm the findings by establishing that the

base oil is of only minor importance for friction behavior and that it is therefore significantly influenced by the additives.

Due to the high cost and effort of experimental investigations, one objective is to minimize the time required. [Acu14, Acu13] developed a test method for this purpose, with which paper friction systems can be systematically characterized quickly. However, this method cannot be applied directly to sinter friction systems, since it leads to large scattering. On this basis, [Sto18a, Sto18b] developed a test methodology that can be applied to both sinter and carbon systems. Their test consists of p-v variations at different load levels. In the context of her investigations on the running-in behavior, [Voe20] also optimizes the duration until a constant or linearly decreasing friction behavior is reached, by suitable test procedures. Here, she develops a methodology for all lining types and for load stages and applications in transient slip. The investigations show that the end of the running-in is a system variable that is strongly influenced by interactions.

Another possibility to streamline test programs while at the same time maintaining high significance lies in the use of statistical methods [Sie17, Sud11]. [Fri17] use statistical test planning to determine the tolerances of double-clutch components during the development process. [Str22], on the other hand, directly tries to determine the CoF as an input variable for thermal simulation in a time-optimal manner using ANOVA and regression models. The same method of a two-stage test plan is used by [Man02] to derive a deep understanding of the system with regard to the influencing variables of the clutch engagement process. [Bis21], on the other hand, uses the methods to derive explanatory models, with the help of which clutch slip can be used as an active damping element in the powertrain.

[Mäk05a] focuses his research on developing test methods for applications in limited slip differentials. For this purpose, a new test rig is being set up which considers the operating modes of a limited slip differential, and extensive measurements of friction, wear and temperature behavior are being carried out. He also confirms the large additive influence on the friction behavior of sintered friction linings. Furthermore, a large influence of the temperature and a small influence of the pressure on the friction behavior is shown.

[Abu06] also deals with the decisive influences on the performance limits in continuous slip operations. In the area of sintered friction linings, very pronounced friction coefficient and temperature fluctuations distributed over the active friction interface of the steel plates were already evident well before the performance limit was reached. He identified the cooling oil volume flow and the level of the base speed (speed of the grooved plate) as having a major influence on the level of friction power to be endured.

[Kat19] show that the manufacturing process of the lining on the friction plates can significantly influence friction behavior. Their results suggest that the E-modulus of the lining is correlated with dynamic friction behavior.

Other influences are in the surface properties of the friction partners. [Nym06, Zou13] show correlations between friction and surface properties, but [Zou13] restrict that this is particularly applicable to dry friction pairings.

2.4 Conclusion of the Literature Review

Thermal behavior of wet clutches is a well-established topic in the engineering research society. Therefore, new findings are not about the one new big thing, but are working incrementally towards small improvements in better understanding of the already known things.

The thermal behavior of clutches represents a central core in the field of research on wet multi-plate clutches, as it decisively defines the service life and functionality of clutches. The thermal behavior is therefore of utmost relevance for both research and users.

The simulation of the thermal behavior of wet clutches based on the basic hydrodynamic and thermal equations involves a variety of modeling approaches. With the help of the calculations in existing research work, important influencing variables such as the lubrication situation, loading, materials, oil and operating conditions can be shown and investigated.

Furthermore, there is still a strong focus on experimental investigations to generate new knowledge and to validate simulation results in this area.

The analysis of the existing literature shows that the potentials of modern engineering tools have not yet been fully transferred to clutches - in particular, the path towards virtual product development and thus the strengthening of the field of thermal simulation can still be extended. Potentials are particularly evident in the areas of friction behavior and input variables for thermal simulations, which have so far been investigated mainly experimentally.

According to the current state of research, friction behavior for application-oriented friction systems will continue to be determined experimentally, since the physical explanation models are not yet transferable to sufficiently complex systems. However, there is the possibility of specifically considering non-physical explanatory models for applications and research in this area. With the help of big data analytics, artificial intelligence (AI), and other statistical explanatory models, great added value can be created, and the number of new experimental studies required can be significantly reduced. The literature research already shows first promising approaches which, however, also point out the still existing need for further research.

In the area of thermal calculation, there are already many good and established alternatives from the field of simulation. However, it is important here to reduce the dependence on input variables from complex tests. Since the friction behavior, as explained in the previous paragraph, is still excluded, the focus should be placed on the area of oil modeling. The oil models used nowadays still need a lot of empirical data that is supported by measurements. There is potential here, for example, concerning oil distribution and oil delivery capacity of clutches. According to the results of the literature research, these can already be determined by calculation. In the application, the focus should also be on the advantages of targeted best- and worst-case calculations that can be carried out regarding, for example, manufacturing tolerances. The effects of wear on the oil carrying capacity of the clutch during operation are also easier to implement in an existing simulation model than would be possible in a real test setup.

Another important aspect is the determination of CHT coefficients. This can be seen as one of the more challenging next steps towards a more purely virtual product development. Here, the literature research shows a large spread of semi-analytical and purely empirical approaches in which it is also openly admitted that the actual physical interpretability of the quantity is softened more in the direction of a calibration factor for the respective system. Other authors show that a purely computer-aided determination is already possible today. These models are more complex implementations, but the expected know-how gain is probably worth this step. There is still the potential to generate an extended physical understanding of the influencing variables for the optimization of the cooling behavior with the help of grooving. Thereby, many small-scale effects can be used and interpreted compared to previous experimental setups.

Users and researchers from the field of industrial clutches can benefit from these approaches. On the one hand, the experimental conditions are particularly challenging, while on the other hand, most publications in the field of highly innovative simulations can rather be assigned to the automotive sector. There is thus a research gap around development, applicability and transferability of state-of-the-art calculations and simulation approaches for the thermal behavior of wet multi-plate clutches in industrial applications.

3 Research Gap, Objectives and Solution Approach

3.1 Research Gap and Objectives

The thermal behavior of clutches from industrial applications has not been sufficiently studied to date. The focus of many published scientific papers, both in the experimental and theoretical context, is on automotive applications.

An important feature of the tribological system of an industrial clutch in the sense of this thesis is the implementation of a pressurized oil supply. It is to be expected that this will influence both the thermal behavior and the frictional behavior of the clutch. Questions that have not yet been answered in this context include the extent to which pressurized oil supply affects the oil distribution within the clutch or, functionally, the transmissible torque. Therefore, fundamental questions relating to the existing oil and pressure distribution in the clutch are still open when influencing variables such as the bore pattern of the oil supply bores in the inner carrier or the operating conditions are varied.

The investigation of the oil distribution offers the possibility to analyze how evenly the oil distribution takes place over all friction interfaces of a clutch system. Furthermore, the dynamics of the filling process is relevant and investigation results on this have so far mostly been published for clutches from non-industrial applications.

The usually low quantities produced in conjunction with the infrastructural challenges due to the clutch dimensions (size, power) make extensive experimental investigations of the thermal behavior and friction behavior in clutches from industrial applications difficult. With the help of simulative calculations for oil distribution as well as the use of thermal clutch models, these operational limitations can be overcome. Nevertheless, there is a need for research in the context of industrial clutches since the specifics of industrial clutches are not represented at all or only inadequately in existing models. There are open questions regarding the transferability of former thermal models to clutches from applications in the industrial environment. It is unclear whether the large thermal masses of the plates and carriers as well as the heat transfers between these components are adequately captured. Furthermore, an adapted modeling of the lubrication situation for industrial clutches must be examined. The provision of real-time capable digital twins of the thermal behavior of wet clutches has also been published so far mainly in the context of automotive applications.

The identified research gaps show an opportunity to expand the existing knowledge base about the thermal behavior of industrial clutches with pressurized oil supply. The objective of the thesis is to reduce the existing gaps through a combination of experimental and theoretical work. For this purpose, reliable simulation methods for the calculation and prediction of the thermal behavior as well as for the simulation of the oil and pressure distribution are developed within the theoretical works. The calculation and prediction of the thermal behavior shall be implemented as a real time temperature model in terms of a digital twin of the clutch. The digtial twin can be used in offline mode for extensive variation calculations, for example in the context of pre-development, and for parameterization for online and predictive operation. In online mode (on controller hardware), the temperature of the clutch components can be calculated live using fed-in sensor signals and predictions can be made for future shifting or while maintaining the current operating state.

With CFD simulations, the steady-state oil and pressure distribution in the clutch per friction interface is investigated. The pressure distribution can then be used, for example, to examine the interactions between the axial force imposed by the piston and the hydrodynamic pressure due to pressurized oil supply. Furthermore, the potential of calculating CHT coefficients by means of CFD simulations is analyzed. The overall objective of the theoretical work is thus to capture the thermal behavior as fully as possible in the form of a real-time capable temperature model (digital twin). Furthermore, the CFD simulations serve to improve the understanding of the system as well as the possible generation of input variables, which otherwise must be determined in a time-consuming manner by means of experimental investigations.

Additionally, experimental investigations are carried out to further increase the understanding of the system and to validate and fully parameterize the theoretical models. Friction behavior and heat transfer coefficients are recorded as input variables for the thermal models. Furthermore, temperature measurements on the component test rig serve to identify relevant effects on the thermal behavior and are used to validate the real-time temperature model and the CFD simulations. With the help of high-speed recordings with 3D printed transparent components, the CFD modeling is additionally validated and results are generated for system understanding with regard to the dynamic filling behavior and the oil distribution in the clutch system.

The objective of the work is thus to combine theoretical and experimental approaches to investigate the thermal behavior of wet industrial clutches in a holistic manner. The main objective is to show the relevant influencing factors on the thermal behavior of industrial clutches with pressurized oil feeding, which are identified by applying the different methods.

3.2 Solution Approach

Chapters 1-3 demonstrate the importance of wet clutches in industrial applications and the need for further research on thermal behavior of clutches from industrial applications. The objectives of the thesis are obtained from the identified gaps in the state of research. Furthermore, these objectives define a suited solution approach.

The applied investigation methods, their interconnections as well as their connections to the identification of influencing factors in the results are visualized in Figure 9.

The approaches presented for investigating the thermal behavior in chapters 5 - 6 of wet multi-plate clutches vary in their degree of innovation. Both the CFD simulations for determining oil and pressure distribution and the associated high-speed camera recordings for visualizing oil flow can be classified as very innovative and are oriented to the latest state of research. In contrast, the developed real-time calculation model and the experimental investigations on temperature and friction behavior enhance and improve established procedures.

The combination and application of all the methods presented enables a holistic view on the thermal behavior of clutches in industrial applications as presented in chapter 7. The strengths and weaknesses of the various investigation methods are cleverly combined to enable the investigation of numerous details.

The interlocking of the various aspects is particularly evident around simulative modeling: Studies on oil distribution and related issues are investigated using computationally intensive 3D models. The thermal behavior of the clutch components, on the other hand, is transferred to a transient 1D model since sufficient quality of results can be achieved with this at very high computing speeds. In addition to answering the research questions, a reduction in the computational and modeling effort is also of great importance for the transferability of the approaches into industrial practice.

Experiments are used in a targeted manner and play a key role in validating the developed computational models. Furthermore, friction behavior is determined as the only input variable that needs to be obtained by measurements at relevant operating points.

Compared to the current state of research where most of the work focuses on one question and the associated modeling, the combination of various methods represents an extension of the existing knowledge. In particular, the objective of developing an efficient and fast calculation method for practical applications, which at the same time considers findings from extensive CFD simulations and validation by experiments, is a unique feature of this work.

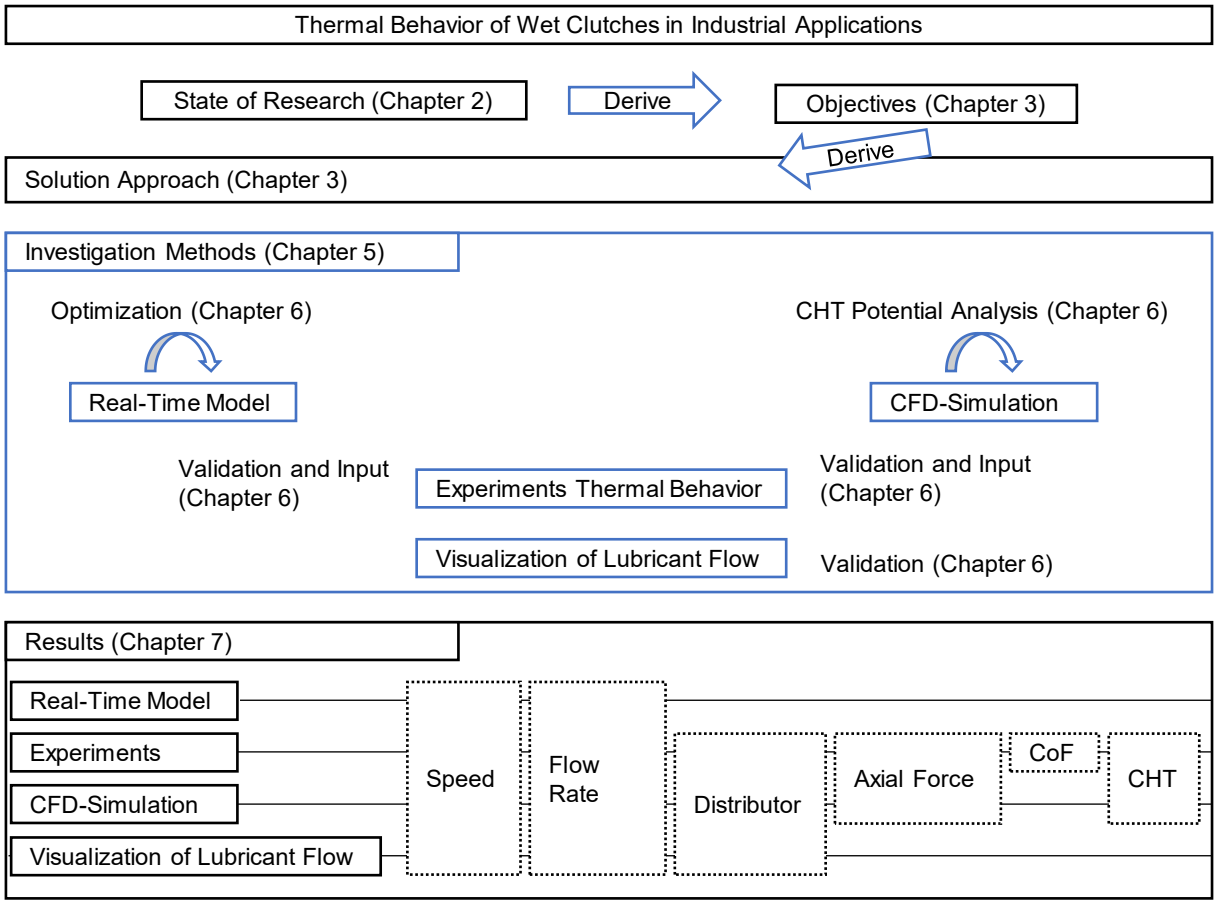

Figure 9: Visualization of the applied investigation methods, interconnections among the methods and influencing factor results

4 Parts and Oil, Experimental and Numerical Tools

4.1 Parts and Oil

The numerical and experimental studies were performed on two differently sized industrial clutches. Excerpts of the description presented below have been published by Groetsch, Motzet, Voelkel, Pflaum and Stahl [Gro22]. The clutches are identified based on their mean diameter d_m = 122/148 mm as clutch D123 and D148. The steel (outer) and friction (inner) plates are from serial production. Figure 10 pictures the plates before the experimental studies (new parts). Both clutches have a waffle groove pattern on the sinter friction linings of the inner plates. The steel plates are different in arrangement and design of the connecting gears to the outer carrier and surface appearance.

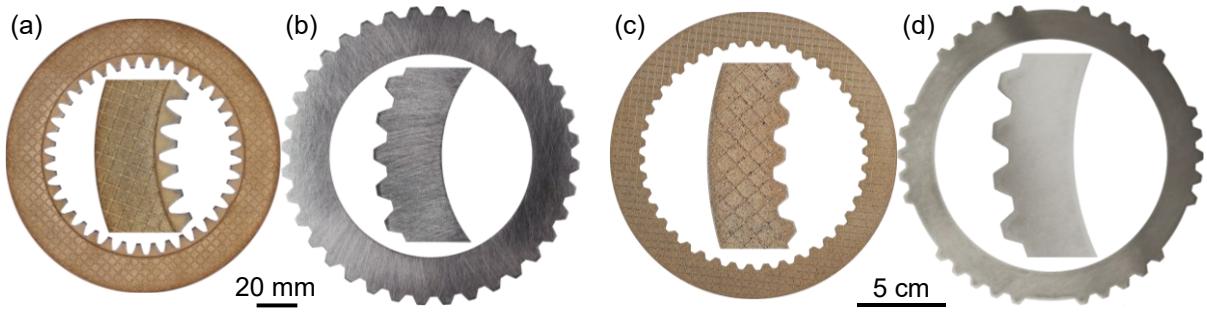

Figure 10: (a) Friction plate (fp) and (b) steel plate (sp) of clutch D123, (c) friction plate and (d) steel plate of clutch D148

More details about the geometric parameters of the clutch components are summarized in Table 1. The volume of the gears is added/subtracted to the diameters at the gear side, such that the volume of the annulus represents the volume of the corresponding part. The technical data of the oil, plate and friction materials are listed in Table 2. Density and viscosity properties of the oil for temperatures not listed in the table are calculated acc. to DIN-51757 [DIN94] and DIN-51563 [DIN11, Gro22].

Table 1: Summary of geometric parameters and materials of clutches D148/D123

identifier	D148			D123		
part	sp	fl	cp	sp	fl	cp
inner diameter /mm	132	127.4	127.4	102	104	95.3
outer diameter /mm	168.4	164	164	147	141	141
thickness /mm	1.5	0.4	1.0	3	0.68	2.3
material	C60	MS-A	C60	C60	MS-B	C60

Table 2: Technical data of oil, plate and friction lining materials

material	C60[a]	MS-A[b]	MS-B[b]	L-301[b]	ATF-B
thermal conductivity at 20 °C / W/mK	46,6	15	50	0.130	
density at 15 °C / kg/m³	7,850	6,800	6,500	891	760
specific thermal capacity at 20 °C / J/kgK	460	460	400	1,860	2,540
kinematic viscosity at 40°C / mm²/s				100	28
kinematic viscosity at 100°C / mm²/s				11.4	12.6
[a]) [Hts21] [b]) manufacturer's data					

4.2 Test Rig KLP-260

The experimental investigations are carried out on the component test rigs KLP-260 and LK-4. The description of KLP-260 presented below has been published by Stockinger, Groetsch, Reiner, Voelkel,

Pflaum and Stahl [Sto21]. The test rig operates in brake mode, where the outer carrier is fixed and the inner carrier rotates as pictured in Figure 11.

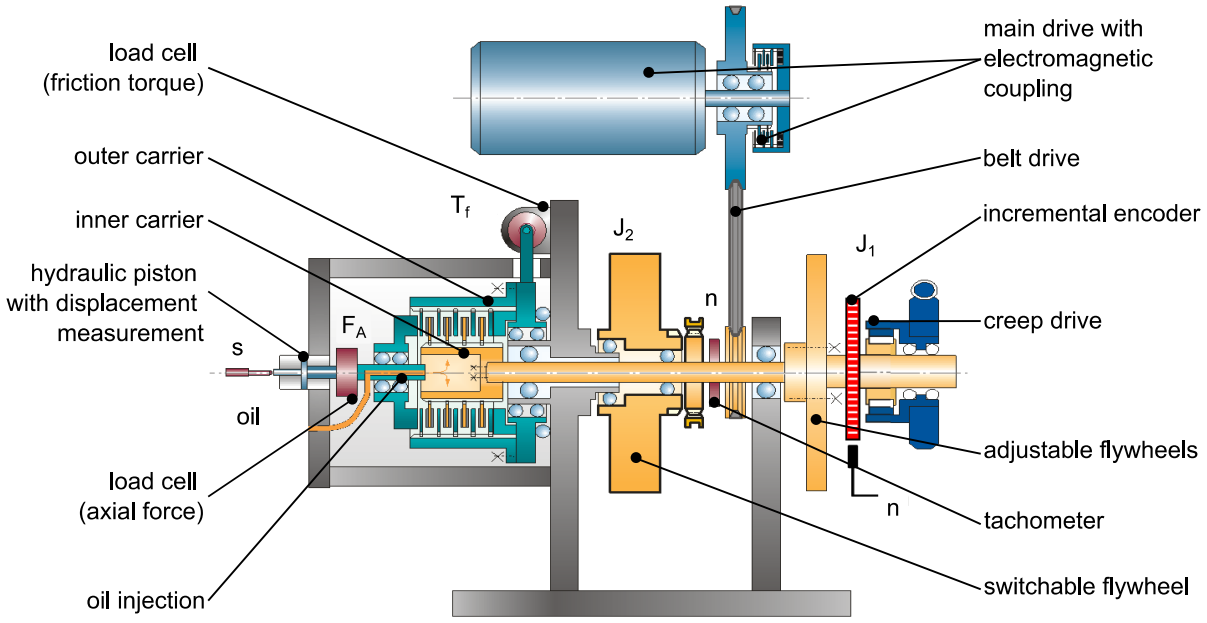

Figure 11: Test rig KLP-260 – schematic sketch from [Mei15]

The test rig enables the mounting of a complete clutch package of a gearbox with the corresponding carriers. The inner plates are placed on the inner carrier, which is installed on the inner shaft and connected to the fly wheels (J_1, J_2). The friction work of the clutch can be adjusted through variable installations of fly wheels J_1 as well as by engagement of the basic inertia J_2.

Pressure is applied by a force controlled hydraulic piston. The friction torque is measured at the outer carrier. Cooling oil can be supplied centrally into the inner carrier (non-pressurized, pressurized, volume flow controlled), externally from the top of the housing or by oil sump. The oil flow rate and the thermostat-controlled feeding temperature can be adjusted in a wide range. For brake engagement tests, the main shaft with the inner carrier and the fly wheels are accelerated by the speed-controlled main drive to a defined differential speed Δn. During the engagement process, the main drive and inner shaft are decoupled by means of electromagnetic coupling. In creeping conditions and in continuous slip mode, a defined axial force is applied on the clutch plates. The creep or main drive then accelerates the clutch to a defined slip speed. The rotational speed in low speed creep is measured with high resolution by an incremental encoder [Mei15, Sto21]. Table 3 summarizes the technical data of the test rig.

Table 3: Technical data of test rig KLP-260 from [Sto21]

variable small fly wheels	J_1 = 0.12 … 0.75 kgm²
basic inertia	J_2 = 1.0 kgm²
plate diameters	d = 75 … 260 mm
max. torque	$T_{f,max}$ = 2,000 Nm
differential speed	Δn = 0 … 7,000 rpm
slip speed	Δn = 0…140 rpm
torque in slip mode	$T_{f,slip,max}$ = 2,000 Nm
max. axial force	F_{ax} = 40 kN
feeding oil temperature	ϑ_{oil} = 30 … 150 °C
max. feeding oil flow rate	$\dot{v}_{Oil}$= 7 l/min

Table 4 summarizes the measurement accuracy of the KLP-260 test rig from [Gro22]. The table includes the measurement accuracy table of the test rig published in [Sto21] by analyzing the uncertainty of the installed oil pressure sensor, taking into account the findings of Baumgartner [Bau20]. She applied the rules of the Guide to the Expression of Uncertainty in Measurement (GUM) [Joi08] and DIN EN ISO 14253-2 [DIN18] to the KLP-260 test rig. Furthermore, it shows the offset of the thermocouples at 0 °C from the norm curve by calibration of the test rig setup with distilled ice water as published in [Jan21].

Table 4: Overview of measurement accuracy of the KLP-260 test rig (confidence level 95 %) from [Gro22]

measured / calculated variable	uncertainty
axial force	+/- 1.3%
torque	+/- 0.4 %
CoF	+/- 1.3 %
speed (main engine)	+/- 0.2%
speed (creep engine)	+/- 0.9%
thermocouple type K class 1	+/- 1.8 K (DIN) +/- 0.3 K (estimate from calibration)
feeding oil pressure	+/- 0.1 bar

4.3 Test Rig LK-4

LK-4 is a clutch test rig focusing on the measurement of the drag torque of multi-plate clutches in the open stage. The description presented below has been published by Groetsch, Niedenthal, Voelkel, Pflaum and Stahl [Gro20]. Figure 12 shows that a complete clutch package (2) consisting of steel and friction plates is mounted in the test rig. The outer carrier (1) is engaged with the outer hollow shaft (8). The inner carrier (3) is mounted on a torque-sensing (resistive wire strains) element (5), which is applied to the inner full shaft (7). This allows for the measurement of drag torque directly at the inner carrier without the influence of sealing or bearing friction.

The test rig can vary the operating conditions of the clutch in a wide range. It is possible to change the rotational speed of the inner and outer carrier independently in both rotational directions, oil injection temperature, oil flow rate (4) and the height of total clearance (6) of the multi-plate clutch. Table 5 summarizes the range of possible operating conditions.

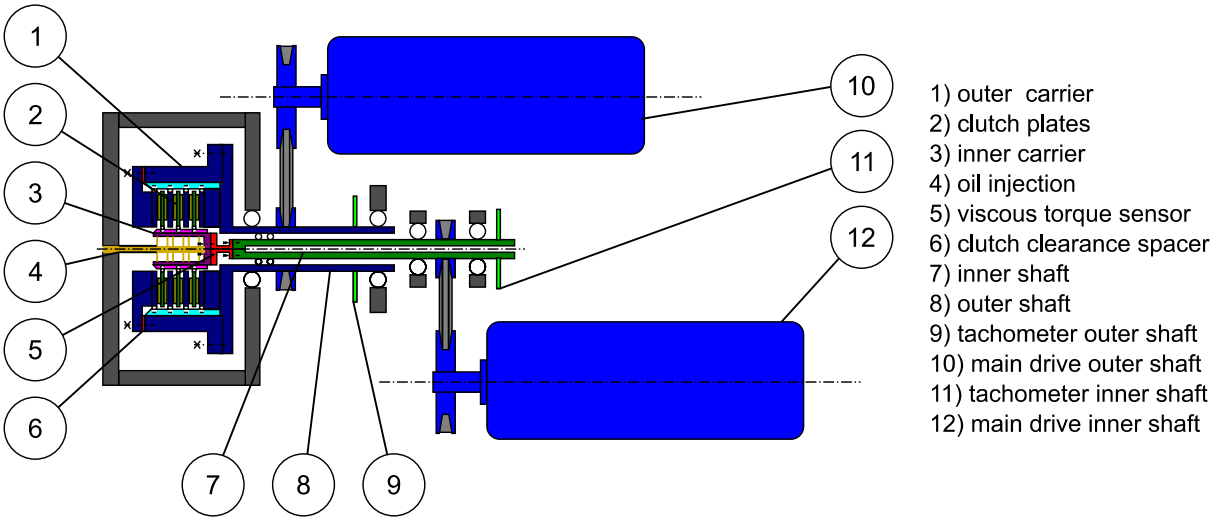

Figure 12: Schematic of wet multi-plate clutch test rig LK-4 from [Gro20]

Table 5: Operating conditions of test rig LK-4 from [Gro20]

speed range outer shaft	n_{full}	+/- 9,000 rpm
speed range inner shaft	n_{hollow}	+/- 9,000 rpm
measuring range torque	T_d	+/- 50 Nm
feeding oil temperature	ϑ_{oil}	30 … 120 °C
feeding oil flow rate	v_{oil}	0 … 20 l/min

4.1 High Speed Camera

Multi-plate clutches typically operate at high speeds. This results in high sliding velocities, which make it almost impossible to assess the behavior of the cooling oil by watching the oil flow in real time. The rapid changes in flow conditions can be assessed by using a high-speed camera. The Photron Fastcam Mini AX [Pho22b] uses a 1-megapixel CMOS sensor that offers a resolution of 1,024 x 1,024 pixels. At full resolution, the maximum frame rate is 6,400 fps, but can be raised to 540,000 fps by gradually reducing the resolution. The camera is used with a Tamron lens [Tam22] with a focal length range of 28-75 mm. The lens is used for all exposures at its longest focal length of 75 mm to achieve the greatest distance to the subject and thus the least distortion. The sensor diagonal of 28.96 mm results in an angle of view of 21.86°. The closest focusing distance of 0.33 m enables detailed images to be taken with a reproduction scale of 1:4.4. Despite the sensor's high light sensitivity of ISO 16000 and the fast lens with a maximum open aperture of F/2.8, a powerful light source is required, since the high frame rate allows only short exposure times. For this purpose, the VD36 LED spotlight [Vis22] is used, which offers a maximum brightness of 36,000 lm at 360 W power. It is also a non-pulsed continuous light source, which allows images to be taken without flickering. The camera has an internal memory of 8 GB, which allows 5,457 images to be captured at full resolution. At different frame rates, for example, maximum recording times of 0.853 s (6,400 fps), 5.457 s (1,000 fps) or 43.656 s (125 fps) are possible. After recording, the data is transferred to the computer via an Ethernet interface, which is also used to control the camera.

(a) (b) (c)

Figure 13: Photron Fastcam Mini AX (a) [Pho22a], Tamron SP AF 28-75 mm F/2.8 XR (b) [Tam22] and Vision Devices VD36 (c) [Vis22] from [Sch22a]

4.2 Simulation Tools

The developed calculation methods of this thesis are based on theoretical studies with numerical models that enable the calculation of oil and pressure distributions and temperatures in the solid (plates and carriers) and fluid parts (oil) of the physical domain. The literature review showed that most research in this area is based on the use of commercial CFD software tools, since the development of own solvers is far beyond the scope of nearly all publications. Comparable to the field of TEHD calculations, the use of commercial software packages applied to thermo-fluid problems of wet clutches is necessary “(…) to make simulation techniques available to a broader audience and to focus research more on physical relationships than on numerical procedures.” translated from [Loh16]. Hence, for the model

developments and numerical studies, the commercial software programs SimericsMP+ and Matlab / Simulink are used, since prior publications showed that they can be used to efficiently calculate oil flow and temperatures in wet clutches (a.o [Gro19a, Gro21b, Gro22, Gro19b, Yas18]).

According to the SimericsMP+ manual [Sim20], SimericsMP+ is a multi-purpose (MP), finite-volume and pressure-based CFD solver. It solves the integral form of the governing equations for the mass and momentum conservation, and (when appropriate) for energy and other scalars such as turbulence and chemical species. This control-volume-based technique first divides the physical domain into discrete control volumes using a computational mesh. The meshing algorithm of the software automatically creates a hexahedron dominant mesh using the binary tree mesh algorithm. This algorithm provides high solution quality even at low mesh resolutions [Din11]. The governing equations for the physical domain are discretized over each control volume to construct algebraic equations for the dependent variables (e.g. speed/velocities, temperature, …). To obtain the solution, the pressure is extracted by solving the pressure-velocity correction equations, which are obtained by coupling the discretized continuity and momentum equations. These discretized governing equations are linearized and the linear equation system is solved.

SimericsMP+ features a unique and intuitive approach to simulate systems with moving, sliding, or rotating geometries [Sim22] and is therefore well-suited for applications with wet clutch systems.

MATLAB is widely used to analyze and design systems and products in science and engineering. MATLAB is a matrix-based language to express computational mathematics in a natural way, which enables, for example, the development of numerical calculation tools or graphical user interfaces. Built-in graphics enable visualization and analysis of complex data and simulation results. [Mat22a]

Simulink is a block diagram environment for multidomain simulation and model-based design. It supports system-level design, simulation, automatic code generation, and continuous test and verification of embedded systems. Therefore, Simulink-models can be integrated in existing gear box software environments. Simulink provides a graphical editor, customizable block libraries, and solvers for modeling and simulating dynamic systems. It is integrated with MATLAB, enabling incorporation of MATLAB algorithms into models and export simulation results to MATLAB for further analysis [Mat22b].

5 Investigation Methods for Thermal Behavior of Wet Clutches

In the following section, the developed and applied methods for investigating thermal behavior of wet industrial clutches are presented. The work is divided into theoretical work and experimental investigations. Within the theoretical work, a real-time model for thermal calculation and prediction is developed and a CFD simulation model is used to calculate oil distribution and pressure in a sealed clutch.

During the experimental investigations, important input variables such as the CoF and heat transfer coefficients are determined. Furthermore, the thermal behavior of clutches from serial production is investigated and used to validate the thermal calculations. In addition, high-speed camera recordings are presented on a test setup with transparent clutch components to validate the CFD simulations.

5.1 Preliminary Considerations and Requirements

The methods used to investigate thermal behavior of wet clutches should meet several requirements. The higher-level objective is to improve knowledge compared with the current state of research. In this context, topics from applications in the industrial environment are of particular interest, such as the special operating conditions (e.g. long continuous slip at high differential speed), the design of oil distributor patterns in the oil supply of industrial carriers and the influence of oil pressure on the thermal behavior in sealed industrial clutches.

This work focuses on high computational speed combined with high robustness and quality of the results. Furthermore, the extension of the statements to 3D is aimed with respect to flow variables. Another important target is the reduction of the required experimental effort - I tried to avoid experimental investigations as far as possible and to use them only for tasks that are not yet simulatively realizable.

For the developed real-time temperature model, a maximum deviation of +/- 10K of calculated temperatures compared to the measurement is acceptable. Typically, the deviations should be in the range of +/- 5K. The calculation should be very fast, so that online operation on controller hardware is possible or extensive variation calculations can be carried out in the shortest possible time in offline operation. Furthermore, the model should be able to be operated directly with sensor signals. The transferability to different clutch systems is considered by a parametric-physical based development approach. Furthermore, a possibility for the prediction of future thermal developments shall be created, especially for the operation on controller hardware, to enable a significant improvement of operational safety.

CFD simulations are used specifically to expand knowledge in the field of oil distribution analyses. The focus is on the calculated pressure distribution in the closed clutch and its influence on the effective surface pressure of the clutch. Furthermore, the influence of different oil distributor patterns in the inner carrier on oil distribution will also be investigated. With the help of the CFD simulations, model ideas can be derived to take account of the flow effects in the thermal simulation. Furthermore, design guidelines can be adapted based on the results.

Experimental investigations are to be implemented at low cost. On the one hand, the number of required experiments should be low, and on the other hand, an easy-to-use experimental method should be used. The method used should nevertheless ensure reproducible results. Tests will be carried out to determine the temperature and friction behavior under practical operating conditions. Furthermore, it is attempted to reduce the future experimental effort by deriving suitable parameterizations for CoF (map, model).

The recordings using a high-speed camera are intended to provide a practical method for validating flow conditions in the clutch. Attention is paid to a simple implementation of the procedure using existing test rigs and measurement technology. In addition to providing insights into the flow conditions, these experiments are intended to verify the validity of assumptions made when modeling oil flows in a sealed industrial clutch under varying operating conditions.

5.2 Real-Time Temperature Calculation and Temperature Prediction

Under the guidance of the author, the development of the real-time temperature calculation and temperature prediction approach was supported by the student research projects of Butzhammer [But18] and Rauscher [Rau19]. The real-time temperature model enables calculation of the thermal behavior of a wet multi-plate clutch based on input signals provided by sensors. The minimum input requirements for the model are speed (input and output speed) and axial force in addition to data on geometry and heat capacities. Based on these inputs, the energy input and cooling conditions are calculated. An implemented logic, which is identified from the input signals, decides on the current operating phase of the clutch. The identification of the operating phases is done according to the scheme shown in Table 6.

Table 6: Identification of operating phase as a function of input signals

operating phase	axial force signal	speed signal
sliding phase	$F_{ax} > 0$	$\lvert\Delta n\rvert > 0$
closed cooling phase	$F_{ax} > 0$	$\lvert\Delta n\rvert \approx 0$
open cooling Phase	$F_{ax} \approx 0$	any

By providing optional input variables, the demands on parameterization of the model can be reduced while improving calculation quality. In the first column of Table 7 all input signals of the real-time model are summarized. The second and third columns indicate which sensors and possibly required additional parameters can be used to provide the required input variables. All input values must be specified during parameterization either as a constant value or in the form of a sensor signal. The units may have to be scaled prior to performing the calculations by conversion factors.

Table 7: Input signals for the real-time model and possibilities in which these can be provided

input signal real-time model	possible inputs	additional requirements
drive speed / rpm	signal drive speed	
	constant value	
output speed / rpm	signal output speed	
	constant value	
axial force / N	signal axial force	
	signal hydraulic pressure	piston area
	signal ramp angle	map force to ramp angle
friction torque / Nm	signal friction torque	
	constant value	
	signal axial force	CoF map and geometry
feeding oil flow rate / mm³/mm²s	signal oil flow rate	friction surface
	signal oil mass flow rate	density and friction area
	constant value	friction surface
oil injection temperature / °C	signal oil injection temperature	
	constant value	
temperature at beginning / °C	signal ambient temperature	
	signal steel plate temperature	
	signal oil injection temperature	
	constant value	

The calculations of the real-time model can be applied to any load scenarios (e.g. stationary / transient slip, load cycles, clutch and brake operation). The oil calculations consider internal lubrication via the inner carrier with or without forced lubrication.

All calculated values can optionally be defined as model outputs with a user defined sample rate. The available output signals are grouped thematically by:

- output temperatures
- output load spectrum
- output oil flow
- output power

All output signals are summarized in Table 8.

Table 8: Available output signals of real-time model

group	signalname
output Temperatures	steel plate temperature node 1 / °C
	steel plate temperature node 2 / °C
	friction lining temperature node 1 / °C
	maximum friction lining temperature / °C
	friction lining temperature node 2 / °C
	friction plate temperature / °C
	inner carrier temperature / °C
	outer carrier temperature / °C
	oil outlet temperature / °C
output load spectrum	operating phase / -
	calculated friction torque / Nm
	current CoF / -
	input signal friction torque / Nm
	input signal differential speed / rpm
	input signal drive speed / rpm
	input signal output speed / rpm
	input signal axial force / N
output oil flow	current oil flow rate / mm³/mm²s
	current possible oil flow rate / mm³/mm²s
output power	current power input steel plate / W
	current power input friction / W
	current power input oil cooling / W
	current power input friction plate / W
	current power input inner carrier / W
	current power input outer carrier / W
	current overall power balance / W

5.2.1 Mathematical Model

The model description presented below has been published by Groetsch, Voelkel, Pflaum and Stahl [Gro21b]. The parametric model for calculating clutch temperatures uses input signals provided by sensors. The geometry of the clutch is transferred into a thermal network [Ste62]. The analogy between electrical and thermal current fields is used for the calculations.

Figure 14 shows a friction pairing of a wet multi-plate clutch including the radial connecting components (outer carrier (oc) and inner carrier (ic)). The clutch consists of alternately arranged outer plates (here: steel plates (sp)) and inner plates (here: friction plates (fp)). A friction plate typically consists of a friction lining carrier plate with friction lining (fl) on both sides. The illustration corresponds to the spatial system boundaries used for the temperature calculation model according to equation (2.13). The calculation domain considers the typically thermal, most severely loaded inner friction pairing (axial middle of the clutch package). Owing to the thermal symmetry, the calculation domain can be reduced again to the consideration of half the plate width.

The right side of Figure 14 shows the thermal network used for the calculations, representing a virtual temperature sensor of all clutch components. The application of the real-time model on a clutch controller in real-time also serves as a digital twin of the thermal behavior of these components. A thermal network consists in the transient case of areas with concentrated resistances R and capacitances C. The calculation area, which is composed of different thermal masses, is therefore discretized in nodes. A node is modeled as thermal capacity. In the thermal-electrical analogy, the temperature of the node corresponds to the voltage at the capacitor. Each node has a temperature T. If there is a temperature difference ΔT between two nodes, this results in a compensating heat flow between them. The thermal resistances correspond to the thermal resistances between the thermal masses. These are either convective resistances R_{conv} or thermal resistances due to heat conduction R_{hc}. The reference potential of the network is the oil injection temperature T_{oil} or the ambient temperature $T_{ambient}$ at the carriers.

The energy input $\dot{Q}_{friction}$, the heat conduction between the steel plate $\dot{Q}_{sp}$ and the friction lining $\dot{Q}_{fl}$ as well as the heat dissipation due to the cooling oil $\dot{Q}_{cool,oil}$ at the friction interface are considered. Energy input and output are implemented in the source/sink terms ($\dot{Q}_{friction\ /\ cool,oil}$).

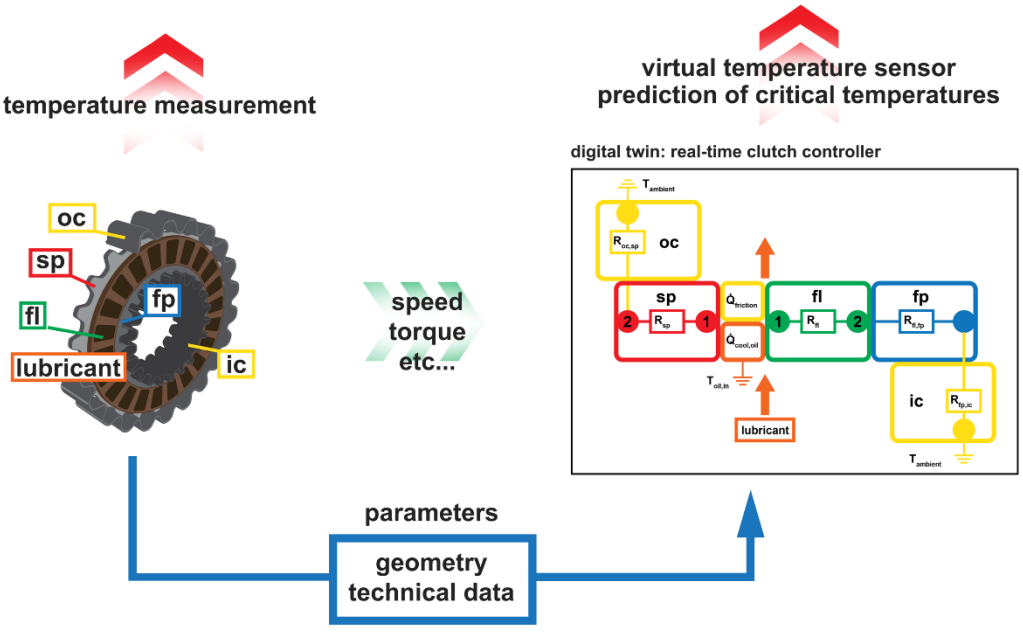

Figure 14: Visualization of the real-time temperature model from [Gro21b]

The development and implementation of the model is based on the derivation and application of the following formulas that can be derived from the fundamental governing equations as described in

Section 2.2. The thermal resistances in Figure 14 are calculated according to equation (5.1) for convective heat transfer and according to equation (5.2) for thermal resistances due to heat conduction [Pol09].

$$R_{conv} = \frac{1}{\alpha \cdot A} \tag{5.1}$$

$$R_{hc} = \frac{s}{\lambda \cdot A} \tag{5.2}$$

According to equation (5.3), the thermal capacities in the thermal network correspond to the product of mass and specific heat capacity [Ste62]. The input parameters for the thermal calculation thus result from the geometry of the calculation domain and the material values of the corresponding material.

$$C_{therm} = \rho \cdot V \cdot c \tag{5.3}$$

The energy input on the friction surface corresponds to the friction work performed per unit of time. It can be assumed that the friction work is completely dissipated as heat [Gei37]. In the real-time temperature model, the friction power is modeled according to equation (5.4).

$$\dot{Q}_f = \Delta\omega \cdot T_f = 2\pi \cdot \Delta n \cdot T_f = 2\pi \cdot \Delta n \cdot \mu\,(p, v, T) \cdot F_{ax} \cdot r_m \tag{5.4}$$

The oil cooling (based on the findings of Hämmerl [Häm95]) is taken into account during the sliding phase by balancing the friction power with the effective power according to equation (5.5)

$$\dot{Q}_{eff} = \dot{Q}_{friction} + \dot{Q}_{cool,oil} \tag{5.5}$$

The friction partners are in contact with each other. This is a coupling condition. For this purpose, the effective power supplied according to equation (5.6) is split into two components in the further calculations. The components are each supplied to the steel plate (sp) or the friction plate (fp).

$$\dot{Q}_{eff} = \dot{Q}_{sp} + \dot{Q}_{fp} \tag{5.6}$$

Further details on the mathematical model can be found in [Gro21c].

5.2.2 Temperature Prediction

The temperature prediction is implemented using a map-based approach to reduce the calculation effort. Figure 15 shows the steps for the commissioning of the prediction module.

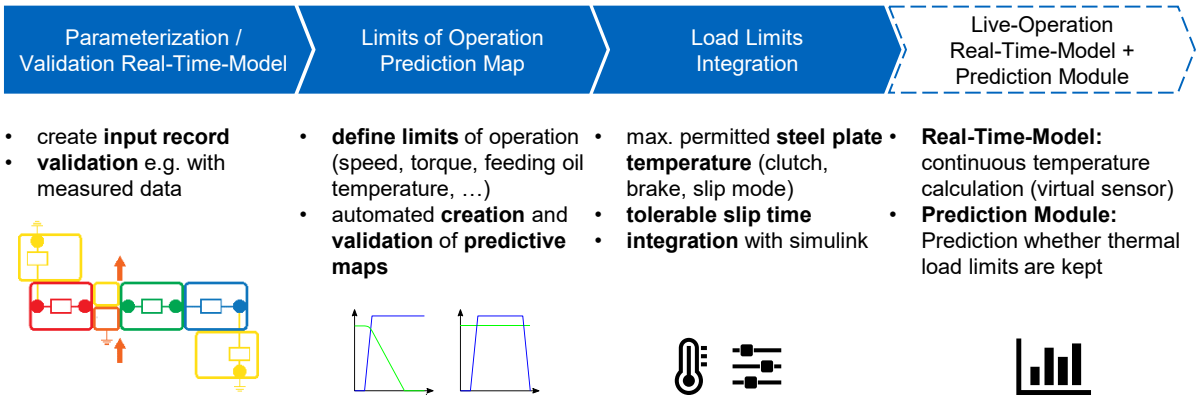

Figure 15: Schematic diagram of how temperature prediction works from [Gro21b]

The first step is parameterization of the real-time model for the desired clutch. The calculation model should also be validated, for example by comparing it with existing measurement data. Next, the operating limits must be defined as min./max. and constant values of the clutch. The specification of the operating limits varies depending on the application, as can be seen from Table 9.

After the operating limits have been defined, a map for the prediction module can be generated and validated automatically. The resolution of the map can be influenced by specifying the number of interpolation points between the specified operating limits. To create the map, simulations are performed

for all parameter combinations using the validated real-time model of the clutch application. Subsequently, the temperature rise in the steel plate (typical temperature at node 2) (brake operation, clutch operation) or the maximum tolerable slip time (continuous slip) is stored for each operating point. The maximum tolerable slip time is defined as the time until the maximum steel plate temperature is exceeded under the current operating conditions or a time threshold is reached. Automated validation is carried out by a subsequent comparison of the central points that are not part of the characteristic map with the result of a simulation.

The prediction module can then be made operational by defining the load limits for the maximum permissible steel plate temperature or tolerable slip time and by integrating the previously created map into the Simulink model. In live operation, the thermal behavior of the clutch is provided in the form of a virtual temperature sensor by continuous temperature calculation of the real-time model. By interpolating from the prediction map under the current operating conditions and comparison with the defined load limits, it can be predicted whether the permissible load limits will be kept in the subsequent shifting operation.

Table 9: Required specifications for the operating limits of the prediction module from [Gro21b]

name of limited value	braking operation	clutch operation	continuous slip
input speed / rpm	X	X	X
output speed / rpm	-	X	X
friction torque / Nm	X	X	X
oil volume flow / mm³/mm²s	X	X	X
oil injection temperature / °C	X	X	X
start temperature calculation / °C	X	X	X
moment of inertia drive / kgm²	X*	X*	-
moment of inertia output / kgm²	X*	X*	-
drive torque / Nm	X*	X*	-
output torque /Nm	X*	X*	-
max. steel plate temperature / °C	-	-	X*
max. simulated time / s	-	-	X*
* constant values			

5.2.3 Characterization of Transient Plate and Oil Temperature Courses

The real-time model calculates all node temperatures and makes them available as output variables for evaluation. According to Figure 14, there are thus two node temperatures of the steel plate and the friction lining, and one node temperature for the lining carrier plate and the inner and outer carrier. The model also calculates the supported oil flow rate per time step and the oil outlet temperature.

For comparison with measurements from the test rig, the inner node temperature of the steel plate is suitable, since this represents the temperature in the center of the plate. Another possibility is the volume-averaged value from both nodes as the mass temperature.

For the evaluation of thermal behavior, the characteristic values ΔT (temperature rise) and T_{max} (maximum temperature) are evaluated among others. In slip operation, ΔT corresponds to the difference between the minimum and maximum temperatures during a slip cycle, i.e. typically the temperature difference between the initial temperature (before the first slip phase) and the maximum temperature after the last slip phase. For shifting cycles, ΔT corresponds to the difference between the maximum temperature in the friction phase and the temperature immediately before the start of the shifting cycle. T_{max} denotes the maximum temperature occurring in a defined interval.

5.3 CFD Model for Calculation of Oil Distribution and Reduction of Axial Force

The CFD model for the calculation of the oil and pressure distribution is developed in the SimericsMP+ commercial software v5.0.15.

5.3.1 Calculation Domains and Meshes

The description presented below has been published by Groetsch, Motzet, Voelkel, Pflaum and Stahl [Gro22]. Furthermore under the guidance of the author, the CFD model development was supported by the student research project of Motzet [Mot21]. The calculation domain of the CFD approach represents the clutch setup in the test rig as shown in Figure 16. The outer carrier is fixed to the housing of the test rig. The inner carrier is engaged with the main drive via the test rig shaft. The axial force is applied on the steel plates by a force controlled hydraulic piston. The oil is supplied to the inner carrier region by the oil injection nozzle. The oil is then distributed to the clutch package through the radial holes in the inner carrier. After passing the waffle grooves (in the plate-area), the oil leaves the clutch package axial and radial at the outer carrier. Two X-rings and a shaft seal ensure that the fluid passes the grooves during static and dynamic operations. Therefore, with sufficient oil supply a single-phase oil flow is expected.

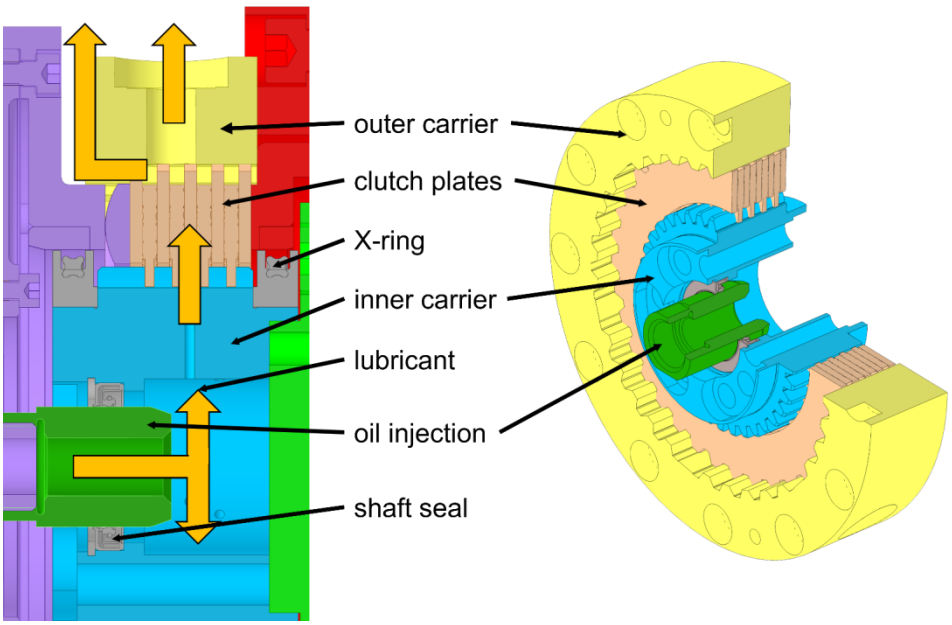

Figure 16: Test rig setup at KLP-260 of multi-plate clutch from [Gro22]

Figure 17 shows the boundaries of the calculation domain for the static case with eight friction interfaces and the naming of the mesh regions. Four regions can be distinguished. The inlet-area contains fluid regions of the oil supply nozzle and the inner carrier as far as the end of the radial holes. The inner carrier-area is made up of the splines between the inner carrier and the clutch plates. Furthermore, the plate-area represents the grooves of the friction plates. The outer carrier-area is derived from the splines between the clutch plates and the outer carrier.

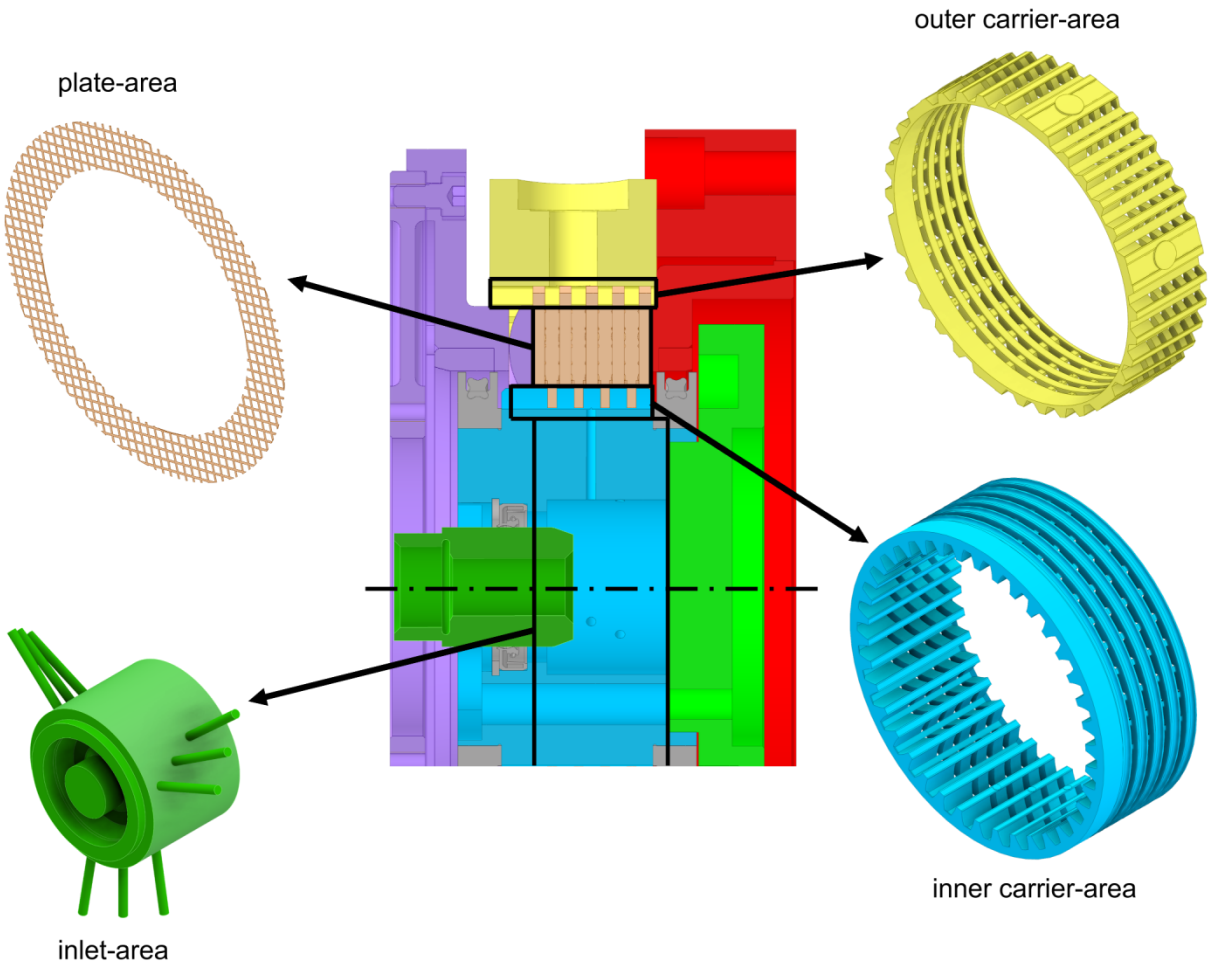

Figure 17: Regions of calculation domain (boundaries marked with black lines) from [Gro22]

There are two variants of the pattern of the oil supply through the inner carrier. The pattern of oil supply holes in the inner carrier can be varied using grub screws. Figure 18 visualizes the difference between the two variants. The axial spacing of the holes for both variants ensures oil supply at each friction interface. The circumferential spacing varies, since variant I supplies fresh oil at every axial position within a third of a turn, and variant II within one turn of the inner carrier.

The computational mesh is created by using the implemented body-fitted binary three-mesh algorithm, which produces a highly efficient hexagonal dominated mesh (a.o. [Din11]). A preliminary mesh study shows that a mesh size with a relative maximum cell size of 0.005 is an optimal trade-off in terms of computational effort and quality of results. Therefore, three different meshes with different cells were used, as summarized in Table 10.

The so called rough, standard, and fine meshes differ in cell size and total number of cells. The meshes have three refinement zones (RZ I – III) to resolve oil shear and large velocity gradients at cross-sectional transitions. The refinement zones are highlighted in Figure 19.

Table 10: Cell properties in preliminary mesh study from [Gro22]

mesh type	relative maximum cell size	no. of cells
rough	0.01 (0.002)*	10 Mio.
standard	0.005 (0.002)*	12 Mio
fine	0.002 (0.001)*	20 Mio
*refinement zones		

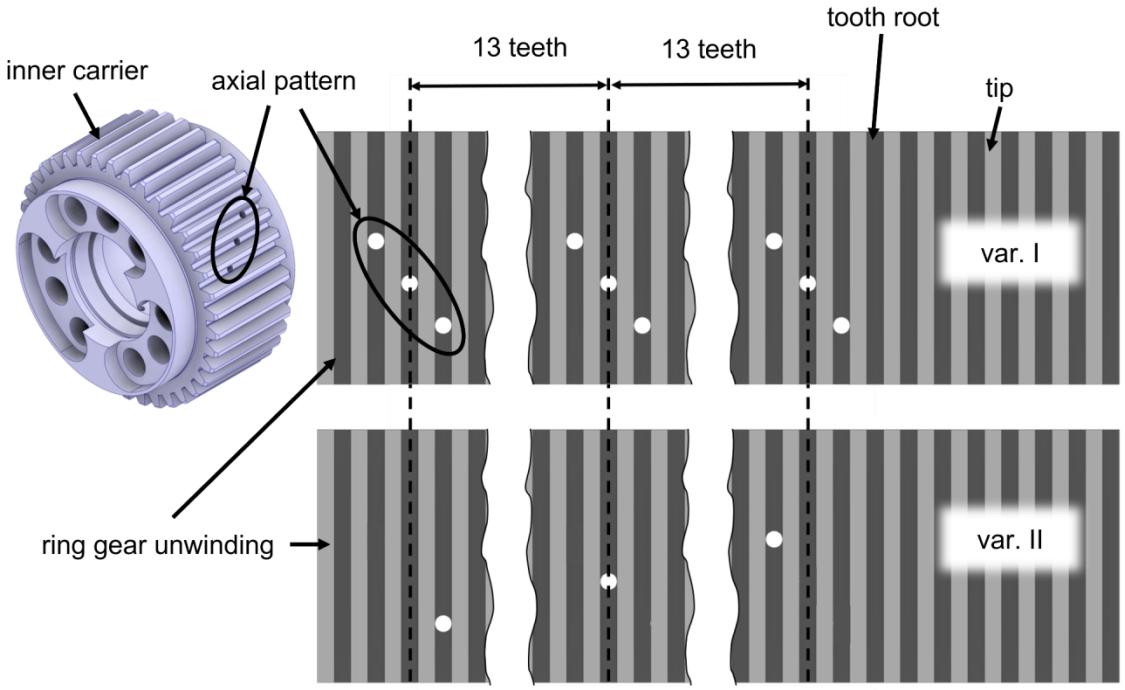

Figure 18: Oil distributor patterns of the inner carrier from [Gro22]

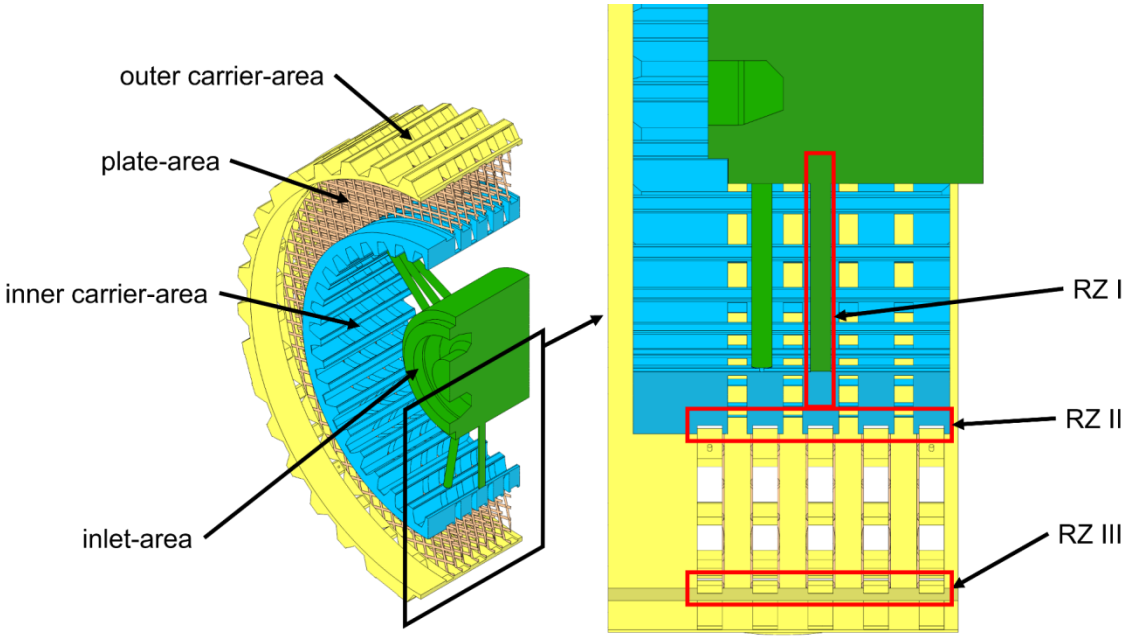

Figure 19: Refinement zones in the calculation domain from [Gro22]

5.3.2 Governing Equations and Solvers

The flow is modeled as laminar, incompressible, and isothermal (see section 6.3.1). Governing equations are defined from the flow module with dynamic mesh motion to solve the continuity (equation (2.9)) and momentum (equations (2.10) (2.11) (2.12)) equations on an arbitrary control volume, whose boundary is moving with a grid velocity. Further details can be found in the software documentation [Sim20].

If the clutch operates long enough in continuous slip, measurements show that the plate temperatures are nearly constant [Pay91]. Considering the small cross section of the grooves and therefore the small volume of oil that must be heated, it seems justifiable to assume an isothermal flow. The motivation for the assumption is the trade-off to reduce computational effort and modeling complexity, while representing the physics accurately enough.

Although assuming steady conditions regarding oil heating in the grooves, the flow is solved as unsteady to capture the effects of the rotating oil distributor holes in the inner carrier.

The CFD solver is based on the finite volume method and a pressure-based solver. Upwind interpolation is used for the pressure solver, and second order upwind for the velocity solver. The algebraic multi-grid method is used to solve the pressure equations, and the conjugate gradient squared method is applied to the velocity equations.

5.3.3 Boundary Conditions and Initialization

Figure 20 shows the calculation domain with oil supply variant I with highlighted in- and outlet areas. At the inlet, the oil flow is specified according to the test conditions (described in section 5.4). The outlets are set to an ambient pressure of 0 bar.

In static operation modes, the remaining walls of the calculation domain are set to stationary solid walls. For the dynamic operation modes (continuous slip), the components adjacent to the calculation domain are divided into input and output sides. Components of the input side have the rotational speed of the drive; components of the output side have the rotational speed of the outer carrier of the clutch.

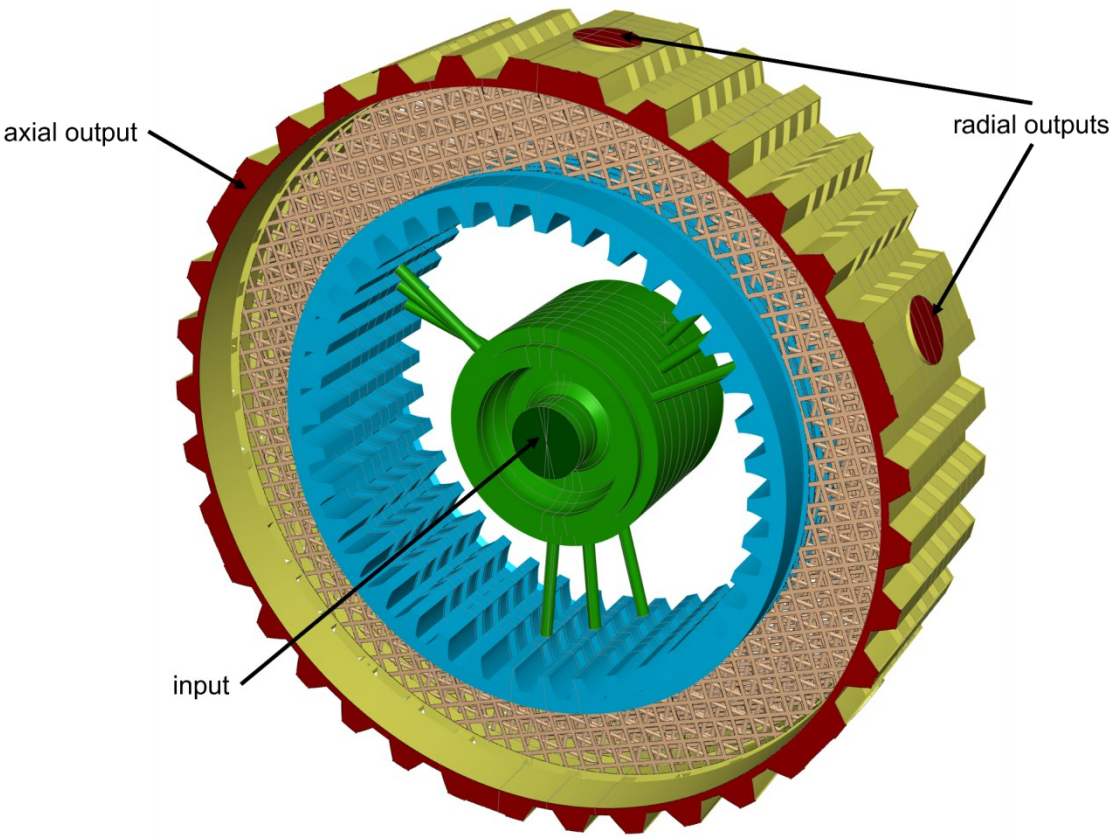

Figure 20: Calculation domain variant I with marked in- and outputs from [Gro22]

The simulations are initialized with oil temperature (representing viscosity / density) and rotational speed of the plates according to the conditions in the test rig. Static cases are initialized with the data recorded during the experimental investigations (described in section 5.4).

Furthermore, for a potential analysis of the calculation of heat transfer coefficients, the calculation domain was reduced to the consideration of one friction interface. The flow area and the boundary conditions for these investigations are shown in Figure 21. The calculation domain includes both the oil flow and temperature distribution in the fluid starting from the oil supply holes in the inner carrier through the grooves of the engaged clutch and the temperature distribution in the solid bodies (lining plates, steel plate). The geometry of the outer carrier is not considered in the model since the influence on the heat transfer between the oil in the grooves and the friction interface is estimated to be low.

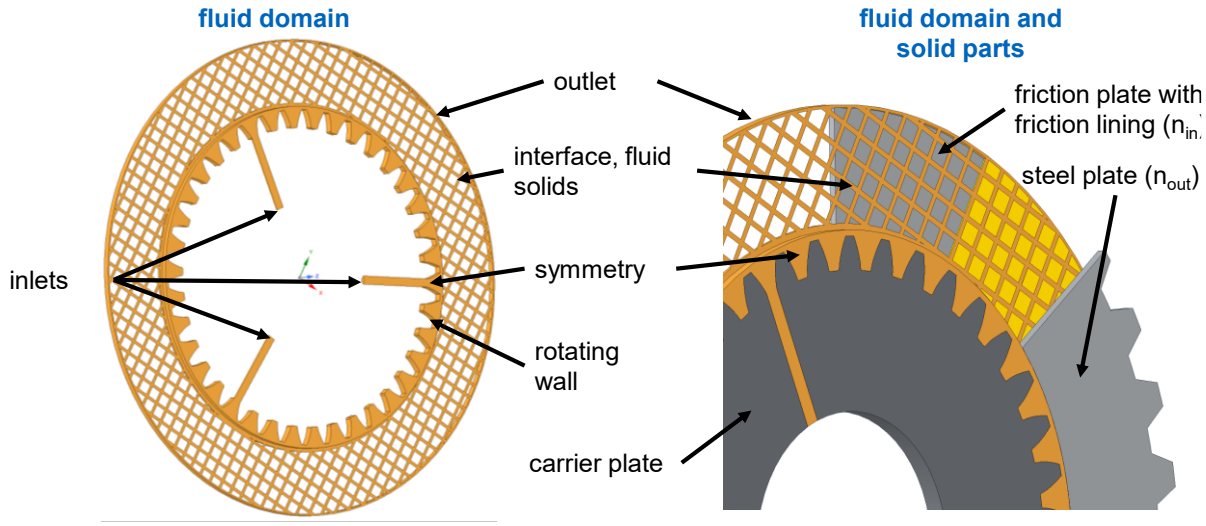

Figure 21: Calculation domain and boundary conditions for CFD simulation in the context of the potential analysis for numerical calculation of heat transfer coefficients

5.3.4 Model of Reduction of Axial Force Due to Hydrodynamic Pressure

One hypothesis is assuming that pressurized oil feeding lowers the axial force at the friction interfaces and therefore also lowers torque transfer capability of the clutch.

Figure 22 shows a schematic representation of the force ratios in the clutch package. Due to pressurized oil feeding, a static oil pressure in the groove gaps (gg) between steel and friction plates builds up and generates axial forces. In the central section of the clutch package (fp 1 …4 and sp 2 … 4), these forces cancel each other out. The forces acting on sp1 and sp5 reduce the nominal contact force (dashed) and the result is the reduced contact force F_{red}.

The reduced contact force through the oil pressure in the grooves ($F_{red/g}$) is calculated acc. to formula (5.7) by the difference of the applied nominal force F_{nom} and the sum of the axial forces in the grooves at each friction interface ($F_{ax/gi}$).

$$F_{red/g} = F_{nom} - \sum F_{ax/g_i} \tag{5.7}$$

Subsequently, the reduced contact force $F_{red/g}$ is scaled with the ratio of gross friction surface (A) and grooved area ($A_{grooves}$) acc. to formula (5.8).

$$F_{red} = F_{red/g} \cdot \frac{A}{A_{grooves}} \tag{5.8}$$

Thus, it is assumed that the calculated pressure in the grooved area approximates the pressure in the tribological contact at the non-grooved sections of the friction interfaces.

The reduced nominal surface pressure in the clutch is then calculated by dividing the resulting contact force (F_{red}) by the gross friction surface area (A).

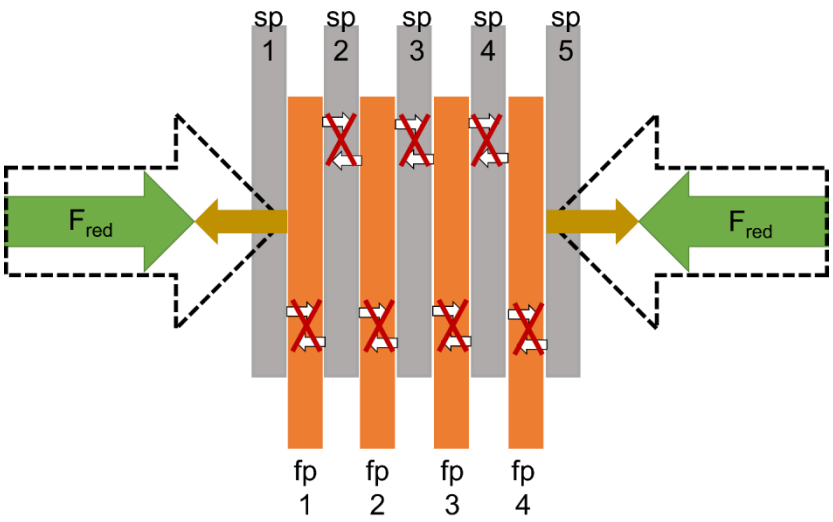

Figure 22: Schematic representation of the force ratios in the clutch package from [Gro22]

5.4 Experimental Investigations of Friction Behavior and Temperature

The test setup at the KLP-260 test rig is described in section 5.3.1; the setup in the LK-4 test rig can be found in section 5.5. The test procedures are split into static and dynamic operations. Static operations are performed with a clutch package consisting of five steel plates and four friction plates, therefore eight friction interfaces. In dynamic operations, the clutch size is reduced to four friction interfaces due to torque limitations of the main drive during continuous slip operations (see Table 3).

All experimental tests are performed after 3,000 running-in cycles (cycle time 15s) have been conducted [Voe20]. Table 11 summarizes the variations of the oil injection temperature and the oil flow rate during static operations.

Table 11: Operating conditions during static operations (ST) from [Gro22]

	ST1	ST2	ST3	ST4
$\dot{v}_{oil}$ / mm³/mm²s	0.5	1.0	1.5	2.0
ϑ_{oil} / °C	40/60	40/60	40/60	40/60

The load stages during running-in and in dynamic operation mode (continuous slip) are summarized in Table 12. The load stages differ by oil flow rates and differential speeds.

Table 12: Load stages during running-in (E) and in continuous slip (dynamic operations) from [Gro22]

	E	LS1	LS2	LS3	LS4	LS5	LS6
$\dot{v}_{oil}$ / mm³/mm²s	1.25	0.75/1.5/2.5	0.75/1.5/2.5	0.75/1.5/2.5	0.75/1.5/2.5	2.5	2.5
$v_{s,m}$ / m/s	10	2.5	5	7.5	10	5	0
ratio n_{sp}/n_{fp}	0	0	0	0	0	0.5	1.0
*numerical study							

In the numerical study, the ratio of rotational speed between steel and friction plates was varied as well. Cycle time during dynamic operations is 900 s, whereas it is a few seconds during static operations to ensure that steady state conditions for temperature and pressure signals are reached. The nominal pressure is held constant at 0.75 N/mm² during static operations and 0.22 N/mm² during dynamic operations. All specific values are normalized by gross friction surface area A. The load stages cover typical working conditions of the clutch in real applications.

In the test rig, the speed of the inner carrier, oil flow rate, oil injection temperature, and clutch pressure (hydraulic piston) are defined and measured. Additionally, the transferred clutch torque, steel plate

temperatures, and the oil pressure near the oil injection nozzle are recorded. Figure 23 shows measurement data during static operations (variant I, L-301, ϑ_{oil} = 40 °C, static operation ST1). To obtain steady state conditions the evaluation interval is chosen such that the pressure and temperature signals are nearly constant. Within this interval, the median and the 2.5th and 97.5th percentile from the continuous signals are calculated.

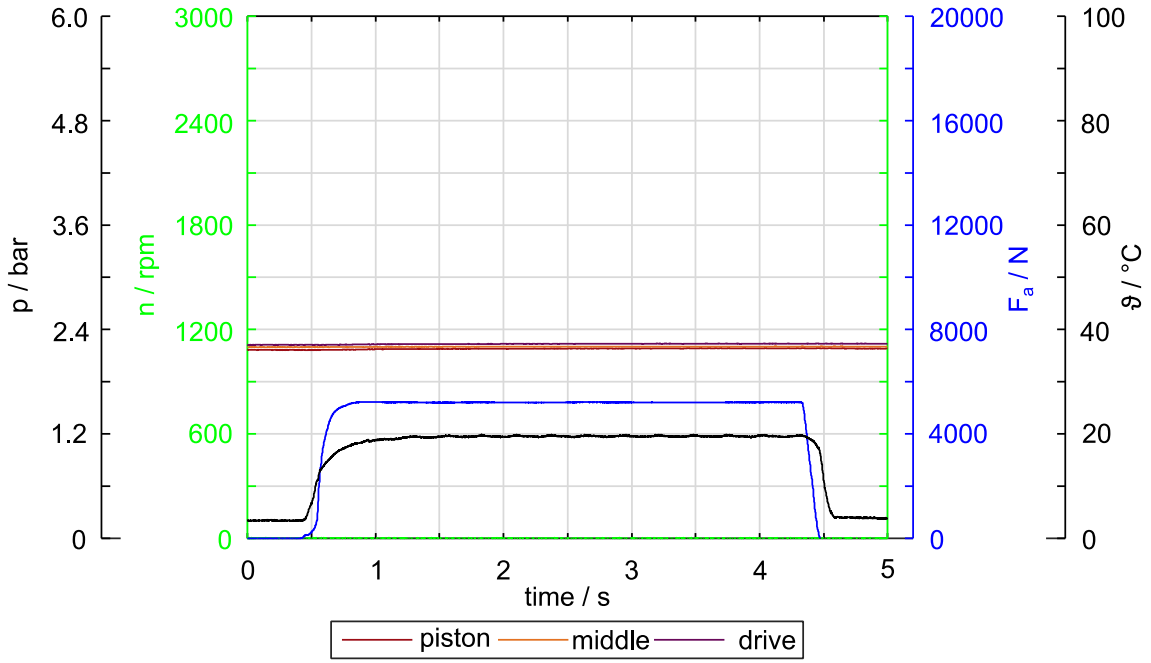

Figure 23: Recorded signals differential speed (n, green), axial force (F_a, blue), oil pressure (p, black) and thermocouples (ϑ red, orange, purple) from test rig, (variant I, L-301, ϑ_{oil} = 40 °C, static operation ST1) from [Gro22]

Temperatures are measured in the first (hydraulic piston side), middle, and last (drive side) steel plates with a thermocouple (NiCr-Ni Type K Class 1, ⌀ 0.5 mm, response time approx. 30 ms calculated acc. to [Pol09]), as pictured in Figure 24. A high-density polysynthetic silver thermal compound was applied on the thermocouples, which were then placed in a circumferential drill hole (⌀ 0.6 mm) positioned at approx. 12 o´clock in the midplane of the steel plates with a drill depth of approx. the mean radius.

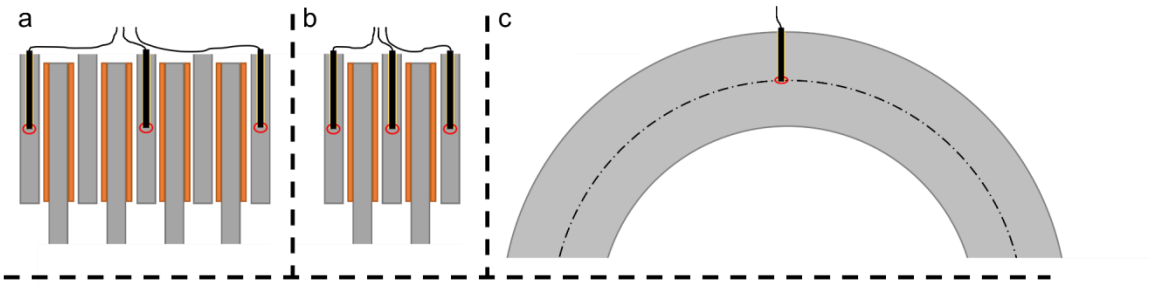

Figure 24: Positions of the thermocouples during (a) static operations, (b) dynamic operations and (c) the circumferential positioning from [Gro22]

For further analyses, the values of the nearly stationary courses of the signals at the end of each load stage are evaluated. The median of the signals of the last minute is determined and compared in bar charts. The scatter bars show the limits of the 2.5th quantile and 97.5th quantile. Thus, 95% of the observed values lie within these limits.

To determine the temperature behavior of the industrial clutch during shifting operations, stitch tests were carried out with a load cycle consisting of four load stages. To distinguish between load stages during continuous slip and shifting cycles, the load stages during shifting operations are defined as load

levels and are abbreviated with LLx. The influencing variables pressure and differential speed were varied. The settings of the load parameters are summarized in Table 13.

The load levels are run in the sequence LL1 ... LL4. The cycle time is 15 s. and the clutch is engaged for 5 s at the beginning of each cycle by applying the axial force. Oil is injected centrally from the inside. The oil injection temperature is 80 °C for this test and the specific oil flow rate is v_{oil} = 1.25 mm³/mm²s. Each load level is repeated ten times.

Table 13: Load parameters of the stitch tests shifting cycles

	LL1	LL2	LL3	LL4
pressure / N/mm²	0,75	1,0	1,0	0,5
max. speed / rpm	1,700	1,300	2,300	1,300
specific friction work / J/mm²	0.5	0.2	0.9	0.2

To determine heat transfer coefficients according to Wohlleber [Woh12] in the sliding phase, further stitch tests were carried out in continuous slip at low speed. During a test, the average steel plate temperature is monitored while increasing the clutch speed from rest in steps of 10 rpm. Each speed level is maintained until the steel plate reaches an almost constant temperature. When the defined limit value of the steel plate temperature is reached (here approx. 200 °C), the tests are terminated to prevent damaging the clutch. The nominal pressure is p = 1.0 N/mm². These tests were carried out at a specific oil flow rate of 1.0 mm³/mm²s and an oil injection temperature of 80 °C.

5.5 Experimental Investigations for Visualization of Oil Flow

Under the guidance of the author, the development of the experimental investigations for visualization of oil flow was supported by the student research project of Schermer [Sch22a]. The investigations were carried out on the LK-4 test rig as shown in Figure 27. The cover of the test rig (1) is produced from plexiglass and is therefore transparent. The oil is supplied pressurized via the inner carrier by a central sleeve (2), where the existing oil supply of the LK 4 test rig is connected. Furthermore, parts of the installation, such as the clutch cover (3) and inner carrier (4), are manufactured using Stereolithography Apparatus (SLA) 3D printing to realize transparent components. The outer carrier (5) is the same as in the tests at the KLP-260 test rig. Transparent steel and lining plates are also produced. The simple geometry of the steel plates is cut with a laser cutter from plexiglass plates of the appropriate thickness. For the complex geometry of the lining plates, the SLA 3D printing process is selected as it is for the components of the installation. The clutch package during the tests consists of the transparent clutch cover representing the first friction interface that is observable through the transparent test rig cover. The following plates (steel, friction in alternating order) are from serial production except for one stitch test, for which the first steel plate is replaced by a transparent version. The last friction plate is integrated into the inner carrier geometry and therefore also replaced. To increase contrast during recordings, the first non-transparent steel plate is coated with a white finish.

Instead of X-Rings, the clutch is sealed by a modified design of the inner carrier as pictured in Figure 26. The 3D printed inner carrier incorporates the last friction plate. The design of the inner carrier features holes and undercuts in places that would only have been possible with a multi-part design in conventional manufacturing processes. By mounting the clutch cover with an O-Ring at the inner diameter on the inner carrier, the clutch is sealed and closed. Since the LK-4 test rig is not able to close the clutch with a piston, it is operated in an always closed mode by applying a low axial force with the clutch cover (p ≈ 0 N/mm²). More details on transparent plate manufacturing and the test rig setup can be found in [Sch22a].

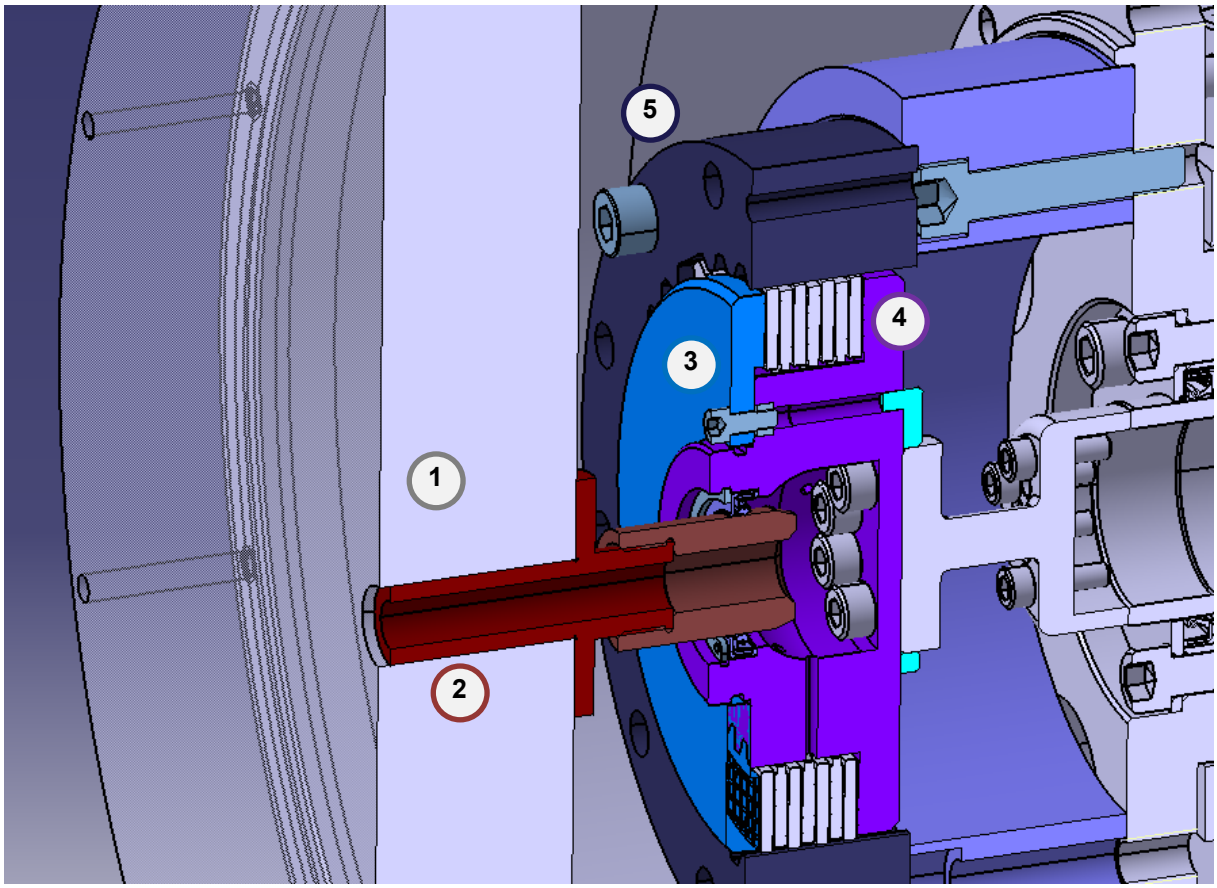

Figure 25: Test Rig Setup at LK-4 with transparent plexiglas cover (1) and clutch D122 from [Sch22a]

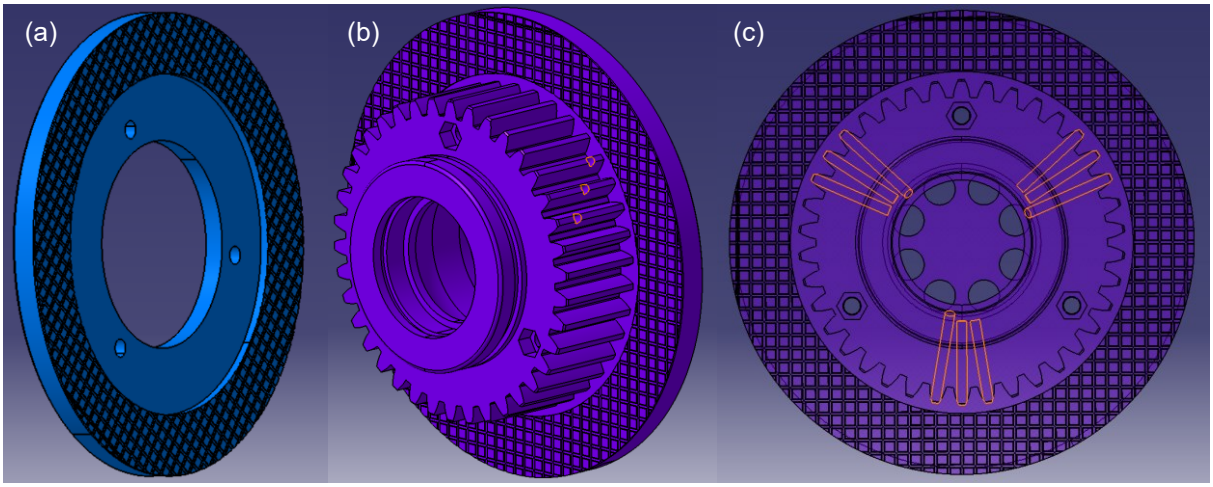

Figure 26: Clutch D122: Clutch cover (a) and inner carrier (b) with integrated spline and orange-marked bore hole pattern of the oil supply (c) from [Sch22a]

The experimental investigations to visualize the oil flow are carried out with four (dynamic operation) and eight (static operation) friction interfaces (as described in section 5.4). Apart from the geometric variations of the test setup, the test program consists of two differential speeds and three specific oil flow rates. The test program consists of LS1 and LS2 as summarized in Table 12. The test rig with the installed test setup with four friction interfaces can be seen in Figure 27. It also shows how the oil supply with a thermocouple for the measurement of the oil injection temperature is mounted via the sleeve on the plexiglass cover. Figure 28 shows the components for installation with eight friction interfaces (top) and the finished assembly for four friction interfaces (bottom).

During the experiments, the influence of differential speed, specific oil flow rate, number of friction interfaces and oil distributor pattern on the filling behavior of the clutches is investigated. For this

purpose, the inner carrier is accelerated without lubrication to the respective differential speed of the load stage. The oil supply is then switched on while observing the filling process and measuring characteristic times. The clearance for the entire clutch package is less than 0.05 mm in each case, resulting in an approximately closed clutch ($p \approx 0$ N/mm²).

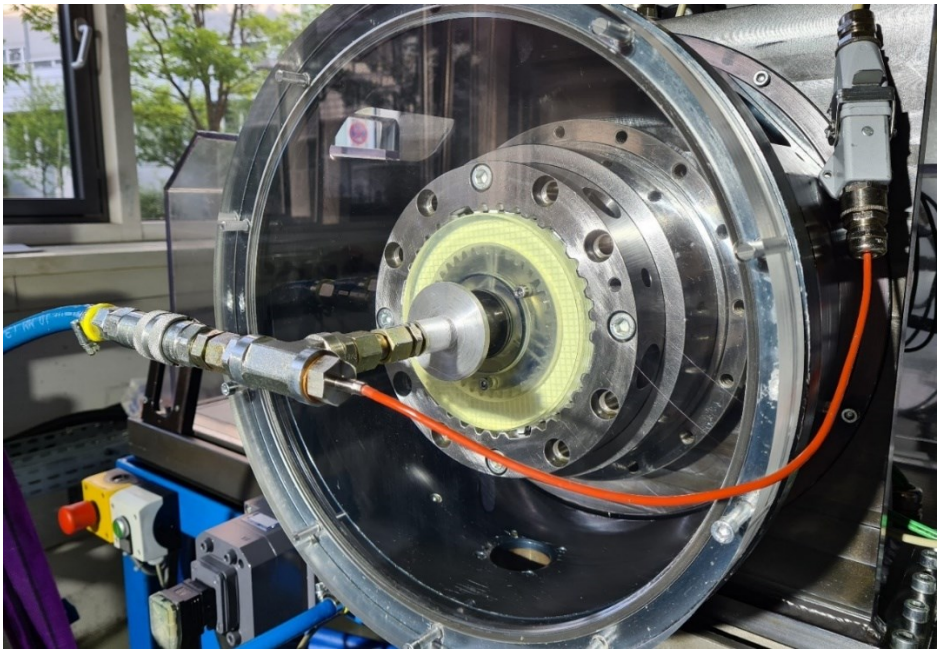

Figure 27: Test rig LK-4 with transparent cover, installed test setup D123 with four friction interfaces and oil supply with thermocouple for oil injection temperature from [Sch22a]

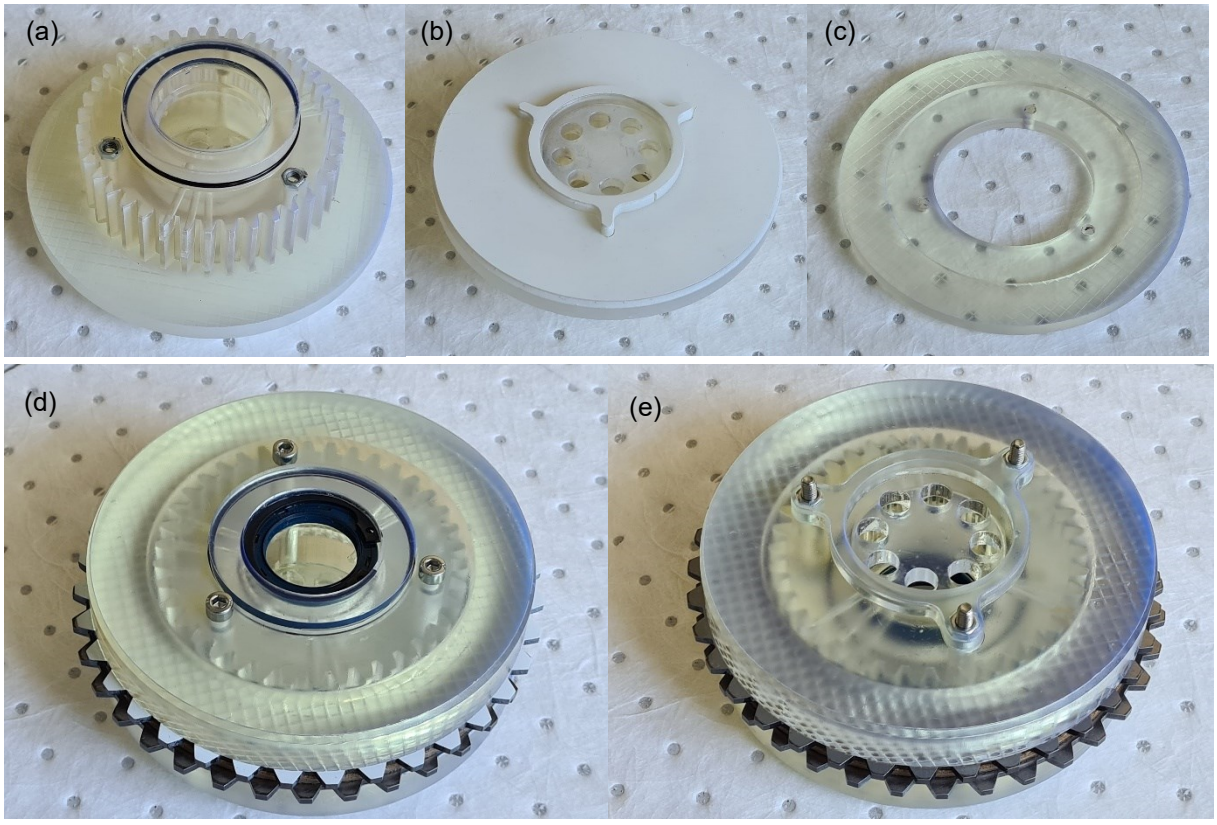

Figure 28: Inner carrier (a), white painted back (b) and clutch cover (c) for eight friction interfaces and complete assembly for four friction interfaces (d and e) from [Sch22a]

6 Validation and Plausibility Checks of Investigation Methods for the Thermal Behavior

The validation and plausibility of the investigations methods is checked in the following paragraphs, except for the investigations on the KLP-260 test rig since the procedures are already well established (a.o. [Gro21a, Mei15, Sto21]).

6.1 Real-Time Temperature Calculation and Temperature Prediction

The results presented below have been published by Groetsch, Voelkel, Pflaum and Stahl [Gro21b, Gro21c].

6.1.1 Plausibility of Plate Temperatures in Comparison to KUPSIM Simulations

The plausibility of the calculations of the real-time model is at first checked using representative load levels for clutch operations in comparison with results of KUPSIM. The calculations are carried out with the same input parameters. Subsequently, a comparison and evaluation of the output parameters is performed. A clutch system is used that has already been experimentally validated with KUPSIM. This procedure ensures that the thermal calculation with KUPSIM is correct. The material and geometric data correspond to clutch D176 with group parallel grooves and a paper friction lining. ATF-B is used as oil (compare section 4.1). All input variables including the input signals of the calculation were taken from the literature [Woh12, Woh11]. The loads of the test consist of four load levels. The load levels are calculated as a load sequence in the order LL1-1* - LL3* - LL4* - LL2* - LL1-2* (from [Gro21b]). The course of axial force and speed of the load levels can be seen in Figure 29.

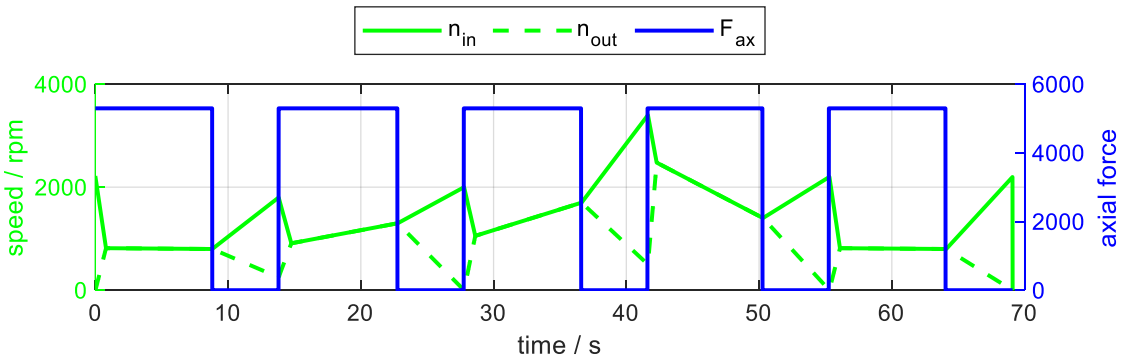

Figure 29: Time curve of input and output speeds and axial force of load levels LL1-1* - LL3* - LL4* - LL2* - LL1-2* from [Gro21b]

In the following, the calculation results of the real-time model are compared with the results from KUPSIM. A specific oil volume flow of 0.65 mm³/mm²s at an oil injection temperature of 80°C is defined as a reference condition. In KUPSIM, the sliding phase is considered spatially resolved in two dimensions. The cooling phases are calculated spatially isothermal. Figure 30 shows the temporal course of the calculated temperatures of steel plate node 2 (S2) of the real-time model and the isothermal steel plate temperature from KUPSIM.

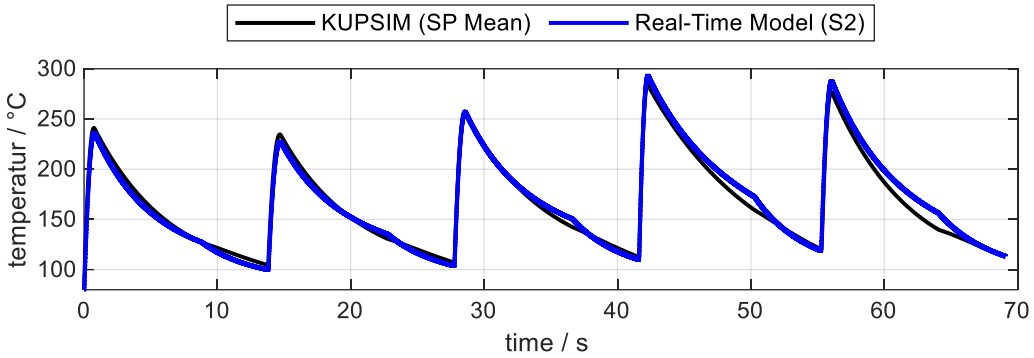

Figure 30: Temperature curves of the isothermal steel plate temperature from KUPSIM and the node temperature (S2) of the real-time model for the load levels LL1-1* - LL3* - LL4* - LL2* - LL1-2* (v_{oil} = 0.65 mm³/mm²s, $\vartheta_{oil,in}$ = 80°C, p = 1.0 N/mm², ATF-B) from [Gro21b]

The isothermal steel plate temperature in KUPSIM in the sliding phase is determined by numerical integration over the two-dimensional domain of the steel plate. A typical temperature characteristic for wet multi-plate clutches is obtained. This is characterized by a strong heating of the plate during the sliding phase and the subsequent exponential cooling phases. The temperature curve in the cooling phases show a change in cooling rate in the transition between the closed (axial force applied) and open (no axial force) cooling phase. This can be explained by the changed heat transfer due to the opening of the clutch (oil flow rate, heat transfer coefficient). The S2 node temperature is in very good agreement with the isothermal steel plate temperature from KUPSIM. The spatially two-dimensional calculation of KUPSIM enables the output of the peak temperature at the friction interface for each sliding phase. In Table 14, the local peak and mean peak temperatures of the steel plates from KUPSIM are compared to the peak temperatures of node S2 on the different load levels. The temperatures in the real-time model follow the calculation in KUPSIM. The differences for the maximum temperatures are due to the one-dimensional modeling. In the real-time model, the heat is distributed to a larger thermal mass per time step. The mean peak temperatures show good agreement (within +/- 10 K).

Table 14: Comparison of the maximum temperatures per load level of node S2 with the maximum steel plate temperature per load level of the spatially two-dimensionally calculated sliding phase in KUPSIM from [Gro21b]

	LL1-1*	LL3*	LL4*	LL2*	LL1-2*
$T_{sp,max,KUPSIM}$ / °C	258	247	273	306	295
$T_{sp,mean,max,KUPSIM}$ / °C	241	235	258	284	277
$T_{sp,max,real\ time\ model}$ / °C	236	227	257	293	288
$\Delta T_{sp,max}$ / K	22	20	16	13	7
$\Delta T_{sp,mean}$ / K	5	8	1	-9	-9

The cooling in the real-time model is slightly lower compared to the spatial resolved calculation in KUPSIM. The cooling phases in the real-time model would therefore be slightly longer than in KUPSIM until complete cooling. This leads to a slightly higher node temperature in sequential shifting operations with almost the same temperature rise.

6.1.2 Validation of Plate Temperatures and Pressure in Comparison to Measurements

Figure 31 shows the comparison of the calculation with the real-time model and the mean of the circumferential distributed temperature measurements (compare section 5.4) in continuous slip using a heat transfer coefficient determined according to Wohlleber (α = 8000 W/m²K (sinter)) [Woh12].

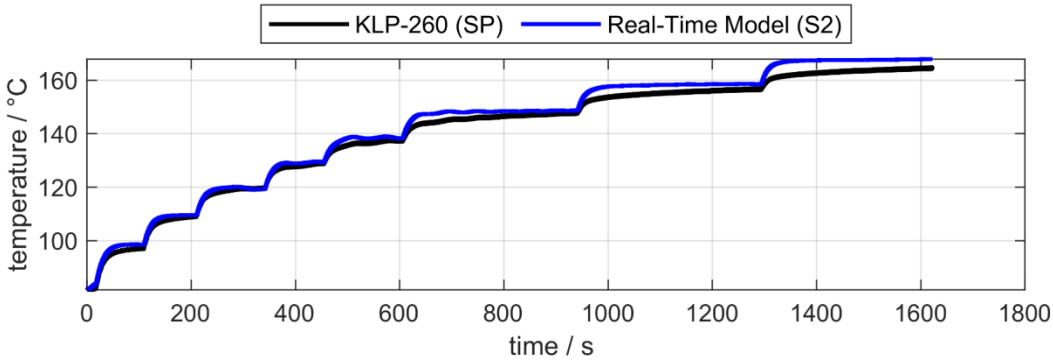

Figure 31: Temperature curves of the measured steel plate temperature and the node temperature (S2) of the real-time model in continuous slip (v_{oil} = 1.0 mm³/mm²s, $\vartheta_{oil,in}$ = 80°C, p = 2.0 N/mm², Industry, D123) from [Gro21b]

The temperature curves show very good agreement. This applies to the dynamic change from one speed plateau to the next higher one as well as to the stability of the calculation while one speed step is held constant. The absolute deviations of the temperatures shortly before the rise to the next speed level are summarized in Table 15. The values confirm the optical impression and show an excellent agreement between measurement and simulation.

Table 15: Comparison of the measured temperatures on the test rig and the temperatures of node S2 shortly before the rise to the next speed level in continuous slip from [Gro21b]

Δn / rpm	10	20	30	40	50	60	70	80
time / s	100	200	300	450	600	900	1,250	1,550
$T_{sp,measurement}$ / °C	97	109	119	129	137	147	156	164
$T_{sp,real\ time\ model}$ / °C	99	109	119	128	139	149	159	168
ΔT_{sp} / K	2	0	0	1	2	2	3	4

In addition to continuous slip operation, the real-time model was also validated for operation with shifting cycles by comparing calculated with measured results on the KLP-260 component test rig. For the calculation, the drive speed (main drive), torque and axial force signals measured on the test rig are fed into the model. The other input signals are specified as constant values. Figure 32 and Figure 33 show the input signals speed (green), friction torque (red) and axial force (blue) over measured time as described in section 5.4.

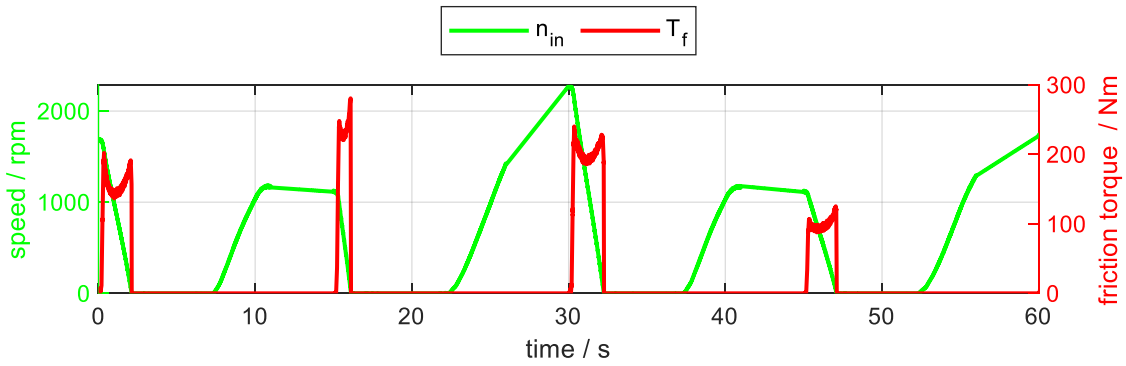

Figure 32: Course of drive speed (n_{in}) and friction torque (T_f) of the load stages for validation with load cycles from [Gro21c]

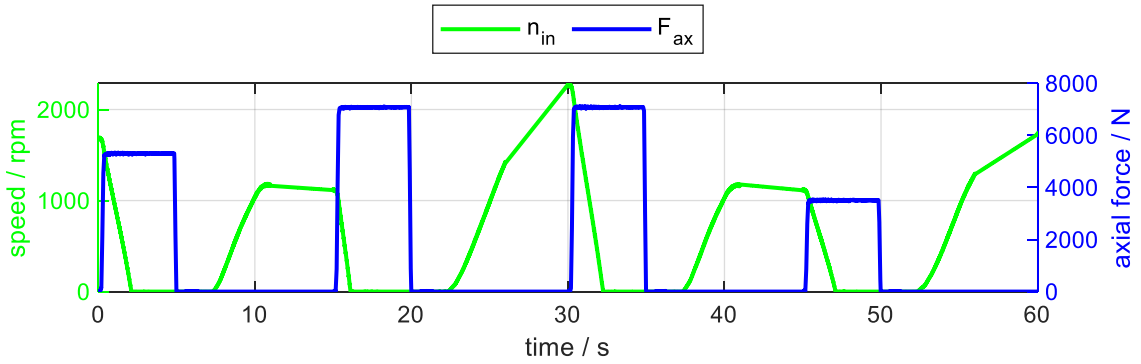

Figure 33: Course of drive speed (n_{in}) and axial force (F_{ax}) of the load stages for validation with load cycles from [Gro21c]

Figure 34 shows a comparison of the measured mean steel plate temperature of load levels LL1 ... LL4 with the calculated temperatures of the real-time model. To show the calculation quality, the dashed gray lines represent the limits +/- 10 K around the measured temperature. The measurement on the test rig is triggered per load level. The measurement time is therefore a few seconds shorter than the cycle time. In areas without a measurement signal, no limits are therefore given for the temperature calculation. The temperature calculation remains in the corridor of +/- 10K of the measurement over all load levels. The model calculates a plausible temperature deviation despite strongly varying operating conditions. Furthermore, the cooling behavior is well represented. Between LL1, LL2 and LL3, the cycle time is sufficient to cool the clutch back almost to the temperature before the start of the cycle. In LL3, the clutch was strongly heated, and the cycle time was not sufficient to cool the clutch back to the initial temperature. Both effects are reproduced by the calculation.

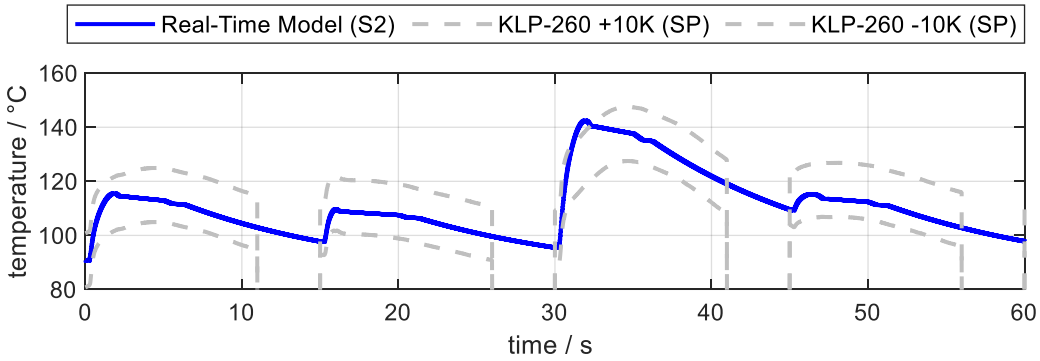

Figure 34: Comparison of the measured mean steel plate temperature (limits +/- 10K) and the real-time model during shifting cycles (D123, v_{oil} = 1.25 mm³/mm²s, $\vartheta_{oil,in}$ = 80°C, L-301) from [Gro21c]

Figure 35 shows the continuation of the stitch test of the load sequence LL1 ... LL4. The load sequence was repeated a total of ten times. The calculation also remains within a range of +/- 10 K around the measured mean steel plate temperature over the full test duration with a total of 40 shifting operations. The comparison of the results of the real-time model with test rig measurements thus shows valid results even for long simulation times and at high shifting frequencies.

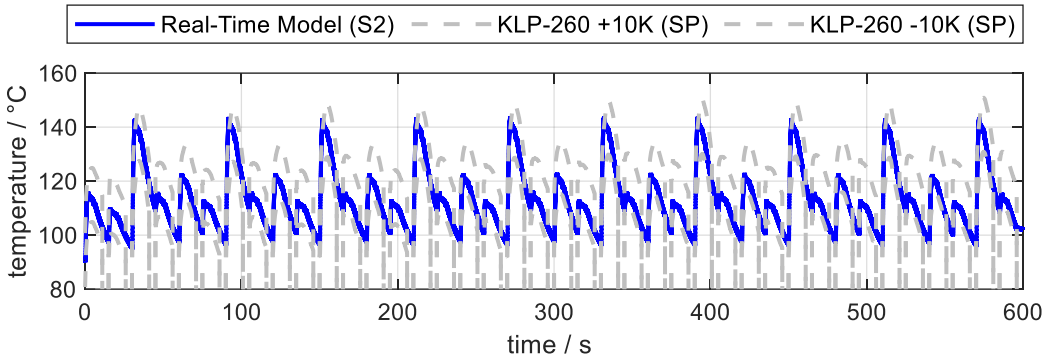

Figure 35: Comparison of the measured mean steel plate temperature (limits +/- 10K) and the real-time model (D123, v_{oil} = 1.25 mm³/mm²s, $\vartheta_{oil,in}$ = 80°C, L-301) from [Gro21c]

6.1.3 Validation of Temperature Prediction

To validate the temperature prediction, the points furthest away are selected between the grids stored in the map (compare section 5.2.2). The inaccuracy that results from interpolation is the greatest there. For all these points, a full simulation is used to calculate the required value. The same value is also generated by interpolation from the map. The deviation of the interpolated values from the simulated values gives information about the accuracy of the prediction module.

Figure 36 shows the results of the validation for a prediction map with 3,125 values (memory requirement approx. 27kB, number of interpolation points = 5 for all parameters). The operating limits were defined for clutch D123. The specific friction work varies in the range of 0.03 ... 1.23 J/mm², the specific friction power in the range of 0.14 ... 4.35, W/mm² and the pressure in the range of 0.7 ... 3.7 N/mm² for a drive inertia of J_{in} = 1.25 kgm². There are 1,024 test points with the greatest distance from the values stored in the map. The figure shows that the deviations between prediction module and real-time model are in the range of 0 ... 4 K. The mean value and the median of the deviations are 3 K. It can furthermore be seen that the prediction is always conservative because it predicts a higher temperature. A high accuracy of the temperature prediction over the given operating range of the clutch is therefore shown.

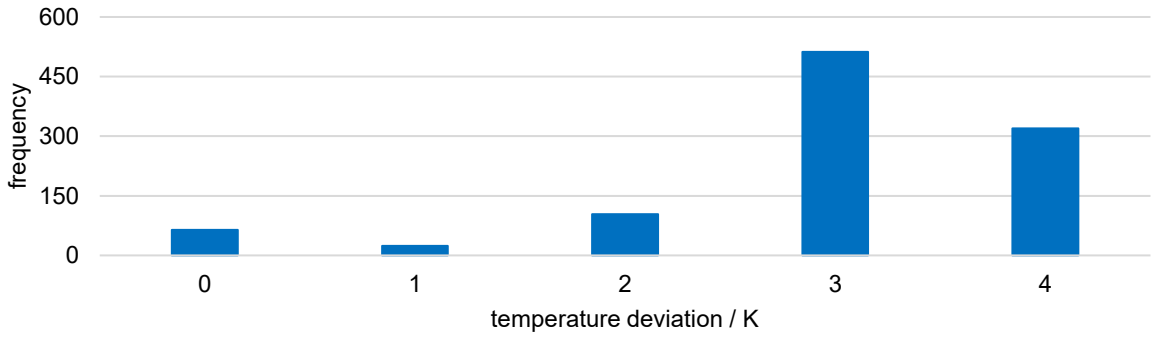

Figure 36: Histogram of temperature deviation from prediction to simulation (brake mode; map: 1024 test points) from [Gro21b]

6.2 Sensitivity Analysis and Optimization of Temperature Prediction Method

The reliability of the prediction module depends largely on the accuracy of the linear interpolation between the values stored in the prediction map.

However, the results of the validation of Figure 36 show a high memory requirement (3,125 values approx. 27kB) for the prediction map and numerous simulations are required to determine the map. In the following, the map generation will therefore be optimized using the D176 clutch (see Section 6.1.1) as an example by means of a sensitivity analysis.

6.2.1 Design of Sensitivity Analysis

The results of the sensitivity analysis give insight into the relevance and effect of the input parameters on the calculation results, and can thus be used to optimize the generation of prediction maps. For the sensitivity analysis, a full factorial test plan is applied for all parameters (see section 5.2.2) on three levels. This results in 729 / 243 / 729 simulations in clutch / brake / continuous slip operation. Then the main influences and interactions between the parameters on the temperature rise (clutch, brake) and the tolerable slip time (slip operation) are graphically illustrated. Subsequently, an evaluation can be made regarding the absolute influence of the parameters on temperature rise and a qualitative evaluation of the course can be performed. If the input parameter has only a minor influence on the temperature rise or the tolerable slip time, a coarse resolution can be selected. Furthermore, a coarser resolution can also be selected if the relationship between the parameters and the temperature rise / tolerable slip time is almost linear. In the case of a non-linear curve and a large influence, on the other hand, the parameter should be resolved more finely.

6.2.2 Evaluation of Sensitivity Analysis

Figure 37 shows an example of the calculated main effects of the input parameters on the temperature rise in clutch operation for all input variables. The input and output speeds thus have the greatest influence on the calculated temperature rise. Furthermore, it can be seen from the slope change in the center that the speed influence is nonlinear. The friction torque also shows a nonlinear relationship to the output variable due to a kink in the curve. However, the direct effect of the friction torque on the temperature rise is significantly lower than the influence of the speed. The other input variables show a linear behavior (no kink) and a very small overall influence on the calculation of the temperature deviation.

Figure 38 shows the interaction diagram during clutch operation. The speed level (both input and output speed) has a significant influence on the temperature rise. The speeds interact with all parameters. The other input variables show no interaction. The observations are consistent with the physical modeling.

In braking mode, the map is reduced by one dimension since the output speed does not have to be considered. The influences of the main effects and interactions are analogous to clutch operation.

The analysis of the main effects in continuous slip shows that the tolerable slip time in the tested range is significantly influenced by the input variables input speed, friction torque and start temperature of the steel plate. Furthermore, there is also an influence of the output speed, which has a small effect due to the low variation in the range 0 ... 5 rpm. The parameters specific oil flow rate and oil injection temperature hardly influence the result. The speed level (both input and output speed), the friction torque and the start temperature of the steel plate have a significant influence on the tolerable slip time and show interactions with the other variables. The other input variables do not show any interactions.

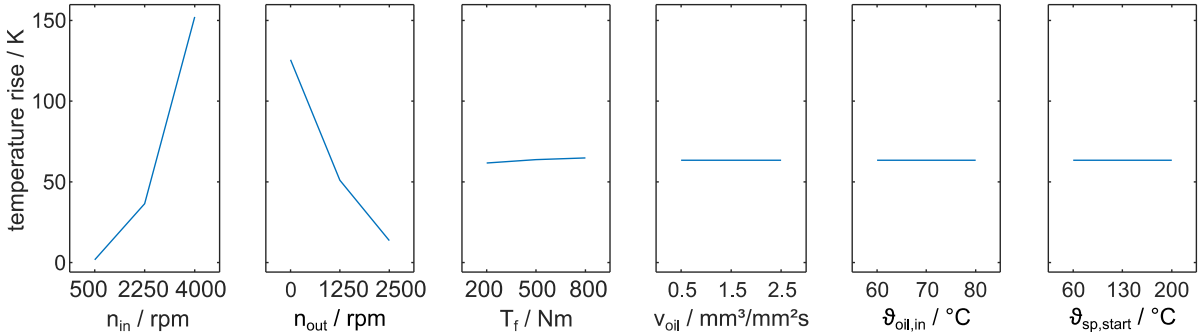

Figure 37: Main effects diagram of the simulated temperature rise for the input parameters input, output speed (n_{in}, n_{out}), friction torque (T_f), supplied specific oil flow rate (v_{oil}), oil injection temperature ($\vartheta_{oil,in}$) and steel plate temperature at the beginning of the calculation ($\vartheta_{sp,start}$) during clutch operation varied on three levels from [Gro21c]

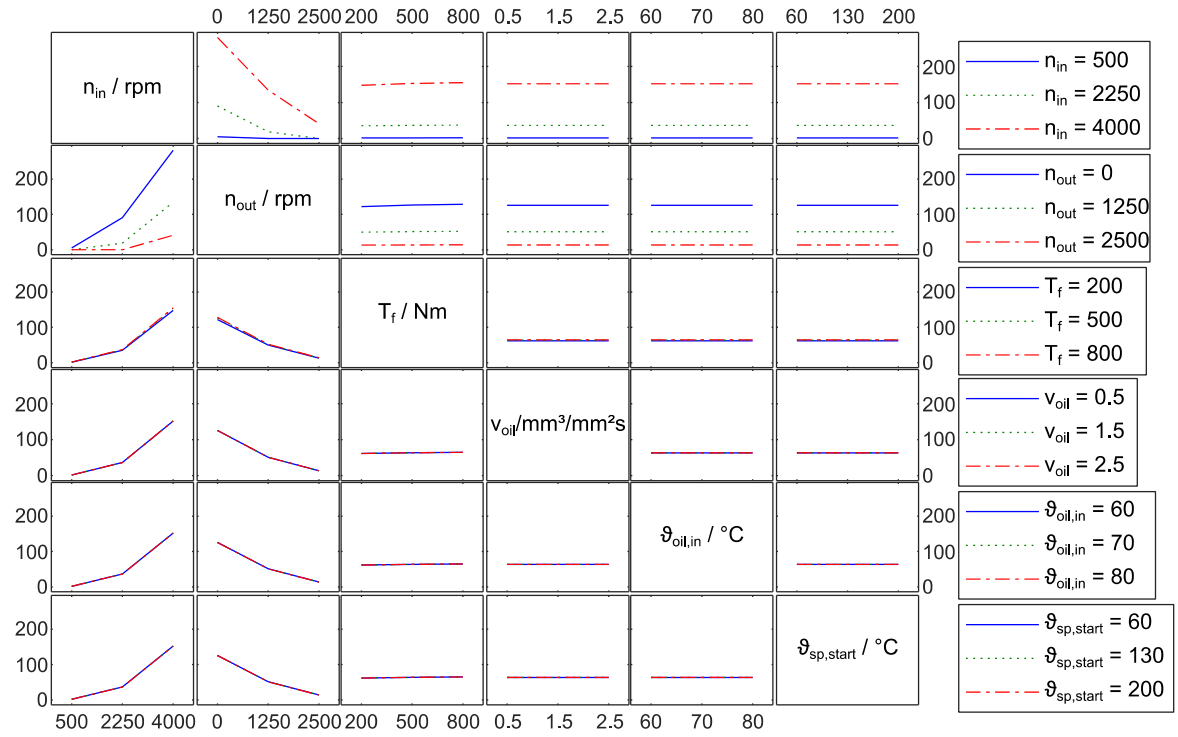

Figure 38: Interaction diagram of the simulated temperature rise for the input parameters input, output speed (n_{in}, n_{out}), friction torque (T_f), supplied specific oil flow rate (v_{oil}), oil injection temperature ($\vartheta_{oil,in}$) and steel plate temperature at the beginning of the calculation ($\vartheta_{sp,start}$) during clutch operation varied on three levels from [Gro21c]

6.2.3 Optimization of Real-Time Temperature Prediction Method

Due to the described main effects and interactions in clutch and brake operation, a high map quality can be achieved by many interpolation points for the speeds and, if necessary (e.g. non-linear friction behavior), for the friction torque. The number of interpolation points for the remaining parameters should be set to as low a value as possible, since they contribute little to improving the prediction of the temperature rise.

In continuous slip, a high map quality can be achieved with many interpolation points for the speeds and the friction torque, since both values show a large and/or non-linear influence. The start temperature of the steel plate shows a large effect, but this is almost linear and can therefore be reproduced well with fewer grid points. The number of grid points for the remaining parameters can be set to a low value, since they contribute little to the improvement of the prediction of the tolerable slip time.

In the following, the optimization of the prediction maps in clutch operation with the aid of the findings from the sensitivity analysis is shown as an example. For this purpose, three prediction maps with different resolutions are created and the calculation quality is validated. The number of grid points used for each parameter is summarized in Table 16. The map that was created for the determination of the main effects and interactions serves as “reference”. Subsequently, the map is designed efficiently by adjusting the number of grid points for “stage I” and “stage II” maps.

Table 16: Variations of the number of interpolation points for the determination of prediction maps during clutch operation from [Gro21c]

	# grid points		
name	reference	stage I	stage II
input speed	3	3	5
output speed	3	3	5
friction torque	3	3	4
specific oil flow rate	3	2	2
oil injection temperature	3	2	2
start temperature	3	2	2
# grid points prediction map	729	144	720
# test points	64	4	40
disk space	6.2kB	1.22kB	6.12kB

For each of these three maps, a test grid was created, located exactly in the middle between the map points. There, the difference of the temperature rise between real-time simulation and prediction was evaluated. Statistical values of this validation are summarized for the three examined maps in Table 17. Furthermore, Figure 39 shows a histogram of the distribution of the temperature deviations for all test points for the “stage II” map.

The comparison of the statistics of “reference” and “stage I” maps show that a reduction in the number of points for the oil flow rate, oil injection temperature and start temperature of the calculation has almost no effect on the accuracy of the calculation. The size of the map can thus be reduced by a factor of five with the same calculation accuracy. “Stage II” represents an optimized variant of the map, considering the findings of the sensitivity analysis. With a slightly lower memory requirement compared to the reference, the accuracy of the prediction can be significantly improved. Figure 39 shows that the deviations between the prediction module with the “stage II” map and the real-time model are in the range of 0 ... 4 K. The mean and median of the deviations are only 3 and 4 K, respectively. Furthermore, the prediction is always conservative since it predicts a higher temperature. Thus, a large optimization potential of the temperature prediction over the given operating range of the clutch is shown. Comparable optimizations were determined in braking and continuous slip operation.

Table 17: Summary of statistics of the validation of optimized temperature prediction in clutch operation for three map resolutions (reference, stage I and stage II) from [Gro21c]

map	reference	stage I	stage II
# test points	64	4	40
mean deviation (arithmetic) / K	15	15	2.9
median / K	18	18	3.7
maximum deviation / K	20	20	3.9

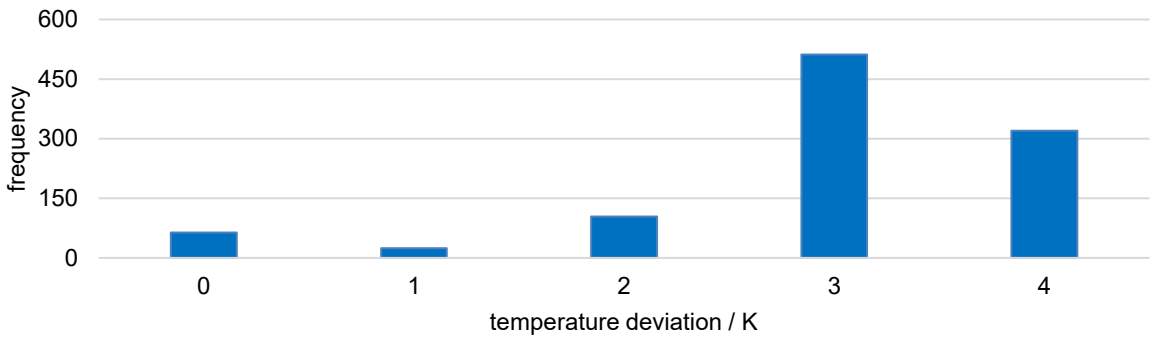

Figure 39: Histogram of temperature deviation from prediction to simulation (clutch mode; D176; optimized map resolution stage II: 40 test points) from [Gro21c]

6.3 CFD-Model for Calculation of Oil Distribution and Reduction of Axial Force

The results presented below have been published by Groetsch, Motzet, Voelkel, Pflaum and Stahl [Gro22]. Furthermore under the guidance of the author, the results were supported by the student research project of Motzet [Mot21].

6.3.1 Plausibility of Flow Modeling Assumptions

The flow modeling assumptions are based on a Reynolds criterion, prior publications, and experimental investigations. The Reynolds number (Re) is calculated by dividing a characteristic flow velocity u and length scale d by the kinematic viscosity v [Pol09].

$$\mathrm{Re} = \frac{\mathrm{u} \cdot \mathrm{d}}{\nu} \tag{6.1}$$

According to [Pay94], the flow inside the grooves can be characterized by the rotational (u: rotational velocity of the plate at inner diameter) or average flow (u: average flow velocity through grooves) Reynolds numbers with the groove width as the characteristic length scale.

It is assumed that circulation of the flow inside the grooves (more details in [Pay91]) is dominated by the main eddy and thus small scale turbulence effects can be neglected [Pay94].

Modeling the oil flow through a grooved clutch as laminar pipe flow [Häm95, Pfl98, Woh12] also assume a laminar flow in the groove region. The calculation of the Reynolds number for the pipe flow model uses the average flow velocity as characteristic velocity, but the characteristic length scale is defined as the spare hydraulic diameter calculated by the division of cross section area (A_{groove}) and length of the contour (c_{groove}) of the groove.

$$\mathrm{d}_{\mathrm{spare,hydraulic}} = 4 \cdot \frac{\mathrm{A}_{\mathrm{groove}}}{\mathrm{c}_{\mathrm{groove}}} \tag{6.2}$$

The summary of calculated Reynolds numbers for critical operating conditions for the CFD model and the limits for transition to turbulent flow regimes in Table 18 show that the laminar assumption is valid to the best of my knowledge.

To adequately fulfill the assumption of an isothermal flow during continuous slip operation, the representative isothermal oil temperature must be estimated. The results of the static cases show that the transition of the oil flow from the inner carrier-area to the grooves has the highest hydraulic resistance due to the shrinking of the cross-section area. Therefore, it is assumed that this region dominates the development of the flow field. The dynamic simulations are initialized with the oil temperature at the inner radius of the friction plates. This temperature is calculated with the thermal clutch design tool KUPSIM [Voe16a, Woh09].

Table 18: Calculated Reynolds numbers and laminar limits for ν = 11,4 mm²/s and $v_{s,mean}$ = 10 m/s from [Gro22]

	value	laminar limit
$Re_{avg,Payvar}$	77	typical below 500 [Pay94]
$Re_{avg,Payvar}$	645	1,800* [Pay94]
$Re_{avg,Pfleger,Haemmerl,Wohlleber}$	28	<< 2,300 [Häm95, Pfl98, Woh12]
*authors use a laminar model for flow with Re = 1,800 and show agreement with the measurements		

Table 19 summarizes the oil temperatures obtained from measurements for the static cases and Table 20 summarizes the oil temperatures from KUPSIM for the dynamic cases.

Table 19: Nominal and measured oil temperatures for static operations from [Gro22]

	ST1		ST2		ST3		ST4	
nominal oil temperature / °C	40	60	40	60	40	60	40	60
measured oil temperature / °C	37	56	38	56	38	57	38	57

Table 20: Oil temperatures from KUPSIM for dynamic operations from [Gro22]

	LS1			LS2			LS3			LS4		
$\dot{v}_{oil}$ / mm³/mm²s	0.75	1.5	2.5	0.75	1.5	2.5	0.75	1.5	2.5	0.75	1.5	2.5
ϑ_{oil} (KUPSIM) / °C	81	68	67	103	78	75	119	88	83	137	96	91

6.3.2 Study on Mesh Independence of Solutions

The mesh study is performed for static operations. All simulations are repeated on each mesh type with the same solver settings, boundary and initialization conditions. Figure 40 shows a section of the investigated meshes. The mesh independence of the oil flow rate through the groove gaps and the axial force due to oil pressure in the grooves are considered as convergence criteria.

rough mesh
max. cell size: 0.01 mm

standard mesh
max. cell size: 0.005 mm

fine mesh
max. cell size: 0.002 mm

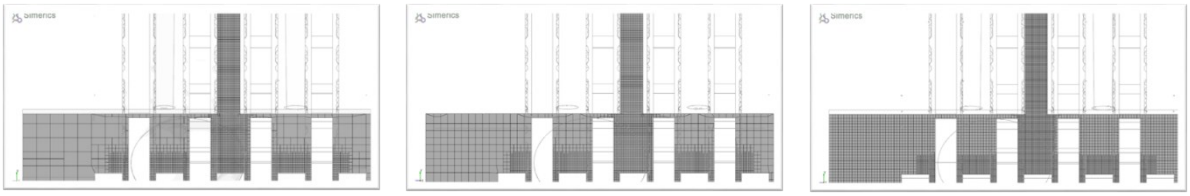

Figure 40: Exemplary sections of the computational meshes of the CFD model from [Mot21]

Figure **41** compares the calculated specific oil flow rate through the groove gaps for each mesh-type. The results are independent of mesh resolution for the studied configurations.

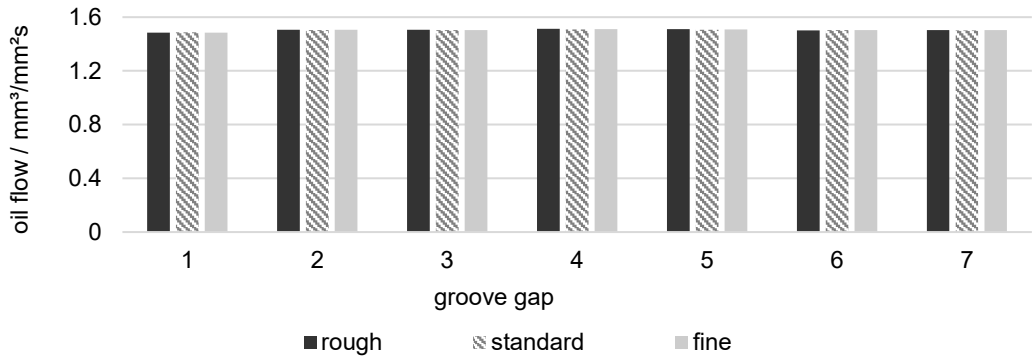

Figure 41: Comparison of oil flow through groove gaps depending on mesh-type (variant I, L-301, ϑ_{oil} = 40 °C, static operation ST3) from [Gro22]

Figure **42** compares the arithmetic mean of the axial force due to oil pressure in the grooves depending on mesh type. A nearly mesh independent solution is achieved with the standard mesh.

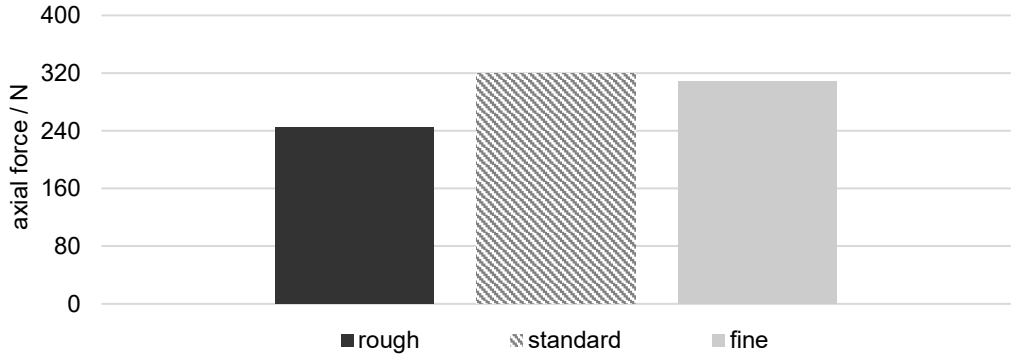

Figure 42: Comparison of axial forces due to oil pressure in the grooves depending on mesh type (variant I, L-301, ϑ_{oil} = 40 °C, static operation ST3) from [Gro22]

The results show that the standard mesh seems to be the optimal compromise between solution accuracy and computational effort and is therefore used for all further calculations.

Based on the results of the mesh study, a time-step-study is executed for the dynamic operating points. The time step is defined in terms of a fixed angular rotation (e.g. [Ter18a]). The study compares the results according to the method in the mesh study by varying the time step between an angular rotation of 1° and 2°. The difference in the results is smaller than 2 %, but calculation times can be nearly halved by using the coarser time step. All dynamic simulations are therefore set up to rotate 2° per time step.

6.3.3 Validation of Calculated Oil Pressure

The numerical model is validated by comparing the calculated pressure in the inlet region with pressure measurements (see section 5.4). Figure 43 shows the increase of oil pressure with rising oil flow rates in both simulation and measurements. The simulation results are consistently lower than measurement data. The difference is within 10 %. The same trend, with comparable relative differences, can be observed for the other static operating points.

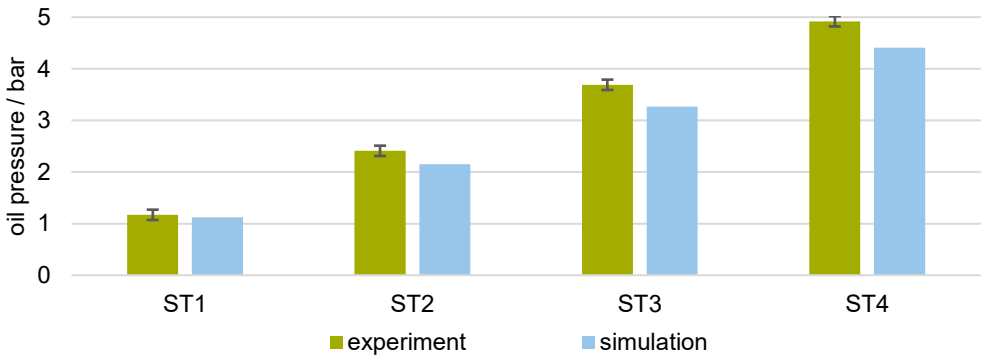

Figure 43: Comparison of oil pressure in the inner carrier region between simulation and measurement data (variant I, L-301, ϑ_{oil} = 40 °C, static operations), error bars indicate 2.5th/97.5th quantile from [Gro22]

In dynamic operations, the pressure likewise increases with rising oil flow rates and the simulation results are consistently calculated lower compared to data from the test rig.

In addition, compared to static cases, the overall pressure level is reduced as rotational speed increases. The most likely causes are a combination of lower oil viscosity in the grooves due to heating during sliding operation and the support of oil transport due to centrifugal forces.

The comparison between numerical and experimental results is challenging due to the numerical results' strong dependence on input parameters (a.o. [Gro20, Pay94]). Since the calculation domain is based on the nominal geometry of the technical drawings, a perfect match between simulation results and measurement data is not expected. Differences can be associated with, e.g., deviations of the groove geometry due to manufacturing processes, uncertainty in the measurements that define input parameters, and the simplifications of the flow problem. Regardless of these circumstances, the validation showed that the simulation model can reproduce the trend and values of the measurement data accurately.

6.3.4 Plausibility of Calculated Heat Transfer Coefficients

The potential analysis for calculation of heat transfer coefficients is a two-step procedure. First, the numerical calculation of the heat transfer is validated by comparison with an analytic solution. For this purpose, the groove geometry is converted into an equivalent pipe cross-section. Table 21 summarizes the geometrical parameters of the groove patterns of the two industrial clutches. Furthermore, the length of the hydraulic and thermal entrance is estimated by means of analytical equations. The thermal entrance length exceeds the groove length for both clutches. The assumption of a thermally fully developed flow does not fit in real world operations and the calculation of the heat transfer coefficient should be performed numerically (see [Pol09]).

Table 21: Geometric and calculated parameters for heat transfer for the groove patterns of clutches D123 and D148

clutch	D123	D148
equivalent pipe diameter	0.12 mm	0.15 mm
groove length	18.5 mm	18.3 mm
hydrodynamic entrance length	0.1 mm	0.2 mm
thermal entrance length	35 mm	43 mm

In the first stage, the validation is based on model assumptions and therefore the calculation method assumes a laminar, thermally and hydraulically fully developed pipe flow with temperature-independent material values. For this pipe flow (cross-section equivalent to groove), the heat transfer coefficients are determined both analytically and by CFD simulation. A specific oil flow rate of 0.5 mm³/mm²s is supplied and the CFD calculations are terminated as soon as the residuals of pressure, velocity and temperature

were less than 1e-6. Table 22 summarizes the results of the calculations. The CFD simulation shows very good agreement with the analytical solution. Thus, the validation of the calculation approach is successful.

Table 22: Comparison of the calculated heat transfer coefficients by means of analytical solution and CFD simulation

clutch	D123	D148
$\alpha_{CFD,outlet}$	1,309 W/m²K	1,880 W/m²K
$\alpha_{analytical,outlet}$	1,309 W/m²K	1,833 W/m²K
$\frac{\alpha_{CFD,outlet} - \alpha_{analytical,outlet}}{\alpha_{analytical,outlet}} \cdot 100\%$	0 %	3 %

In the second stage of the potential analysis, the heat transfer coefficient is determined for an operating point of clutch D123 on a CFD model considering the real clutch geometry. The aim of the second stage is to prove that the calculations can be transferred to real clutch geometries and operating conditions. The qualitative evaluation of the temperature distribution on the steel plate from the CFD calculation shows an almost linear increase in temperature as a function of radius. Stage two of the potential analysis was thus successfully completed by demonstrating the transferability of the calculation approach. As a result, a three-dimensionally resolved oil and temperature distribution as well as the heat transfer coefficients between the components are available. The calculation time per operating point is approx. 10 hours on a node of the CoolMuc2 cluster (28 cores). For application of the new method and for the evaluation of the reliability of the calculated values, extensive validations and, if necessary, parameter variations are still necessary, which cannot be covered within the scope of a potential analysis.

6.4 Experimental Investigations for Visualization of Oil Flow

Under the guidance of the author, the results concerning experimental investigations for the visualization of oil flow were supported by the student research project of Schermer [Sch22a]. The following subchapters give a brief overview about the main findings.

6.4.1 Geometrical Quality of 3D Printed Parts

To check the quality of the 3D printed components for visualizing the oil flow, the focus is placed on the grooves of the friction lining, since the dimensions of the grooves lie within the range of the minimum vertical print resolution of the 3D printer. The quality of the printed geometry and parts from series production is examined using the optical 3D measurement method Focus Variation.

Figure 44 shows the adoption of the measured groove cross-section of a plate from serial production in comparison to the nominal cross-section of the groove from the production drawing. The depth and radius of the groove are reproduced very accurately in the manufacturing of the groove and can be adopted for 3D printing. The edge of the groove is rounded during manufacturing. This effect is approximated with a radius of 0.25 mm in 3D printing.

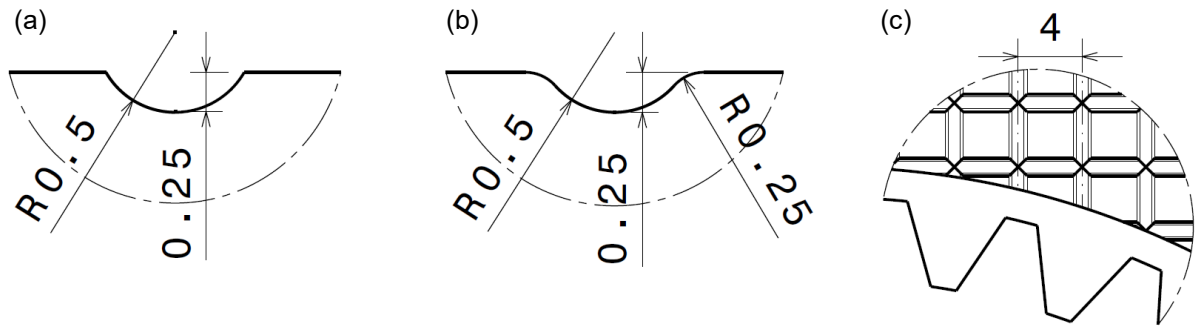

Figure 44: Data of grooves in friction lining D123: nominal groove cross-section from production drawing (a), adopted groove cross-section from measurement of series parts (b) and groove pattern (c) from [Sch22a]

When manufacturing in the 3D printer, all alignments of the components in the installation space are possible. Furthermore, the layer thickness can be varied during printing. Depending on the orientation of the components, additional support structures are printed. To ensure high printing quality, support structures should not be applied to surfaces such as friction interfaces with high surface quality requirements. Figure 45 shows examples of different component orientations and the associated support structures. To check the influence of the printer settings on surface quality, components are printed in horizontal, vertical and diagonal orientation. In the case of diagonal alignments, the components are aligned at an angle of 45° to the base plate. Furthermore, the layer thickness is varied from 50 to 100 µm.

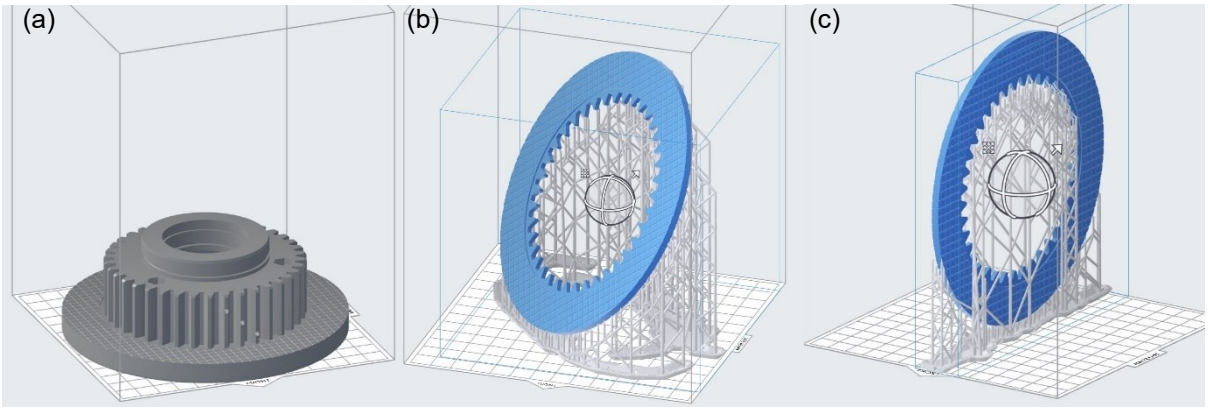

Figure 45: Different orientations of components for 3D printing: inner carrier with friction lining in horizontal orientation (a), friction plate in diagonal orientation (b) and friction plate in vertical orientation (c) from [Sch22a]

To investigate the surface quality, the contour of the groove on the friction interface is measured with the optical focus variation after printing. The vertical and horizontal resolution of the measurement is 1.75 µm.

Figure 46 shows an example of the comparison of the groove cross-section of the printed components with vertical and diagonal orientation with a layer thickness of 50 µm. It is noticeable that two measurements of the vertical orientation roughly correspond to the course of the diagonal measurements, while the other two show a significantly narrower groove. The vertically printed plate is oriented along its axis of rotation such that half of the grooves are upright in the printing space, while the others lie in its x/y plane. The quality of the upright grooves only depends on the precision of the UV laser and therefore matches the CAD data well. The groove cross-sections that run in the plane also depend on the accuracy of the individual resin layers. In addition, one side of these groove cross sections represents an overhang. While the printer can create this overhang, it obviously must compromise on precision. The vertical orientation is thus not recommended for an exact reproduction of the groove geometry.

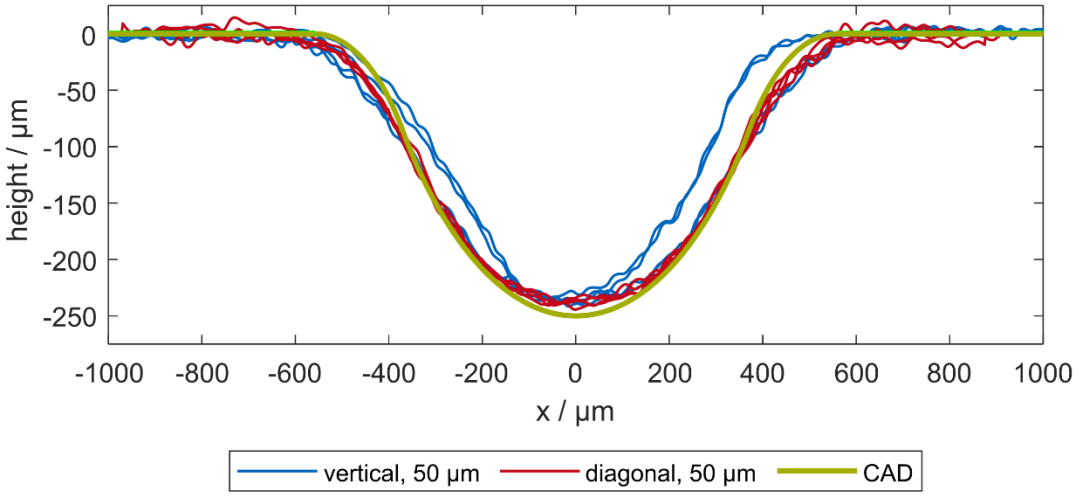

Figure 46: Four contour measurements each of the printed groove cross sections (layer thickness 50 µm) in vertical and diagonal orientation in comparison with the CAD data from [Sch22a]

Further investigations have shown that the diagonal orientation with a layer thickness of 50 µm provides suitable printing results for the planned investigations (see [Sch22a]).

In addition to the quality of the printing geometry with small details in the µm range, the accuracy of the entire component geometry is also assessed. For this purpose, the dimensions of the inner carrier and the clutch cover are checked. All of the outer diameter, inner diameter and small bores show deviations of +/- 1% maximum.

The vertical dimensions, on the other hand, show an absolute deviation in the range of +0.63 mm to +0.82 mm. This is within the range of the printer's correction of the z-compression to the printing platform. Comparing the vertical measurements within the part instead of to the printing platform, the same percentage deviation of +/- 1% is found as for the horizontal dimensions before. Since the inner carrier and the clutch cover are oriented to each other in terms of their printing direction in the assembled state, the z-compression has no influence on the planned test execution.

6.4.2 Transparency of the Material

The more transparent the parts are, the more reliable are the statements that can be made about the lubrication situation. Therefore, the improvement of the component transparency by polishing as well as with an additional wetting with mineral oil is investigated.

Figure 47 shows a transparent test print part with a thickness of 3.25 mm. The test graphic in the background consists of lines of thickness 2.0 mm to 0.5 mm and helps to assess the transparency of the printed part. Figure 47 (a) shows the component without treatment after washing with isopropanol. For Figure 47 (b), the surfaces on the front and back were treated by hand with a plexiglass polish. The remaining surface texture on the right half shows the progress after about two minutes, while the left half was polished for about five minutes. Figure 47 (c) shows the same area after it has been wetted and rubbed with mineral oil. The difference in polishing progress between the left and right sides is almost negligible.

The components are therefore pretreated for all tests with the plexiglass polish before being dipped in the mineral oil used for the corresponding test.

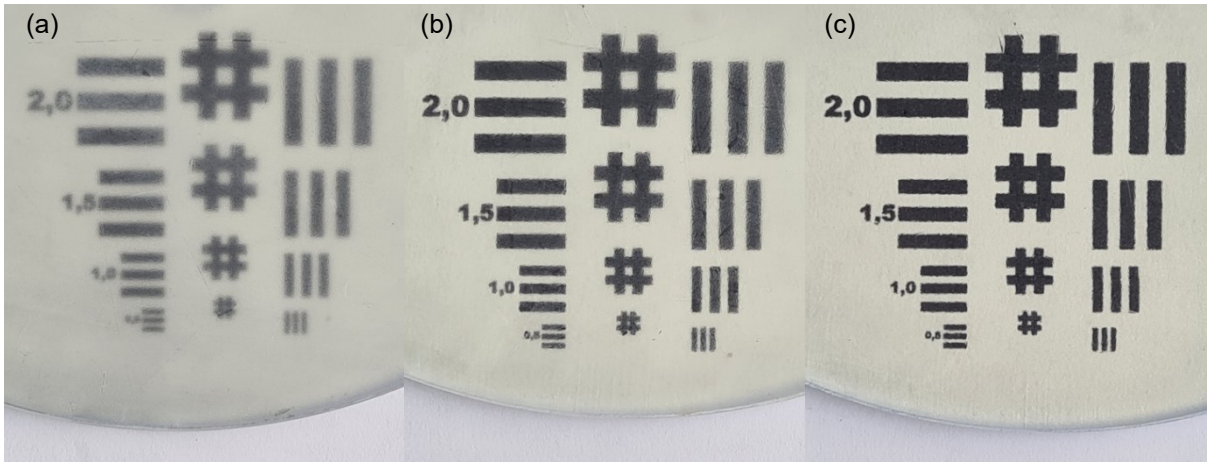

Figure 47: Test print with a thickness of 3.25 mm: no treatment (a), treated with plexiglas polish (b) and additionally rubbed with mineral oil (c) from [Sch22a]

7 Results and Discussion

This chapter presents and discusses the influences of investigated parameters on the thermal behavior. For this purpose, circumstances that have a significant influence on thermal behavior, such as the oil filling behavior, oil distribution and the influence of the oil on axial force in sealed clutches, are considered. Furthermore, temperature behavior is investigated on the basis of characteristic values (e.g. temperature rise, heat transfer coefficients). The results of the different investigation methods are presented and interpreted in the conclusions. The temperature calculations of the real-time model have already been used for the validation and can therefore be found in chapter 6.1.

7.1 Visualization of Oil and Dynamic Filling Behavior

To describe the results of the measurements according to the setup and test conditions described in section 5.5, the symbols (o, x, --- and Δ) are introduced. Therefore, Figure 48 shows exemplary snapshots of the four characteristic points in time that are used to characterize dynamic filling behavior. The symbols (o, x, --- and Δ) mark characteristic times. In the top left image (o), oil reaches the first two oil distributor holes, while the third is still empty. The top right image (x) shows all three holes filled with oil and with no air bubbles. The moment when the oil reaches the observed interface (---) is defined as the zero point in time. Accordingly, all events before and after this moment are provided with negative and positive times. The direction of rotation of the inner carrier is counterclockwise. The oil is distributed along the stationary steel plate until the entire interface is filled with oil (Δ). More details and results concerning the visualization of oil flow can be found in [Sch22a].

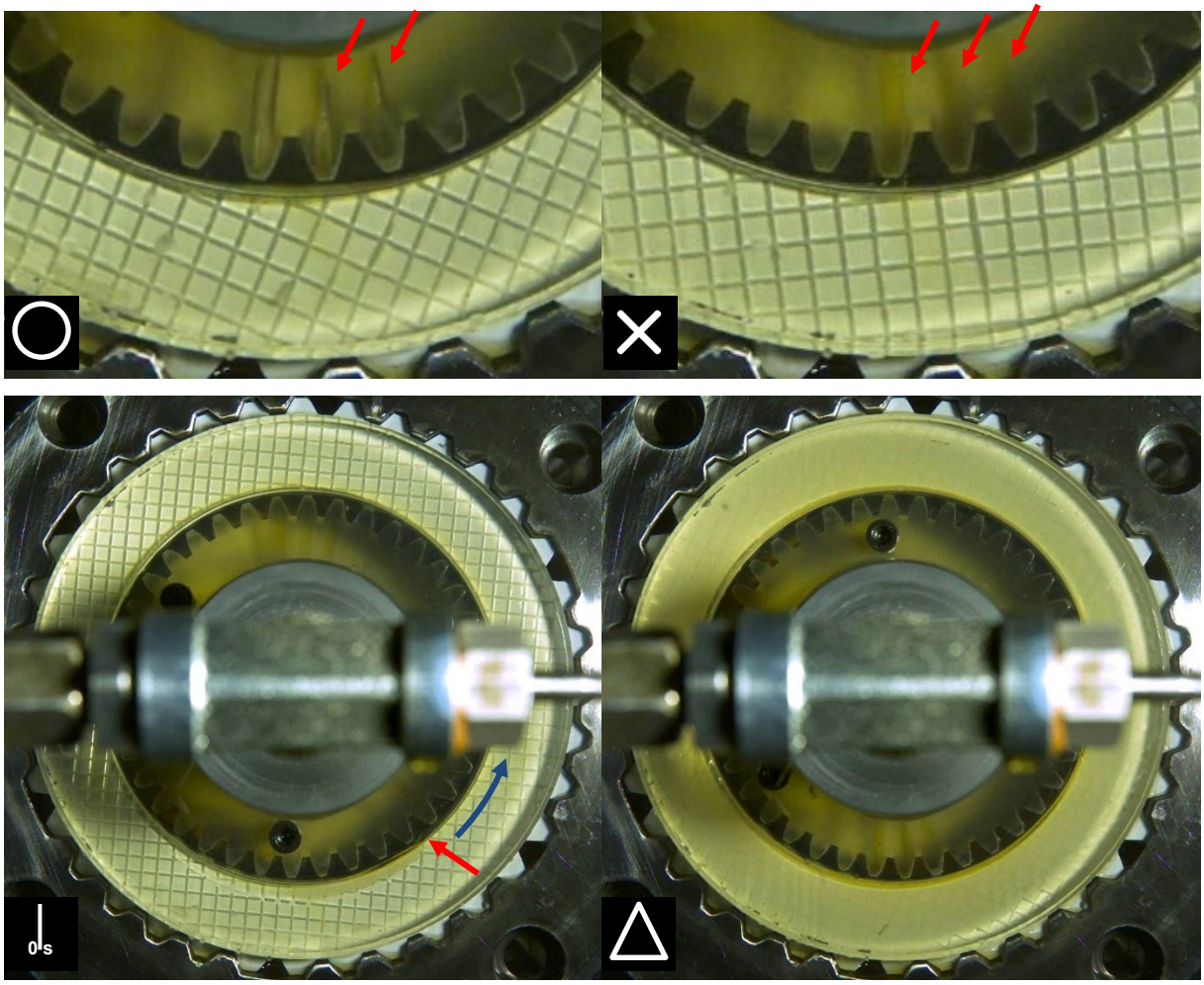

Figure 48: Exemplary snapshots of the observed time points (LS1, D123, 8 friction interfaces): Oil reaches oil distributor holes (o), no air in oil distributor holes (x), oil reaching first interface (---) and first interface filled (Δ) from [Sch22a].

7.1.1 Filling Behavior with Eight Friction Interfaces

Figure 49 shows the effect of the variation of the oil flow rate on the characteristic times (o, x and Δ) in the time domain for two load stages (LS1, LS2 details in Table 12). The setup corresponds to geometry variant I from the CFD simulation. One repetition was performed for each load stage. The specific oil flow rate v_{oil} is plotted on the y-axis, while the load stages correspond to a variation of the differential speed Δn that is indicated by the colors blue (LS1) and orange (LS2).

The results show that all processes are faster with increasing flow rate since the characteristic times are closer together. With increasing flow rate, the clutch requires less time to convey the oil from the oil distributor holes (o) to the first interface, and less time to fill the entire interface (Δ). The same relationship can be seen regarding differential speed. If the speed increases, the processes also run faster. In particular, the time required to supply the oil from the oil distributor holes (o) into the interface is shortened when the differential speed is increased. The repetition of the load levels proves that the behavior of the oil filling behavior is repeatable. The two measuring points of the characteristic times (o) and (Δ) are close to each other in each case.

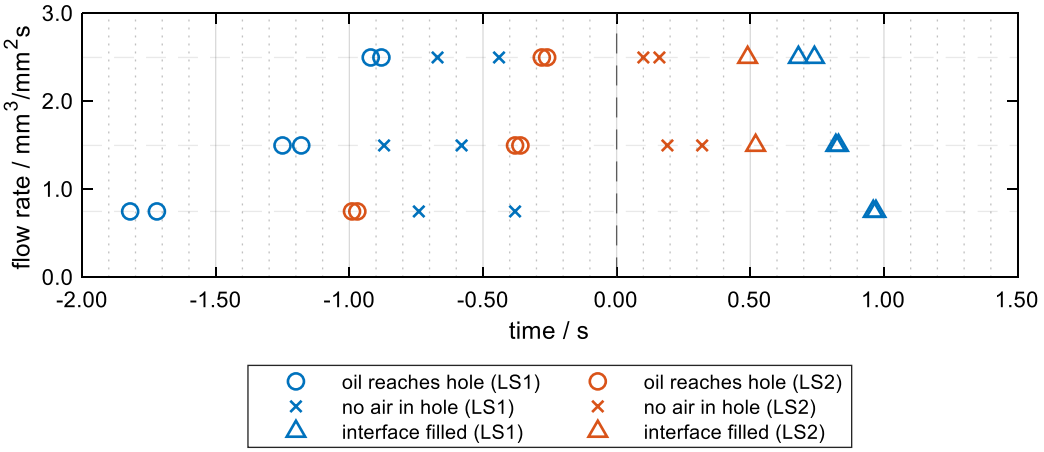

Figure 49: Differences in dynamic filling behavior in time domain with eight friction interfaces depending on specific oil flow rate $\dot{v}_{oil}$ and differential speed Δn (LS1, LS2), oil reaches the interface at 0s, D123, variant I from [Sch22a]

Larger variations can be seen when observing the characteristic time (x) at which the oil distributor holes in the inner carrier are filled with oil. At low speeds, the oil distributor holes are already free of air before the oil reaches the first interface. At high speeds, on the other hand, it takes longer, so that the oil distributor holes are not free of air until the oil reaches the interface. A plausible explanation is that this behavior is related to the conveying effect of the centrifugal force. If the speed is high enough, more oil is conveyed radially outward at the beginning than is supplied (see [Düm84]).

The correlation between rotational speed and flow rate also explains the filling behavior at the lowest flow rate of 0.75 mm³/mm²s. At load stage LS1 with $\dot{v}_{oil} = 0.75\ mm^3/mm^2$, Figure 49 shows that it takes a long time for the holes to be free of air (x) compared to the load stages with higher flow rates. At load stage LS2 with $\dot{v}_{oil} = 0.75\ mm^3/mm^2$, the holes are never free of air in the period under consideration. It can be assumed that the high centrifugal force continuously conveys more oil to the outside than supplied. This also means that the first interface is never completely filled with oil.

The axial positions of the oil distributor holes of the inner carrier are located below the three inner steel plates. This means that oil flows directly onto the six inner friction interfaces. The first and last friction interface therefore depend on axial distribution of the oil in the splines. The combination of high speed and low flow rate ($\dot{v}_{oil} = 0.75\ mm^3/mm^2$) in LS2 ensures that the delivered oil is conveyed radially outward by centrifugal forces before it can distribute axially to the first interface. Due to the symmetrical design of the clutch, the observed phenomena should also apply to the last interface. In both repetitions of LS2 with $\dot{v}_{oil} = 0.75\ mm^3/mm^2$, only small amounts of oil flow into the interface. The oil is then

dragged along the stationary steel plate by the rotating lining interface and conveyed slowly to the outside. The interface remains permanently half-filled this way.

7.1.2 Filling Behavior with Four Friction Interfaces

Figure 50 shows the identified characteristic times (o, x and Δ) in the time domain for the different load stages and flow rates with four friction interfaces. This setup corresponds to geometry variant I from the CFD simulation.

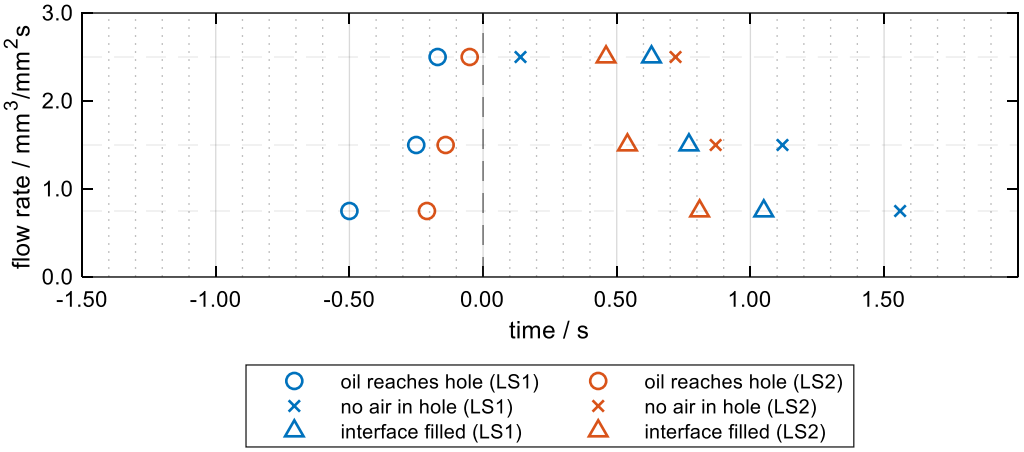

Figure 50: Differences in dynamic filling behavior in time domain with four friction interfaces depending on specific oil flow rate $\dot{v}_{oil}$ and differential speed Δn (LS1, LS2), oil reaches the interface at 0s, D123, variant I from [Sch22a]

In this test setup, the axial position of the first friction interface is directly lubricated from the oil distributor holes. Therefore, no axial distribution of the oil into the splines is required to enter the friction interface. Compared to the setup with eight friction interfaces, the oil enters the interface earlier (o). Higher speed and flow rates also accelerate the filling process.

The setup with four friction interfaces gets completely filled with oil at all load stages and flow rates. Thus, the single-phase flow assumption of the CFD simulation is experimentally validated.

Analyzing the clutch geometry, assuming that the flow at the first interface in the setup with four friction interfaces is nearly equal to the flow in the third interface of the setup with eight friction interfaces seems appropriate. For proof of this assumption, a test with a transparent “steel” plate was installed. However, the complex geometry of the 3D-printed friction plate makes it difficult to assess the oil flow in the third gap due to the many reflections in the grooves. In addition, the groove pattern of the clutch cover and the plate overlap, making visibility even more difficult.

Figure 51 (a) shows the oil-free test setup and Figure 51 (c) shows the moment when the oil reaches the first interface. This can be seen from the clear edge that forms when the oil wets the clutch cover. In Figure 51 (b), the oil already enters the interfaces between the rear plates. However, the moment at which the oil reaches the third or second gap is difficult to define. It does, however, confirm the assumption that in the design with eight friction interfaces, the direct lubricated interfaces in the center of the clutch package are more likely to be supplied with oil than the first interface, which relies on axial distribution of the oil.

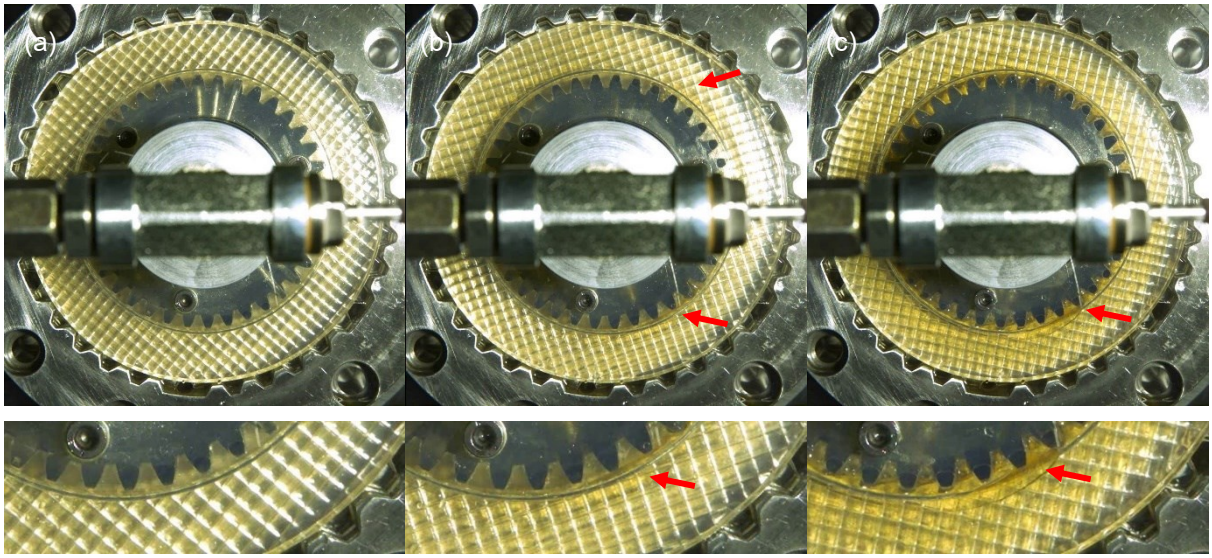

Figure 51: Test image of the test setup with eight friction interfaces with view into the third air gap (first “steel” and “lining” plate are transparent), D123, variant I from [Sch22a]

7.1.3 Influence of Oil Distributor Pattern on the Filling Behavior

The following section shows the influence of the variation of the oil distributor pattern in the inner carrier on the oil supply. For this purpose, six of the nine holes in the inner carrier are sealed with a plug. Thus, the oil distributor pattern variant II is achieved, as described in section 5.3.1.

By comparing Figure 50 and Figure 52, it is obviously that the moment (x) at which the oil distributor holes in the inner carrier are filled with oil is earlier since the same flow rate transitions through a third of the former cross-section. Another difference between the results under varying oil distributor patterns are the times when the first interface is filled at LS1. The filling procedure with variant II takes a little longer, since the three axial positions are flushed with oil only once instead of three times per revolution. At high speed (LS2), the conveying effect of the centrifugal force has enough influence to fill the interface quickly.

Comparing Figure 50 and Figure 52 also shows that the oil distributor pattern variant has a very small influence on the steady-state flow behavior. Both patterns achieve complete filling of the interface (Δ). This observation is consistent with the results from the CFD simulation in section 7.2.3.

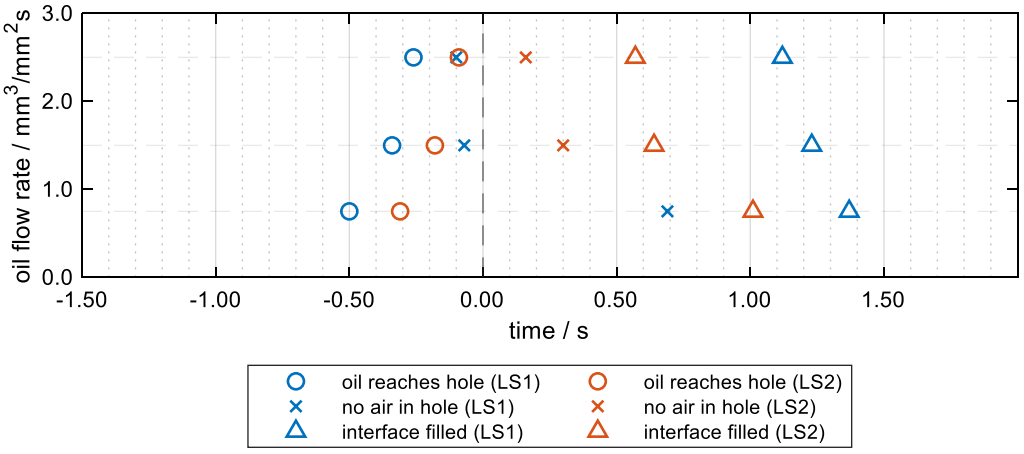

Figure 52: Dynamic filling behavior with four friction interfaces depending on specific oil flow rate v_{oil} and differential speed Δn, oil reaches the interface at 0s, D123, variant II from [Sch22a]

In contrast, the results in Figure 53 of the filling behavior with eight friction interfaces and the oil distributor pattern variant II differ from the results of variant I (compared to Figure 49). Here, only the lowest and highest flow rates were recorded. A little more time elapses until the oil from the holes

reaches the first interface, while filling the interface takes significantly longer. Even when the interface fills completely with oil and reaches a steady state, it can be assumed that the heat dissipation in this gap is weaker than at the better supplied inner interfaces. Together with the previous findings, it can be concluded that the filling behavior and oil distribution of the clutch benefits more from uniform axial distribution of the oil holes in the inner carrier, ensuring direct lubrication of the interfaces than from uniform radial distribution of the oil distributor holes.

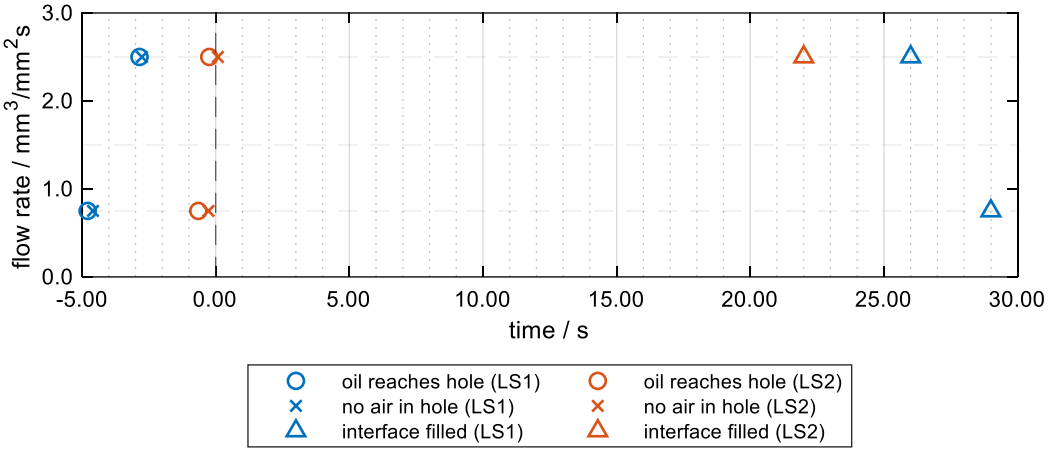

Figure 53: Dynamic filling behavior with eight friction interfaces depending on specific oil flow rate v_{oil} and differential speed Δn, oil reaches the interface at 0s, D123, variant II from [Sch22a]

7.2 Thermal Behavior and Temperature Distribution

In the following, the results of the experimental and simulative investigations are analyzed.

7.2.1 Influence of Lubrication and Clutch Type

In the following, the results of the investigations on the brake test rig KLP-260 during continuous slip are described. The setup and test conditions are detailed in section 5.4.

Figure 54 and Figure 55 show the axial temperature distribution and the mass temperature of the outer carrier at load stage LS1 at different oil flow rates for different clutches. The test setup is preconditioned to an oil injection temperature of 60 °C by lubricating it at least 30 minutes before the tests start. The tests without lubrication were started at room temperature of approx. 30 °C. An increase in the supplied oil flow rate leads to a reduction in all measured temperatures in the area under investigation. This is because the lubrication of the interfaces is not solely dependent on the conveying effect of the centrifugal force, since the clutch is sealed and there is no possibility of axial outflow. Thus, even at low speeds, a higher oil flow rate contributes to the cooling of the plate package. Furthermore, the variations in the axial temperature distribution are very small. The measuring positions on the steel plates at the output and piston side typically indicate a temperature that is about 1 ... 2 K lower than at the measuring position in the center steel plate. Therefore, the temperature in the middle steel plate is usually considered in the following observations. The temperature development in the outer carrier changes with the temperature level in the steel plates and is significantly lower than that of the steel plates due to the large thermal mass and because there is no friction interface at the carrier.

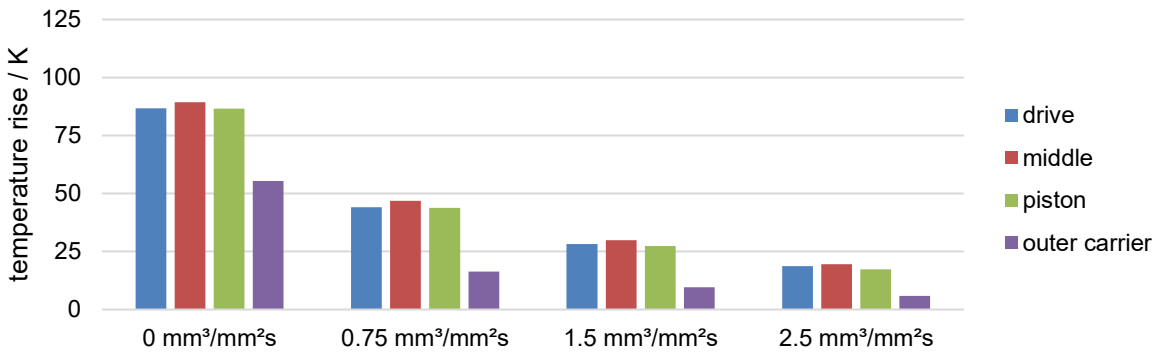

Figure 54: Comparison of median temperature rise at different locations in continuous slip LS1, D148, variant I, L-301 at different specific oil flow rates, ϑ_{oil} = 60 °C

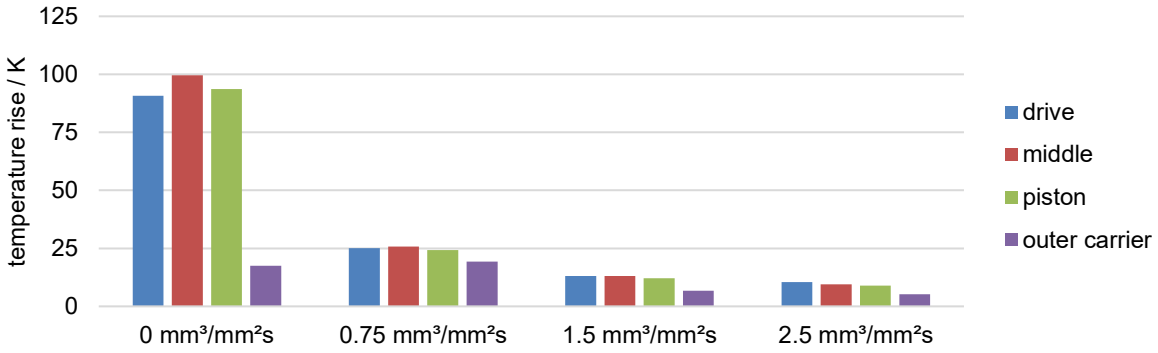

Figure 55: Comparison of median temperature rise at different locations in continuous slip LS1, D123, variant I, L-301 at different specific oil flow rates, ϑ_{oil} = 60 °C

7.2.2 Variations in Operating Conditions

The influence of a variation of the speed in continuous slip on the average steel plate temperature is pictured in Figure 56 and Figure 57 for two different clutches. In each case, the results of an initial test and a repetition of the test at a later point in time are shown. The results indicate a continuous increase in the mean steel plate temperature as a function of the applied friction power. There is a higher temperature level with D148 compared to the tests with D123. On the one hand, this is due to the larger contact area with the connecting components of the thicker plates (D123). In addition, the D148 plates generate higher frictional power under otherwise identical operating conditions due to a higher CoF. Both clutch systems could be operated with internal lubrication in the planned test range without violating the abort criterion of a mean steel plate temperature above 200 °C.

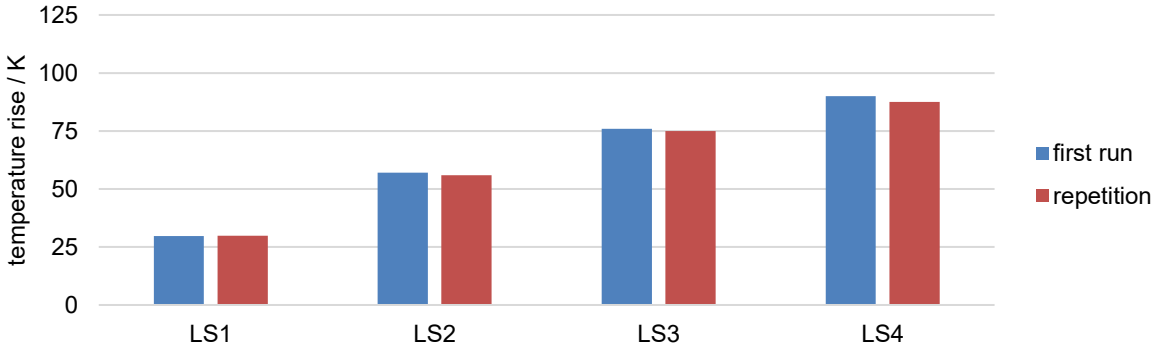

Figure 56: Comparison of the medians of the temperature rise during continuous slip of the first run and a repetition, D148, variant I, v_{oil} = 1.5 mm³/mm²s, L-301, ϑ_{oil} = 60 °C

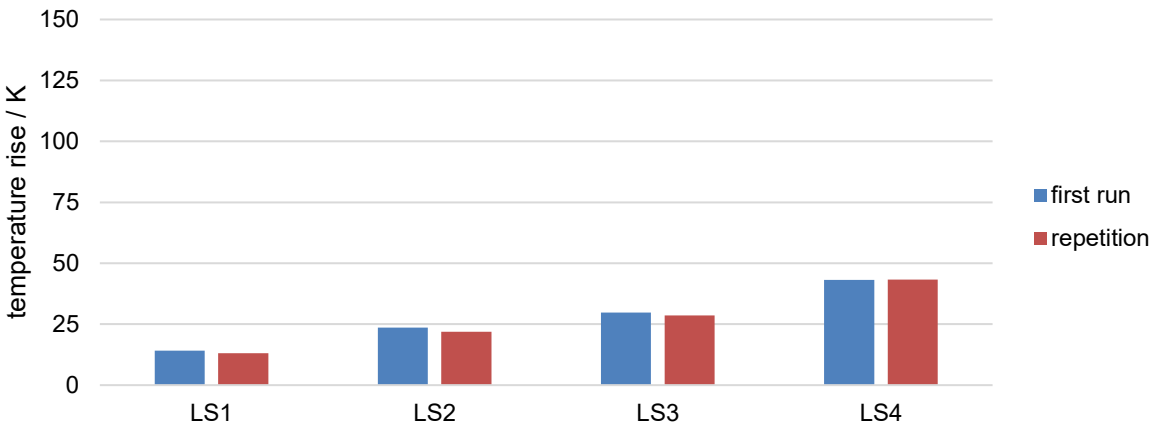

Figure 57: Comparison of the medians of the temperature rise during continuous slip of the first run and a repetition, D123, variant I, v_{oil} = 1.5 mm³/mm²s, L-301, ϑ_{oil} = 60 °C

Figure 58 and Figure 59 show exemplary box plots of the temperature rise during shifting cycles. Compared to continuous slip, the axial position has a greater influence on the temperature rise (see Figure 54 and Figure 55). The values of the median temperature rise at the measuring point on the drive and piston sides are significantly lower than the median of the temperature rise in the middle steel plate.

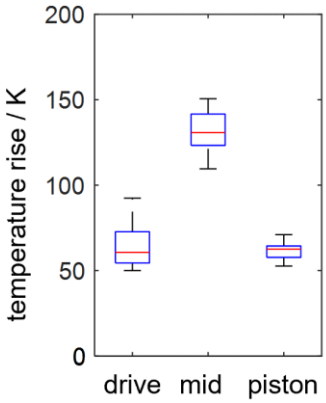

Figure 58: Temperature rise at different axial measuring positions for load level LL4, D148, variant I, internal lubrication v_{oil} = 1.0 mm³/mm²s, L-301, ϑ_{oil} = 60 °C

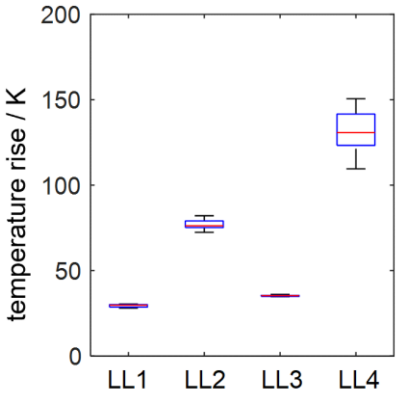

Figure 59: Temperature rise at different operating conditions in the middle steel plate during shifting cycles, D148, variant I, internal lubrication v_{oil} = 1.0 mm³/mm²s, L-301, ϑ_{oil} = 60 °C

Figure 59 illustrates the influence of operating conditions on the temperature rise during shifting cycles. The critical temperature rise in the middle steel plate is shown. At low sliding speeds (LL 1/3), a lower temperature rise occurs than at the load stages with higher sliding speeds (LL 2/4). Furthermore, higher temperature rises are accompanied by a larger scatter band. An increase in surface pressure also increases the temperature rise (LL1 vs LL3 or LL2 vs LL4).

7.2.3 Variations of Oil Distributor Patterns

Figure 60 to Figure 62 show experimental results for quantifying the influence of the design of the oil distributor pattern through the inner carrier (variant I / II) during continuous slip. Figure 60 and Figure 61 show the measured pressure in the oil supply. This can be regarded as representative pressure for the region in the inner carrier, since there is no reduction in the cross-sectional geometry up to the oil feed holes, and the hydraulic pressure should therefore be the same. The measurements show that the oil pressure decreases with increasing differential speed. This observation is independent of the pattern of oil feed holes. Reducing the number of oil feed holes from 9 (variant I) to 3 (variant II) leads to an

increase in oil pressure in the inner carrier in all load stages. This can be largely attributed to the reduction in the hydraulic cross-section at constant volume flow.

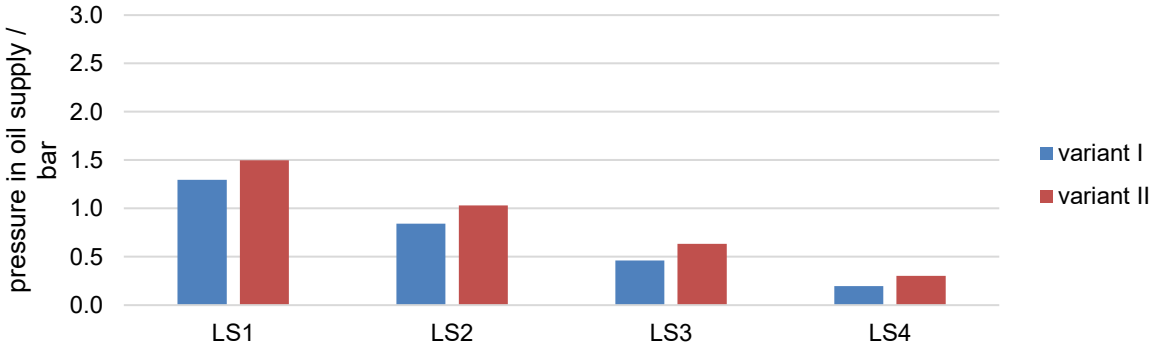

Figure 60: Comparison of the pressure in the oil supply in continuous slip, D148, oil distributor patterns with variants I/II, internal lubrication v_{oil} = 2.5 mm³/mm²s, L-301, ϑ_{oil} = 60 °C

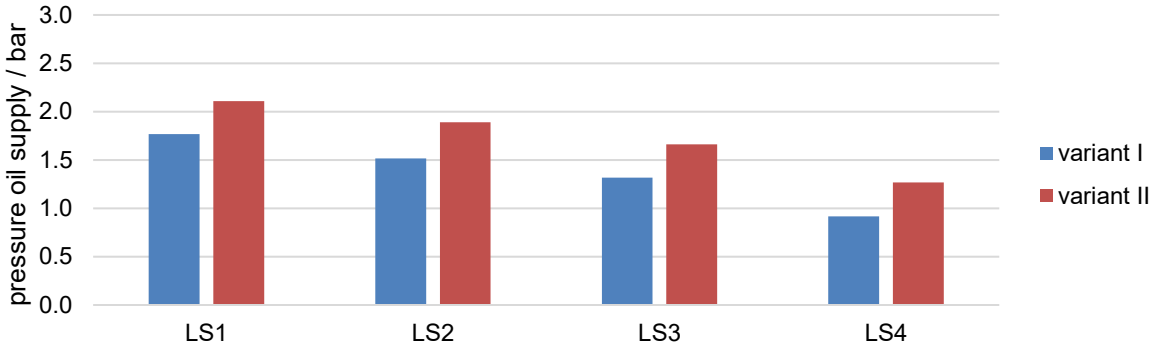

Figure 61: Comparison of the pressure in the oil supply in continuous slip, D123, oil distributor patterns with variants I/II, internal lubrication v_{oil} = 2.5 mm³/mm²s, L-301, ϑ_{oil} = 60 °C

Figure 62 shows the temperature rise during load stages LS1 to LS4 in continuous slip in a comparison of the two oil distributor variants with variation of the oil flow rate at the different axial measuring positions. On the left are the results of variant I (9 oil holes), on the right the results of variant II (3 oil holes).

In addition to the temperature rise, the arithmetic mean of the measured CoF ($\mu_{stat,120}$) during the last 120 s of the load stage and the nominal specific friction power (q_p) are also plotted. Due to the large variations of friction behavior of the investigated sintered friction linings, load stages that show the most similar friction behavior possible were selected for the comparison of the oil distributor variants. This ensures that the energy input is nearly the same, and that the temperature differences can be attributed to the changed lubrication situation.

Analogous to the results from chapter 7.2.1, the temperatures drop with increasing oil flow rate. This effect can be observed at all load stages and for both oil distributor variants.

Axial differences in the temperature rise within the clutch are also very small at all load stages (compare section 7.2.1). It is noticeable that under some test conditions with oil distributor variant I the highest temperature rise occurs at the measuring point in the steel plate near the drive instead of at the measuring point in the middle steel plate. However, since the differences are in the range of 1K and below, the causes of this effect were not investigated further.

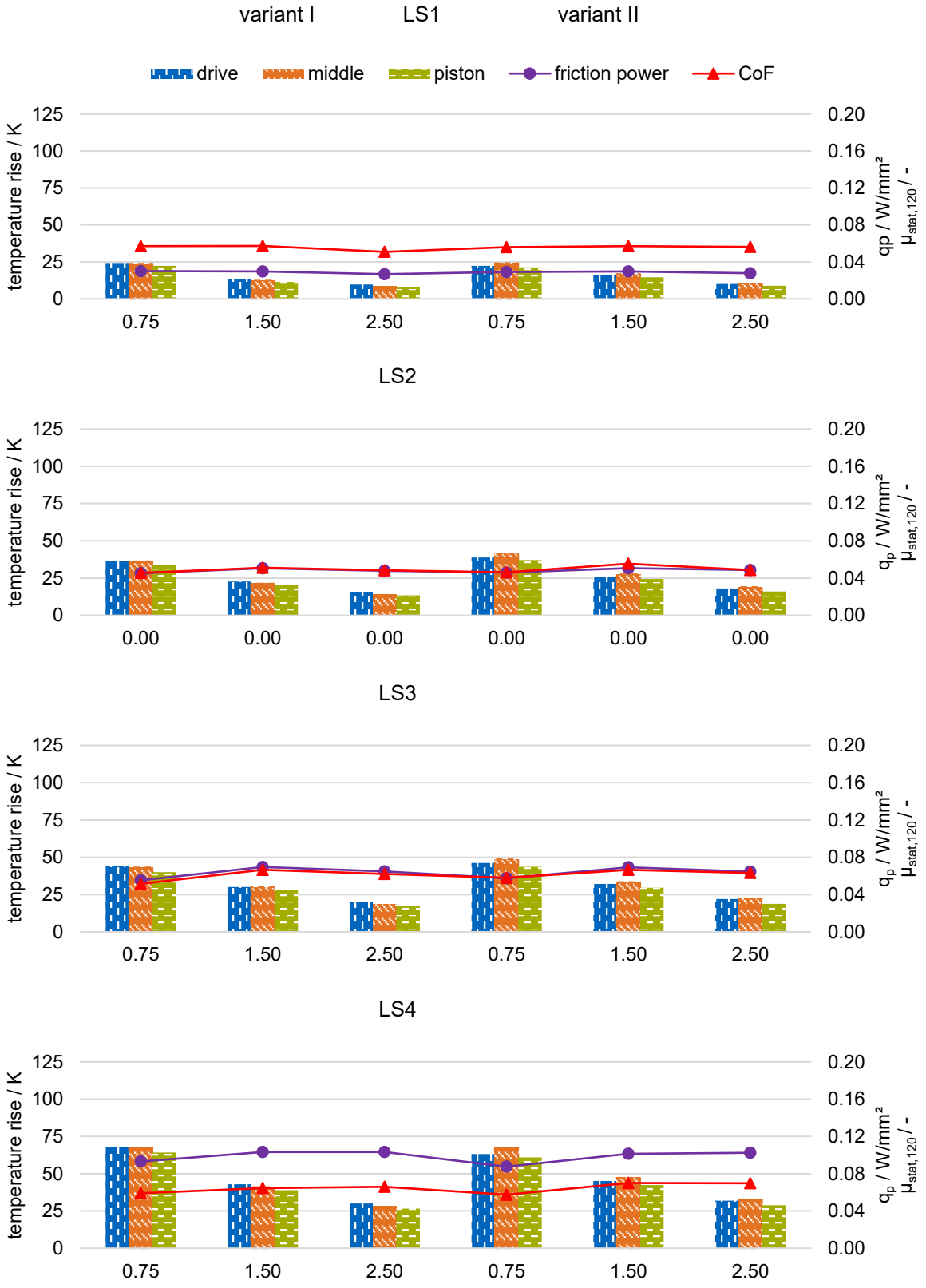

Figure 62: Comparison of temperature rises of load stages LS1 to LS4 with variations of oil flow rate, v_{oil} = 0.75 / 1.5 / 2.5 mm³/(mm²s), variant I (left) and variant II (right), D123, L-301, ϑ_{oil} = 60 °C from [Jan21]

At most load stages, temperature rises with oil distributor variant I are somewhat lower. However, the differences are very small, and in two cases (LS1 $\dot{v}_{oil} = 0.75\ mm^3/mm^2s$, LS4 $\dot{v}_{oil} = 0.75\ mm^3/mm^2s$), the temperature rises are even somewhat lower with variant II. However, it is not possible to speak of a

clear effect here, since the slightly different temperatures in both cases can also be explained by the lower frictional power.

Overall, there is no discernible influence of the oil distributor variant in the inner carrier on thermal behavior. The temperature rises are almost the same for both variants. However, the axial position, the specific friction power, and the supplied oil flow rate clearly influence the thermal behavior.

7.2.4 CFD Simulation: Variations of Oil Distributor Pattern and Operating Conditions

Figure 63 compares oil distribution at each friction interface for variant I and variant II of the oil distributor patterns from CFD simulation in the inner carrier during static operations. The variation in oil distributor patterns does not influence the oil supply at the friction interfaces. The share of total flow rate (ratio of flow rate at friction interface divided by total flow rate) at each friction interface is nearly constant.

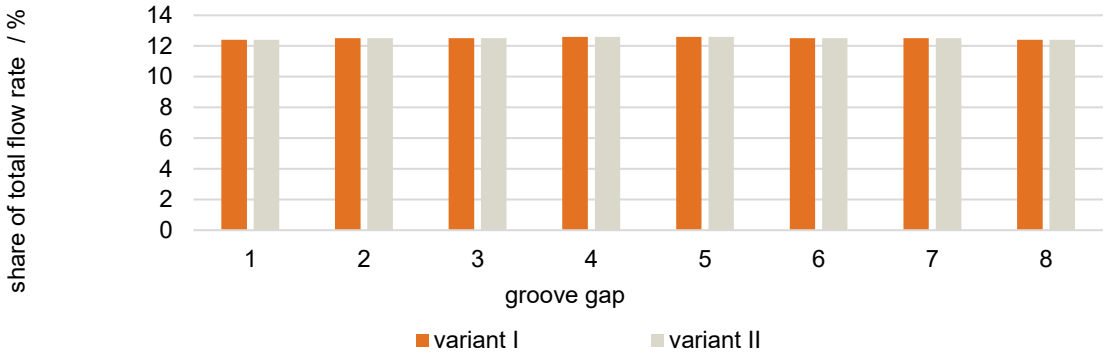

Figure 63: Share of total flow rate at each groove gap with variations in oil distributor patterns (D122, L-301, ϑ_{oil} = 40 °C, static operation ST3) from [Gro22]

The same can be observed for the dynamic cases, as Figure 64 shows. There seems to be no difference in the oil supply, despite the reduction of the radial holes in the inner carrier between variant I and variant II.

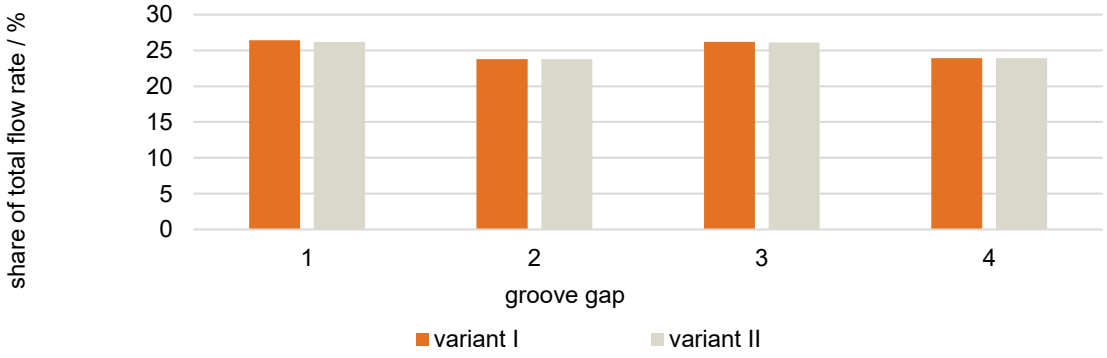

Figure 64: Share of total flow rate at each groove gap with variations in oil distributor patterns (D122, L-301, $\dot{v}_{oil}$ = 2.5 mm³/mm²s, dynamic operation LS4) from [Gro22]

For the sake of completeness, Figure 65 and Figure 66 show the comparison of the reduced surface pressure under variation of the oil distributor pattern. Since the supplied oil at each friction interface is nearly the same in both cases, there is also no difference in the reduction of the nominal surface pressure.

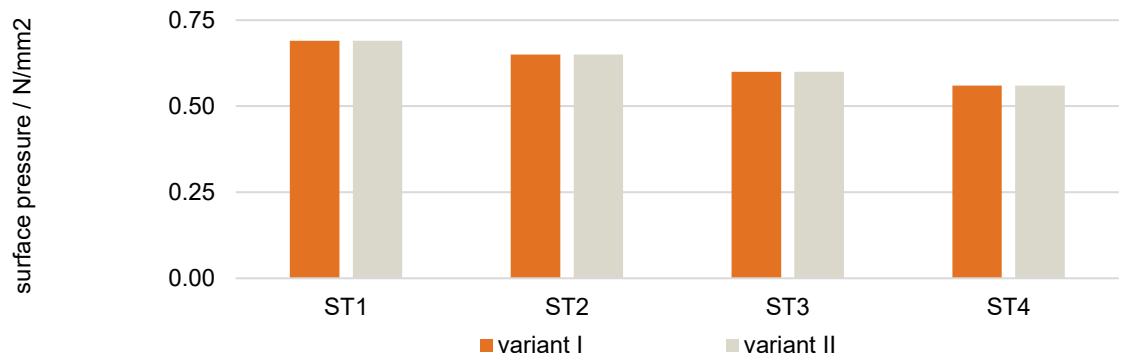

Figure 65: Comparison of reduced surface pressure with variations in oil distributor patterns (D122, L-301, ϑ_{oil} = 40 °C, static operation, p_{nom}=0.75 N/mm²) from [Gro22]

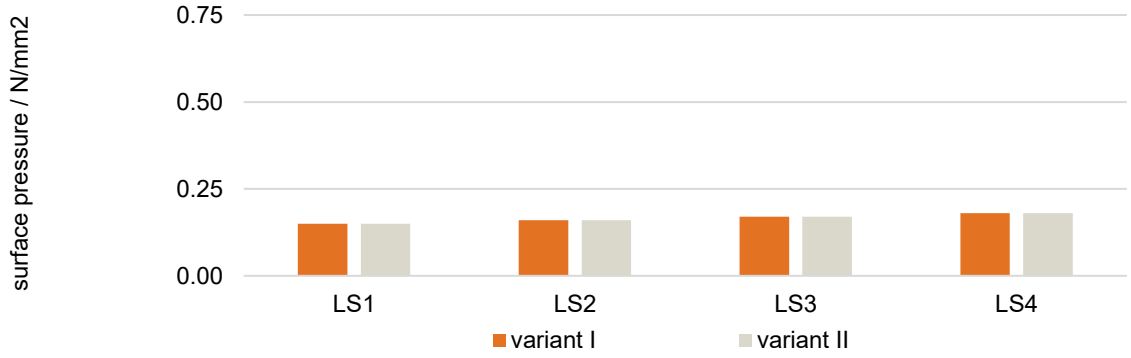

Figure 66: Comparison of reduced surface pressure with variations in oil distributor patterns (D122, L-301, $\dot{v}_{spez}$ = 2.5 mm³/mm²s, dynamic operation, p_{nom}=0.22 N/mm²) from [Gro22]

These results are different from published studies of automotive/motorcycle clutches, in which the authors state that the oil distributor pattern of the oil supply is the main cause for differences in the oil supply at each friction interface [Grü13, Ter18a]. Since the clutch designs in this thesis are sealed, the flow behaves like a hydraulic flow. Therefore, if the value of supplied oil and operating conditions such as rotational speed are constant, oil distribution seems to be independent of oil supply patterns.

7.2.5 Heat Transfer Coefficients during Continuous Slip

The possibility for the simulative determination of the heat transfer coefficients has already been presented within the scope of a potential study in chapter 6.3.4. In the following, results of the practical determination of heat transfer coefficients from measured data and simulation results according to Wohlleber's iterative method are presented [Woh12].

Figure 67 shows an example of the heat transfer coefficients determined in the stitch tests for the operating ranges during continuous slip at low speed investigated for clutch D123. A small scatter band of the determined heat transfer coefficients for this friction pairing can be seen. The average heat transfer coefficient is 8,400 W/m²K and the variation over the different operating points is about +/- 400 W/m²K.

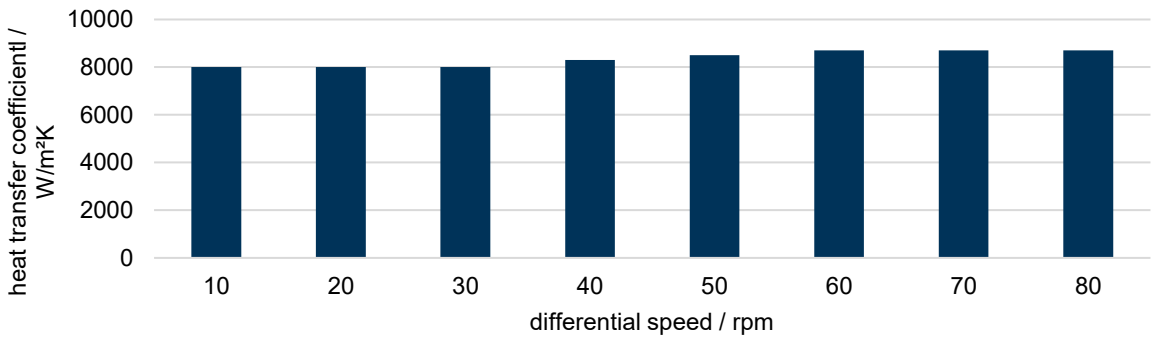

Figure 67: Determined heat transfer coefficients (D123, L-301, $\dot{v}_{spez}$ = 1.0 mm³/mm²s, p = 1.0 N/mm²)

Figure 68 presents the comparison of the calculated and measured steel plate temperatures of the middle plate using the heat transfer coefficients from Figure 67. The deviations between simulation and measurement are very small (< +/- 5 K).

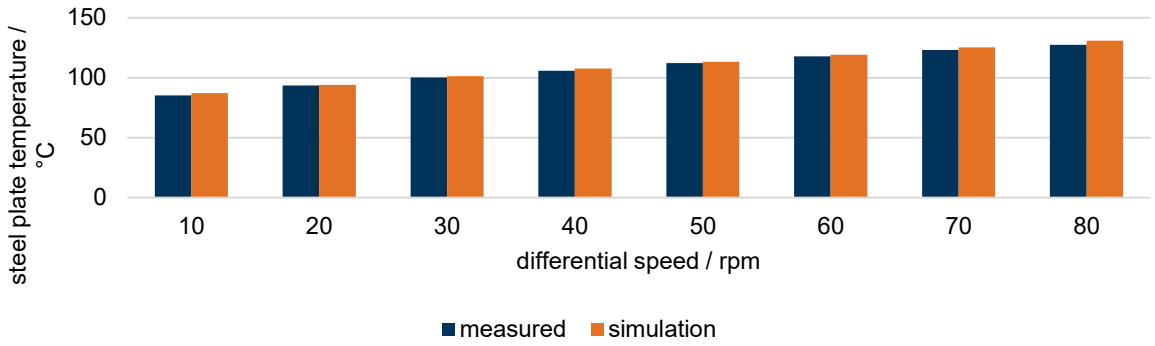

Figure 68: Comparison of the mean steel plate temperature from simulation and measurement (D123, L-301, $\dot{v}_{spez}$ = 1.0 mm³/mm²s)

7.2.6 Reduction of Axial Force due to Pressure Distribution

According to the model described in section 5.3.4, it is possible to calculate the reduced nominal surface pressure in the clutch package from the pressure distribution in the groove channels at the friction interfaces.

Figure 69 (static operation) and Figure 70 (dynamic operation) visualize the pressure distributions of the complete CFD calculation domain. The pressure in the static case (Figure 69) has a nearly constant value in the inlet and outlet regions. In the groove gaps, the pressure drops linearly from the inlet to outlet pressure value. The significant reduction of hydraulic cross-section between the inlet/outlet regions and the groove gaps seems to be the cause of this.

In the dynamic cases at lower sliding velocities (2.5 … 5 m/s), the qualitative pressure distribution is the same as in the static cases. The absolute pressure values are lower than in the static cases, most likely due to the reduction of hydraulic resistance due to the centrifugal forces.

At higher sliding velocities (7.5 … 10 m/s), the pressure distribution looks slightly different. Figure 70 shows an example of pressure distribution in the complete calculation domain for a sliding velocity of 7.5 m/s. The pressure in the inner area slightly increases up to the transition from the inner carrier- to the groove-region, and then decreases linearly with increasing diameter according to the other cases (static / lower velocities).

The small increase in pressure in the inner carrier region seems to be caused by the isothermal modeling approach. Due to the lower fluid viscosity in combination with the centrifugal forces due to increased sliding velocities, the hydraulic resistance of the oil distributor is significantly reduced. This leads to increased oil velocities in the spline zone of the inner carrier-area, but due to the reduction in cross-section at the transition to the grooves, the flow is blocked and the pressure thus rises.

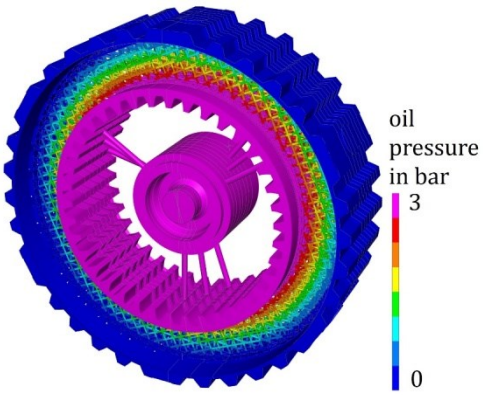

Figure 69: Pressure distribution (D123, variant I, L-301, ϑ_{oil} = 40 °C, static operation ST3, $\dot{v}_{oil}$ = 1.5 mm³/mm²s) from [Gro22]

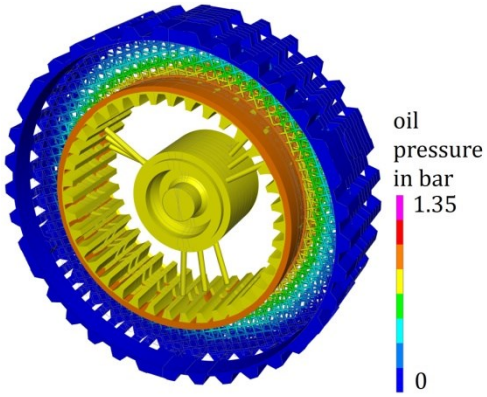

Figure 70: Pressure distribution (D123, variant I, L-301, ϑ_{oil} = 83 °C, dynamic operation LS3, $\dot{v}_{oil}$ = 2.5 mm³/mm²s) from [Gro22]

Figure 71 compares nominal and reduced surface pressures for the static operating points. An increase of oil flow leads to higher pressure in the groove gaps, and thus reduces the effects of the externally supplied axial force at the friction interfaces by lowering the expected nominal surface pressure at the friction interfaces. For static operations, the nominal surface pressure is reduced in the range of 3 … 23 % with increasing supplied flow rates.

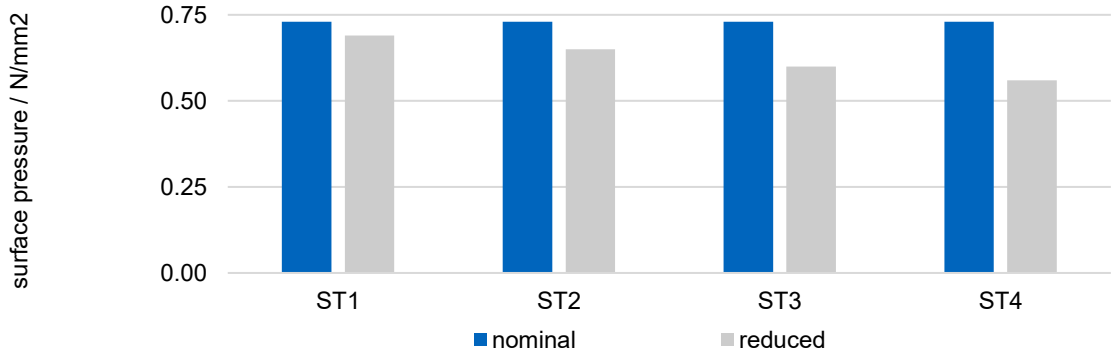

Figure 71: Comparison of nominal and reduced surface pressures (D123, variant I, L-301, ϑ_{oil} = 40 °C, static operation) from [Gro22]

Figure 72 shows the results during dynamic operations. A decreasing sliding velocity leads to an increase of hydraulic pressure since the oil flow reduces the axial force. The maximum reduction of the nominal pressure for dynamic operations is as high as 29 %.

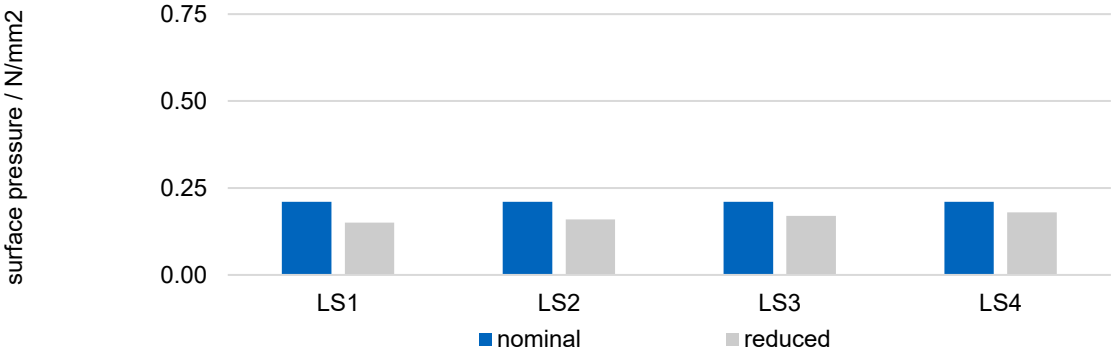

Figure 72: Comparison of nominal and reduced surface pressure (D123, variant I, L-301, dynamic operation, $\dot{v}_{spez}$ = 2.5 mm³/mm²s) from [Gro22]

7.3 Overall Summary of Results

The objective of the simulative and experimental investigations was the identification of influencing factors on thermal behavior of sealed industrial wet clutches with pressurized oil supply.

Two clutches from industrial applications were therefore studied. The clutch D148 has a higher CoF compared to D123, leading to increased friction power at the same load stage. Furthermore, the steel plates of D148 are thinner than the plates of D123 which results in a smaller thermal mass and contact surface to radial connecting parts. Thereby, temperatures of clutch D148 are higher in all load stages.

There is a minor axial temperature distribution in continuous slip operations. The differences between the plate temperatures in the middle steel plate and the axially outer plates (drive, piston) are within a few degrees K. In contrast, during shifting cycles the measurements show a significant difference between the middle and outer steel plate temperatures. During shifting cycles, the time of thermal energy input (sliding phase) is much shorter compared to continuous slip operations. That is why a significant amount of heat can leave the inner steel plates by conduction to connecting parts and convective oil cooling before it reaches the outer plates. Additionally, the temperature gradient to the connecting parts is usually higher due to a longer cooling time. However, the middle steel plate usually reaches the highest temperature in all tests. Therefore, performing thermal calculations with the focus on the so called critical middle steel plate, as implemented in the real-time model, seems appropriate.

Besides the possibility of calculating heat transfer coefficients with CFD simulations, the iterative approach by combining experimental results and simulation data enables quantification of heat transfer in the clutches. Using this approach, robust values for the heat transfer coefficients can be determined during continuous slip operation. The determination during shifting cycles is more complex and not the focus of this thesis. The determined heat transfer coefficients facilitate the parameterization of the simulation models (e.g. real-time model), enabling high quality of the calculated temperatures with deviations of less than 5K compared to the measurement data. Nevertheless, future approaches should use CFD simulations for the estimation of heat transfer coefficients.

The results of the investigations set up the discussion on the effects of differential speed, clutch pressure, feeding oil pressure, oil flow rate and design of the oil distributor pattern in the inner carrier on thermal behavior of the clutches.

Regarding differential speed, the main finding is that higher speeds lead to higher temperatures in the clutch. This applies to both continuous slip and shifting cycle operation modes. The main reason for this is that differential speed determines friction power / work and thus thermal load of the system. The influence of speed on the temperature rise is nonlinear, as the underlying physics and results of the optimization of the real-time model calculations show. Therefore, speed is a key parameter defining thermal behavior of a wet clutch system. Furthermore, the filling behavior of the clutch is accelerated by higher speeds.

Another important factor is clutch pressure. A rise of clutch pressure also leads to a higher thermal load of the clutch and raises the temperatures. This behavior could be validated with the measurements and calculations during shifting cycles and continuous slip.

The special case of a sealed lubrication system in the clutches from industrial applications results in a hydrodynamic pressure at the friction interfaces that can reduce clutch pressure and therefore the transferable torque. The direct measurement of this effect in the test rig is not possible, but CFD simulations implement the calculation of the hydrodynamic pressure at the friction interfaces. For validation of the CFD simulation, the calculated oil pressures in the inner carrier of the numerical simulations were compared with test rig data. The validation showed that the CFD model is capable of reproducing variations in flow rate (static) and rotational speed (dynamic) in good agreement with the test rig data.

The results show a significant reduction of nominal pressure of more than 20 % during static and dynamic operations. However, due to the isothermal modeling approach, these results could be

overestimated. Nevertheless, reducing the oil pressure at the friction interfaces is important to ensure full torque transfer capability of the sealed clutch system.

The oil flow rate has a major influence on thermal behavior of the clutches. Starting with investigations on the filling behavior, the results show an acceleration of the filling behavior with increasing oil flow rate. Furthermore, if insufficient oil is supplied, the friction interfaces are not completely filled with oil. The cooling performance of the clutch system correlates with the amount of supplied oil regardless of the applied loads. A higher oil flow rate lowers the temperature rise in the clutch even at low speeds, since there is no need for sufficient centrifugal force to convey the oil. However, the obvious interaction between flow rate and hydrodynamic pressure at the friction interface must be considered when trying to optimize the cooling conditions by increasing the oil flow rate in a sealed clutch system.

The variation of the oil distributor pattern in the inner carrier was investigated in detail by means of experiments and CFD simulations. For this purpose, the number of friction interfaces and the oil supply through the inner carrier were varied during the investigations. In the case of the clutch with four friction interfaces, the oil holes are located axially directly below the friction interfaces. In the clutch with eight friction interfaces, the first and last friction interface are only lubricated indirectly by axial distribution in the splines of the inner carrier. It therefore took longer for the oil to reach the friction interface. For both configurations (four and eight friction interfaces), the number of oil supply holes in the inner carrier was then reduced. For the clutch with four friction interfaces and direct lubrication to the friction interfaces, only slight changes in the filling behavior were observed, while the clutch with eight friction surfaces exhibited large delays in filling behavior due to the required axial distribution of the oil. At high differential speeds and thus high radial oil conveying effect of the plates, axial distribution of the oil was restricted to such an extent that the outer friction interfaces in the configuration with eight friction interfaces were no longer completely filled with oil. It can therefore be concluded that good axial distribution of the oil distributor holes is more important than their radial distribution, since the differential speed supports the distribution of the oil in circumferential direction. In addition, the filling behavior is then significantly influenced by the supplied oil volume flow.

Experimental investigations on the thermal behavior showed a significant influence of the oil flow rate on thermal behavior independent of speed level (load stage). However, contrary to expectations at the beginning of the investigations, the variations in the oil distributor pattern showed almost no influence on the temperature level. The results of CFD simulations show that the outer friction interfaces in static operations with eight friction interfaces seem to be supplied with slightly less oil than direct lubricated friction interfaces in the middle of the clutch package. During dynamic operations (four interfaces), minor variations of the oil supply at each interface are identified if the ratio of rotational speeds between the steel and friction plates is less than one. In summary, the oil distributor pattern showed no influence on the oil supply to each friction interface as long as enough oil is supplied, each friction interface is directly lubricated or the rotational speed is low enough to enable axial oil flow in the spline zone of the inner carrier. Under these circumstances, there is nearly no change when the oil distributor pattern in the inner carrier is varied. The calculated oil distribution to the individual friction interfaces, and the reduction of the nominal surface pressure in static and dynamic operations do not change.

The application of different investigation methods enables a holistic view on the thermal behavior of the wet clutches while reducing costs in terms of calculation time and modeling complexity. Although based on a one-dimensional spatial resolution, the real-time model can reproduce all identified thermal effects from the experiments except for axial temperature distribution. By comparing temperature measurements and real-time temperature calculations, the validity of the model formation for various clutch applications and load cases was demonstrated. The deviation between measurements and calculations are typically very small (< 5K). The temperature prediction allows a highly accurate (deviations typically < 5K) conservative prediction of the thermal load for future shifting operations. The model can thus contribute to the increase of operational safety of wet multi-plate clutches, while at the same time ensuring critical component design. The results help to identify and quantify important influencing factors, and even nonlinear behavior is correctly reproduced. This enables very efficient

design studies, parameter variations, recalculation, and monitoring of clutch systems in all stages of the development process and during real-world application.

On the other hand, the CFD simulation facilitates in-depth studies of oil flow on the cost of higher modeling complexity and computational effort. Quantities that are difficult or even impossible to measure, including oil distribution, hydrodynamic pressure at the friction interface and heat transfer coefficients can be determined for this.

Neither at the chair nor in the literature is there a well-established procedure for observing the flow conditions in a wet multi-plate clutch under practical conditions; thus experiments with 3D printed transparent parts and a high-speed camera were developed and conducted. Despite transparent materials, the test setups largely corresponded to the geometries of the original parts from serial production. The high-speed camera recordings provide further insights into oil distribution and filling behavior, particularly regarding the first friction interface of the clutch. With the recordings, assumptions and results of the CFD simulations can be validated and made plausible on real-life geometries. For example, the assumption of a single-phase flow in the CFD model was confirmed. This method proves to be suitable for generating high quality results with a manageable effort.

8 Recommendations for Industrial Application

The results obtained will be discussed again in the following section from the perspective of practical application. The focus here is on showing the extent to which the results can be incorporated to industrial practice and in which areas further investigations may be required. The recommendations are derived from the knowledge gained during the development of the previous results. The discussion contains recommendations of the author in the sense of an outlook or as hints regarding a procedure which the author considers reasonable. These outlooks/hints do not claim to be scientifically validated. Furthermore, the findings regarding the influencing factors on the thermal behavior are again reflected in the context of practical application.

8.1 Recommendations for Implementation

In the following, a possible approach to implement the holistic approach implemented in the work is given.

- Consideration 1: Regardless of the subsequent objective, accurate determination of the thermal behavior requires the most exact possible knowledge of the friction behavior in the operating range to be investigated. Based on this knowledge, the acceptable effort for the determination of the CoF can be determined. For a rough prediction, the assumption of a constant CoF estimated by empirical knowledge may be sufficient at first. However, since the CoFs often do not show a constant behavior, the calculation quality can be significantly improved by using a CoF map or a statistical CoF model. For the creation of statistical CoF models, for example, the history of CoF measurements available in operation or an experimental plan developed by means of Design of Experiments (DoE) can be used. For high reliability requirements during online operation, for example, in combination with prediction to prevent overloads, feeding the friction torque signal is probably the optimum. In this case, all changes in the CoF behavior during operation are immediately taken into account in the calculation. In this case, however, it must be critically questioned whether a direct measurement of the corresponding temperatures during operation is not possible with similar effort. An experimental determination of the friction behavior seems to be necessary in most cases for the determination of reliable input data.
- Consideration 2: The CFD simulations presented provide a deep insight into the flow behavior within the clutch. They make it possible to determine the input variables of oil carrying capacity and CHTs. Furthermore, it can be determined whether complete and uniform lubrication of the clutch is achieved with the set oil flow rate and to what extent the hydrodynamic pressure at the friction surfaces reduces the effective pressure and thus the transmissible torque of the clutch. It must be borne in mind, however, that the results presented are valid only for steady-state operation of a fully filled closed clutch in continuous slip. In practice, other operating modes and non-stationary effects (e.g. filling behavior) may be relevant here, for example partial filling of the sealed clutch or variable speed ratios, which should be taken into account when transferring the approach. Furthermore, CFD modeling is not mandatory for parameterization of the thermal models and can therefore be omitted completely. However, from the author's point of view, the determination of the static oil carrying capacity by means of CFD simulation is recommendable in any case, since this requires considerably less effort than an experimental determination. Furthermore, a complete thermal calculation of the clutch by means of CFD would also be possible. For this purpose, the CFD model used to determine CHTs (see Consideration 3) can be used. However, this would involve an immense increase in the computational effort, which does not appear to be a target-oriented general recommendation at the present time (see Consideration 4).
- -Consideration 3: For the parameterization of all temperature models, CHTs are needed to describe the convective heat transfers. For lower accuracy requirements, these can initially be taken from existing empirical knowledge or published tables. For higher accuracy requirements, however, they should be determined for the corresponding system in the desired operating

range. Here, either with the help of an iterative procedure, corresponding coefficients can be determined by adjusting the values in the simulation until a reasonable agreement with existing or to be acquired measurement data is reached. Alternatively, the possibility of determining the CHTs by means of CFD simulations was demonstrated in this work. In this case, a very high quality of results could be demonstrated in comparison with analytical calculations. However, the transferability of these findings to a clutch system was only carried out in the sense of a potential analysis, since there are higher requirements here, particularly about the necessary computing resources. Which approach should be used depends strongly on existing and future available CFD infrastructure. Currently, a hybrid approach seems to make sense.

- Consideration 4: Once all relevant input variables have been determined, the question of the required spatial model depth for the computational determination of the thermal behavior arises. The results of the thermal simulations show that in most cases a very high quality of results is achieved using the real-time temperature model (1D modeling). Except for the spatial temperature distribution, all relevant thermal effects determined in the experimental test series can be reproduced simulatively. The deviations between the measured mass temperature of the clutch components and the simulations are very small. Therefore, as long as no special questions are focused that exclude 1D modeling (e.g. spatial temperature distributions), it is recommended. 1D modeling enables integration into automated variation recalculations in the context of pre-development, as well as accurate recalculations for later development cycles. Furthermore, integration on the clutch controller of the 1D model (digital twin), which is continuously developed during development, is directly possible.
- Consideration 5: The high-speed camera images on the 3D printed components provide an insight into the oil distribution of the wet clutch, analogous to the CFD simulations. However, a variety of challenges emerged in the practical implementation of this. The identification of relevant effects is possible almost exclusively in the first plane captured by the camera. Furthermore, the evaluation is of a rather qualitative nature. In 3D printing, a certain learning curve must also be considered to obtain the desired geometric quality. The recordings in connection with prototype parts thus seem suitable for answering specific questions such as the validation of some assumptions of a CFD simulation. A general recommendation for the application of this investigation method for the characterization of the thermal behavior of an industrial clutch cannot be derived from the experiences within the scope of this work.

8.2 Variables Influencing the Thermal Behavior

In the following section, the most important influencing variables are discussed again in the context of application. In each case, the extent to which the corresponding parameter influences the temperature rise, the filling behavior, the uniformity of the oil distribution and the oil pressure within the clutch is summarized. If possible, the author will provide information on how to take the corresponding effects into account in the application.

8.2.1 Oil Distributor Pattern Design

Two variants of oil distributors are studied. The first distributor variant has nine bore holes that are on three different axial positions and otherwise circumferential even distributed. The second variant has three holes that are axially distributed. Two clutch sizes with four and eight friction interfaces are investigated. The axial spacing is selected such that for the clutch with four interfaces every friction interface is directly lubricated. For the clutch with eight interfaces, the first and last interfaces are not directly lubricated. The results show that the effects of the circumferential spacing on the thermal behavior is negligible, while the axial spacing has a significant influence especially on the time it takes to fill all interfaces with oil and the temperature rise within the clutch. Furthermore, with indirect lubrication, for higher rotational speeds an uneven oil distribution evolves because the oil cannot be distributed within the gears of the inner carrier due to centrifugal forces that force the oil outwards. The oil pressure at the friction interfaces is independent of the oil distributor and clutch configuration. The

implied recommendation for practical application is thus to design the inner carrier of a sealed industrial clutch such that beneath every friction interface oil is supplied. The findings are summarized in Table 23.

Table 23: Summary of the effects of decreasing the number of circumferential oil bore holes from three (variant I) to one (variant II) bore holes at each axial location

	temperature rise	time to fill interface with oil	uniform oil distribution	oil pressure at interfaces
direct lubrication	o	o	o	o
indirect lubrication	-	-	-[1]	o
+: positive effect | o minor or neutral effect | - negative effect [1]) depends on speed				

8.2.2 Oil Flow Rate

The temperature rise in a sealed industrial clutch is reduced and oil distribution improves by increasing the oil flow rate. However, there is a downside to increasing oil flow rate. The oil pressure at the friction interfaces increases, reducing the effective axial force in the clutch and consequently reducing the torque that can be transmitted by the clutch system. Additionally, the drag torque of the clutch, the load on the seals, and the power needed to operate the oil pump are increased. An adaptable cooling oil supply strategy seems optimal, which maximizes oil supply during high thermal loads and reduces or turns off oil supply when clutch temperatures are low enough. Implementing such a feeding oil control strategy could be aided by the application of the real-time model as a virtual sensor or digital twin of the thermal behavior of the clutch. The findings from the study of this thesis suggest that an adaptable cooling oil supply strategy is an effective way to balance the benefits and drawbacks of increasing oil flow rate. Table 24 summarizes the results obtained during the study.

Table 24: Summary of the effects of increasing oil flow rate

	temperature rise	time to fill interface with oil	uniform oil distribution	oil pressure at interfaces
oil flow rate	+	+	+	-
+: positive effect | o minor or neutral effect | - negative effect				

8.2.3 CoF, Sliding velocity and Clutch Pressure

To ensure the proper functioning of a clutch system, it is important to consider the CoF and the operating conditions such as sliding velocity and clutch pressure, as they significantly affect the thermal behavior. As the quantities of the variables are mostly given by the application recommendations are typically out of the scope of clutch optimization and must be addressed by the designers of the environment (e.g. placement in gearbox). The determined effects are summarized in Table 25.

Table 25: Summary of the effects of increasing speed and clutch pressure

	temperature rise	time to fill interface with oil	uniform oil distribution	oil pressure at interfaces
sliding velocity	-	+	o	+
pressure	-	o	o	o
CoF	-	o	o	o
+: positive effect | o minor or neutral effect | - negative effect				

9 Summary and Outlook

9.1 Summary

Within the scope of this work, thermal behavior of wet industrial multi-plate clutches was the subject of extensive experimental and theoretical investigations. Important influencing variables such as the cooling oil flow and oil distribution through the closed clutch, as well as other operating and environmental parameters on thermal behavior were systematically investigated. The most important work carried out and the results of the various investigation methods are summarized below.

Real-Time Temperature Calculation Model and Temperature Prediction:

As part of the theoretical investigations, a simulation model was implemented for generally applicable modeling and real-time determination, and the prediction of the temperatures of a wet multi-plate clutch. The real-time model was designed to be parameterizable for a wide range of applications and operating scenarios and was validated by means of extensive measurements on the component test rig. Furthermore, relevant input variables and parameters for the real-time model were identified and determined. The real-time model can calculate present and future temperatures with a few input signals provided by sensors or from existing measurement data. This enables monitoring of the thermal behavior of the clutch during operation in the sense of a virtual sensor or extensive parameter studies due to the low computational costs. Additionally, a prediction module was implemented to predict critical future operating conditions. Critical shifting and slip states can be prevented with thermal prediction of possible shifting scenarios. Therefore, this allows more efficient clutch dimensioning and a design with lower safety margins. The prediction module was optimized using the results of extensive sensitivity analyses. Non-linear influences of the input variables speed and torque on thermal behavior were identified.

CFD Simulation of Oil Distribution and Reduction of Axial Force due to Oil Supply:

Ensuring sufficient oil coverage on each friction interface of industrial clutches is achieved by pressurized oil supply. The challenge of building capable test rigs to study oil and pressure distribution inside a practical relevant loaded clutch and the limited availability of test parts due to small batch sizes determine the demand for CFD simulations.

The development of CFD simulations by application of a transient moving mesh approach with a laminar, incompressible, and isothermal flow model in a fluid domain representing the test rig setup enables investigations of oil and pressure distributions at the friction interfaces of a closed clutch. The investigations are validated by comparing pressure measurements with simulation results. The influences of varying operating conditions (oil flow, speed) and geometry of oil supply in the inner carrier on the oil and pressure distributions are analyzed. Regardless of operating conditions or geometrical variations of the inner carrier, a nearly uniform oil supply to all friction interfaces is achieved. The hydraulic oil pressure lowers the effective axial force at the friction interfaces, and therefore reduces torque transfer capacity up to 29%, depending on operating conditions.

CFD Simulation Potential Analysis of Calculation of Heat Transfer Coefficients:

As part of a potential analysis, heat transfer coefficients were determined using a CFD simulation. The calculation area was reduced to the average friction pairing and consists of the flow at the friction interface and the solids of the steel and lining plate. Furthermore, the energy equation was integrated. Verification of the calculation method was performed by comparing a simplified numerical calculation of the heat transfer of a pipe flow with its analytical solution. The length and diameter of the pipe correspond to the groove cross-section and groove length of the respective grooves on the clutch. The validation showed very good agreement between numerical and analytical solutions with deviations in the range of 0 ... 3%. Furthermore, the length of the hydraulic and thermal inlet was estimated by means of analytical equations. The thermal inlet length exceeds the groove length for both groove patterns. The assumption of a thermally formed flow can thus not be made in real operation, and the calculation of the heat transfer coefficient can only be performed numerically (not analytically). Transferability of the

calculation method to the real clutch geometry was carried out and showed that the calculation is possible, but is associated with a large computational effort. The result is a three-dimensionally resolved oil and temperature distribution as well as the heat transfer coefficients between the components. For reliable application of the new method, the evaluation of the calculated values, extensive validations and, if necessary, parameter variations are still necessary, which cannot be covered within the framework of a potential analysis. The developed calculation model can be used as a basis for future research in this field.

Experimental Investigations of the Thermal Behavior:

The experimental investigations on the thermal behavior of wet multi-plate clutches were mainly carried out in continuous slip. In addition, stitch tests were performed with shifting cycles and static investigations. Two clutches from industrial applications with sintered friction lining (D148 and D123) were used for the experiments. The temperatures of the steel plates were recorded axially and radially in the middle of the plate in the clutch package, on the steel plate at the piston side, in the center and on the drive side. The focus of the investigations was to determine the influences of oil flow rate, oil supply design and operating conditions (speed, pressure) on thermal behavior.

The tests show clear influences of pressurized oil feeding on thermal behavior. Increasing the oil flow rate leads to lower temperature rises, regardless of speed level. Analogous to the results from the CFD simulations, varying the oil distributor pattern has almost no influence on the determined temperature rises. In continuous slip, the axial temperature profiles of the steel plates are very balanced; during shifting cycles, the outer steel plates heat up significantly less than the middle one. Speed, clutch pressure and CoF level also significantly influence thermal behavior in accordance with physical expectations. Heat transfer coefficients determined iteratively from experiment and simulation in continuous slip show an acceptable scatter band and very good agreement between calculated and simulated temperatures.

Experimental Investigations of Visualization of Oil Flow:

For the experimental investigation of the flow conditions in a closed wet multi-plate clutch, an existing test rig of the chair was converted for optical validation of the flow conditions. Rapid prototyping methods (SLA 3D printing, laser cutter) were used to produce transparent clutch components. Subsequently, investigations were carried out with a high-speed camera under pressurized lubrication. Despite transparent materials, the test setups largely corresponded to the geometries of the original multi-plate clutches. For the tests with pressurized lubrication, the original outer carrier was used, whereas a transparent inner carrier was designed that corresponds to the original component in terms of splines and oil distributor, but enables seeing the oil supply holes. The SLA 3D printing process was chosen to manufacture the inner carrier and lining plates. The steel plates were cut from plexiglass using a laser cutter.

For the transparent resin used in the SLA 3D printer, a layer thickness of 50 µm turned out to be a good compromise for the desirable levels of detail, surface quality and printing speed. The geometric freedom and fast iterations of the part design turned out to be the greatest strength of SLA printing.

Furthermore, the experimental investigations confirm the findings and assumptions of the CFD simulations. With good axial distribution of the oil distributor holes, all interfaces fill at the load levels investigated and the reduction in the number of holes in the circumferential direction has a negligible effect on the oil and pressure distribution on the friction interfaces.

The application of a wide range of investigation methods provides a comprehensive insight into the thermal behavior of wet multi-plate clutches. The results can help in the design and optimization of future clutches. In particular, the summary and interpretation of the results in section 7.3 and chapter 8 can be helpful.

9.2 Outlook

The focus of the presented investigations was on studies of sealed clutches from industrial applications. The holistic approach can probably also be profitably used to investigate other clutch systems and influencing parameters.

In addition to this global perspective, all the research methods used also offer scope for further development. For example, in the sense of further virtualization of the development and research process on thermal behavior, the focus can be on a further reduction of the dependence on experimental investigations. An important milestone regarding these issues was demonstrated by showing the possibility of determining heat transfer coefficients by means of CFD simulations instead of experiments. The validation of the existing model as well as the calculation of an extensive experimental space allows, if necessary, identification of the most important influencing variables on heat transfer in real groove geometries. The insight into the flow, temperature and local heat transfer coefficients would additionally support physical interpretation of the results.

In addition to heat dissipation, improved modeling of the energy input into the clutch system also provides opportunities for further investigations. On the one hand, current progress in quantum computing may enable calculation of CoFs in practical friction pairs within the current century (e.g. [Liu21, Llo20]). Furthermore, the already started research on statistical and empirical models with good prediction quality can also be used to improve thermal modeling.

10 Literature

Standards, Guidelines and Patents

[AT303] AT389165T; AU2003294850A1; WO2005057151A1; EP1692477A1; EP1692477B1; EP1692477B2: Pfeifer R., Verfahren zum Bestimmen der Lamellentemperatur einer Lamellenkupplung (2003).

[DIN94] DIN 51757: Testing of mineral oils and related materials – Determination of density (1994).

[DIN11] DIN 51563: Testing of Mineral Oils and Related Materials – Determination of Viscosity Temperature Relation – Slope m (2011).

[DIN18] DIN EN ISO 14253-2:2018-09: Geometrical product specifications (GPS) - Inspection by measurement of workpieces and measuring equipment - Part 2: Guidance for the estimation of uncertainty in GPS measurement, in calibration of measuring equipment and in product verification (2018).

[Joi08] JCGM 100:2008: Evaluation of measurement data - Guide to the expression of uncertainty in measurement (2008).

[Ver71] VDI 2240: Wellenkupplungen - Systematische Einteilung nach ihren Eigenschaften (1971).

Books, Journal Articles, Dissertations, Student Theses

[Abu06] Abu Snima, K.: Kenngrößen und Belastungsgrenzen von nasslaufenden Lamellenkupplungen unter Dauerschlupfbeanspruchung, Dissertation, Technische Universität Karlsruhe (2006).

[Acu14] Acuner, R.; Pflaum, H.; Stahl, K.: Friction screening test for wet multiple disc clutches with paper type friction material. Proceedings of the Society of Tribologists and Lubrication Engineers Annual Meeting and Exhibition 2014, Florida (2014).

[Acu13] Acuner, R.; Pflaum, H.; Stahl, K.: FVA-Nr. 490 IV - Heft 1051 - Abschlussbericht Reibungszahl-Kurztest - Öleinfluss Reibcharakteristik am Modell nasslaufende Lamellenkupplung; Entwicklung eines Reibungszahlkurztests. Forschungsvereinigung Antriebstechnik e.V., Frankfurt/Main (2013).

[Alb10] Albers, A.; Bernhardt, J.; Ott, S.: Untersuchung der Ölströmung in geschmierten Friktionssystemen am Beispiel einer nasslaufenden Lamellenkupplung. Tribologie und Schmierungstechnik 3/2011. Issue: 58, S. 5–8 (2010).

[Alb12] Albers, A.; Brezger, F.; Koch, C.: Development of a new validation environment for CFD simulations on the example of a lubricated clutch. Getriebe in Fahrzeugen 2012 VDI-Berichte: 2158, Friedrichshafen (2012).

[Alb18] Albers, A.; Ott, S.; Kniel, J.; Eisele, M.; Basiewicz, M.: Investigation of the thermo-mechanical behaviour of clutches using fibre optic sensing technology with high spatial measurement density. Proceedings of the Institution of Mechanical Engineers, Part J: Journal of Engineering Tribology Vol. 232. Issue: 1, S. 26–35 (2018).

[Asa18] Asai, K.; Ito, T.: Effect of Facing Groove Design on Drag Torque of Automatic Transmission Wet Clutches. WCX World Congress Experience, SAE Technical Paper Series, Detroit (2018).

[Bac10] Back, O.; Echtler, P.; Bergheim, M.: Potential of Sintered Friction Linings in Synchronizers. Getriebe in Fahrzeugen 2010 VDI-Berichte: 2081, Friedrichshafen (2010).

[Bar15] Barr, M.; Srinivasan, K.: Estimation of Wet Clutch Friction Parameters in Automotive Transmissions. SAE 2015 World Congress & Exhibition, SAE Technical Paper Series, Detroit (2015).

[Bar10] Bartel, D.: Simulation von Tribosystemen - Grundlagen und Anwendungen, Zugl.: Magdeburg, Univ., Fak. für Maschinenbau, Habil.-Schr., 2009. Vieweg + Teubner, Wiesbaden, 1. Aufl. (2010).

[Bas16] Bassi, A.; Milani, M.; Montorsi, L.; Terzi, S.: Dynamic Analysis of the Lubrication in a Wet Clutch of a Hydromechanical Variable Transmission. SAE International Journal of Commercial Vehicles 9. Issue: 2, S. 280–290 (2016).

[Bau20] Baumgartner, A.: Reibungsverhalten nasslaufender Lamellenkupplungen – Messunsicherheiten und Auswertemethoden, Masterarbeit, Lehrstuhl für Maschinenelemente, Technische Universität München (2020).

[Beh18] Behzad, M.; Saxena, V.; Schaefer, M.: Thermal-Hydrodynamic Optimization of Grooves in a Wet Clutch. Dritev - Drivetrain for vehicles, EDrive, Transmissions in mobile machines VDI-Berichte: 2328, Bonn (2018).

[Ber17] Bernhardt, J.: Entwicklung von Friktionssystemen am Beispiel einer nasslaufenden Lamellenkupplung, Dissertation, Karlsruher Institut für Technologie (2017).

[Bin18] Bin, W.; yongyong, H.; Wei, W.; jianbin, L.: Simulation and experiment of viscous torque for disengaged wet clutches of tracked vehicle. Proceedings of the Institution of Mechanical Engineers, Part J: Journal of Engineering Tribology Vol. 0. Issue: 0, 1-12 (2018).

[Bis21] Bischofberger, A.; Ott, S.; Albers, A.: Einfluss von Betriebsgrößen auf die Schwingungsreduzierungswirkung im nasslaufenden Kupplungssystem: Empirische Modellbildung – Kennfelder und Skalierbarkeit. Forschung im Ingenieurwesen - Engineering Research 85. Issue: 4, S. 933–944 (2021).

[Bjö13] Björling, M.; Habchi, W.; Bair, S.; Larsson, R.; Marklund, P.: Towards the true prediction of EHL friction. Tribology International 66, S. 19–26 (2013).

[But18] Butzhammer, M.: Weiterentwicklung der thermischen Modellbildung einer nasslaufenden Lamellenkupplung in Matlab/Simulink, Semesterarbeit, Lehrstuhl für Maschinenelemente, Technische Universität München (2018).

[Che11] Chen, G.; Baldwin, K.; Czarnecki, E.: Real Time Virtual Temperature Sensor for Transmission Clutches. SAE International Journal of Engines 4. Issue: 1, S. 1523–1535 (2011).

[Cho12] Cho Jungdon: A Multi-Physics Model for Wet Clutch Dynamics, Dissertation, The University of Michigan (2012).

[Cui14a] Cui, H.; Yao, S.; Yan, Q.; Feng, S.; Liu, Q.: Mathematical model and experiment validation of fluid torque by shear stress under influence of fluid temperature in hydro-viscous clutch. Chinese Journal of Mechanical Engineering 27. Issue: 1, S. 32–40 (2014).

[Cui14b] Cui, J.; Wang, C.; Xie, F.; Xuan, R.; Shen, G.: Numerical investigation on transient thermal behavior of multidisk friction pairs in hydro-viscous drive. Applied Thermal Engineering 67. Issue: 1-2, S. 409–422 (2014).

[Czé09] Czél, B.; Váradi, K.; Albers, A.; Mitariu, M.: Fe thermal analysis of a ceramic clutch. Tribology International 42, S. 714–723 (2009).

[Czi20] Czichos, H.; Habig, K.-H.: Tribologie-Handbuch. Springer Vieweg, Wiesbaden, 5. Auflage (2020).

[Dav00] Davis, C. L.; Sadeghi, F.; Krousgrill, C. M.: A simplified approach to modeling thermal effects in wet clutch engagement: Analytical and experimental comparison. Journal of Tribology 122. Issue: 1, S. 110–118 (2000).

[Din11] Ding, H.; Visser, F. C.; Jiang, Y.; Furmanczyk, M.: Demonstration and Validation of a 3D CFD Simulation Tool Predicting Pump Performance and Cavitation for Industrial Applications. Journal of Fluids Engineering 133, S. 1–14 (2011).

[Drä13] Dräxl, T.; Pflaum, H.: FVV-Nr. 1012 - Heft 985 - Abschlussbericht Schleppverluste Lamellenkupplungen - Wirkungsgradverbesserung durch Reduzierung der Schleppverluste an Lamellenkupplungen. Forschungsvereinigung Verbrennungskraftmaschinen e.V., Frankfurt/Main (2013).

[Drä16] Dräxl, T.; Pflaum, H.: FVA-Nr. 671/I - Heft 1117 - Abschlussbericht Schleppverluste Lamellenkupplungen II - Wirkungsgradverbesserung durch Reduzierung der Schleppverluste an Lamellenkupplungen, Abschlussbericht. Forschungsvereinigung Antriebstechnik e.V., Frankfurt/Main (2016).

[Drä15] Dräxl, T.; Pflaum, H.; Stahl, K.: Neue Erkenntnisse über Schleppverluste an Lamellenkupplungen. VDI-Fachtagung "Kupplungen und Kupplungssysteme in Antrieben", VDI-Berichte Nr. 2245, S. 149–161 (2015).

[Düm84] Dümeland, M.: Weiterentwicklung störungsbehafteter technischer Produkte nach konstruktionsmethodischen Kriterien, Dissertation, Ruhr-Universität Bochum (1984).

[Dur06] Durst, F.: Grundlagen der Strömungsmechanik - Eine Einführung in die Theorie der Strömung von Fluiden. Springer-Verlag, Berlin, Heidelberg, 1. Aufl. (2006).

[Egu01] Eguchi, M.; Nakahara, T.: Friction-Velocity Characteristics of a Paper-Based Wet Friction Material in Low Sliding Velocity (Part 1): Boundary Film Model Supposing Eyring Viscosity. Japanese Journal of Tribology. Issue: 46, S. 162–170 (2001).

[Fis16] Fischer, R.; Küçükay, F.; Jürgens, G.; Pollak, B.: Das Getriebebuch. Springer Vieweg, Wiesbaden, 2., überarbeitete Auflage (2016).

[Fis94] Fish, R. L.; Truncone, S. A.: Tracking Wet Friction Performance Via Energy Dispersive X-Ray Spectroscopy. SAE International Congress & Exposition SAE Technical Paper Series, Detroit (1994).

[Fri17] Frisch, H.; Schulz, R. K.; Sittig, K.; Dörfler, D.; Möller, K.: Untersuchung der Drehmomentgleichförmigkeit durch geometrische Zwangserregung bei nasslaufenden Doppelkupplungen. Kupplungen und Kupplungssysteme in Antrieben VDI-Berichte: 2309, Karlsruhe (2017).

[Gao02] Gao, H.; Barber, G. C.; Shillor, M.: Numerical Simulation of Engagement of a Wet Clutch With Skewed Surface Roughness. Journal of Tribology 124. Issue: 2, S. 305–312 (2002).

[Gei37] Geiger J.: Die Erwärmung von Kupplungen und Bremsen. Automobiltechnische Zeitschrift 9. Issue: 7, S. 34–35 (1937).

[Göp21] Göppert, G.: Adaptation of a wet clutch torque model in electrified drivelines. Forschung im Ingenieurwesen - Engineering Research 85. Issue: 4, S. 913–922 (2021).

[Gro19a] Groetsch, D.; Niedenthal, R.; Voelkel, K.; Pflaum, H.; Stahl, K.: Effiziente CFD-Simulationen zur Berechnung des Schleppmoments nasslaufender Lamellenkupplungen im Abgleich mit Prüfstandmessungen. Forschung im Ingenieurwesen - Engineering Research 83. Issue: 2, S. 227–237 (2019).

[Gro21a] Groetsch, D.; Stockinger, U.; Schneider, T.; Reiner, F.; Voelkel, K.; Pflaum, H.; Stahl, K.: Experimental investigations of spontaneous damage to wet multi-plate clutches with

carbon friction linings. Forschung im Ingenieurwesen - Engineering Research 85. Issue: 4, S. 1043–1052 (2021).

[Gro21b] Groetsch, D.; Voelkel, K.; Pflaum, H.; Stahl, K.: Real-time temperature calculation and temperature prediction of wet multi-plate clutches. Forschung im Ingenieurwesen - Engineering Research 85. Issue: 4, S. 923–932 (2021).

[Gro22] Groetsch, D.; Motzet, R.; Voelkel, K.; Pflaum, H.; Stahl, K.: Analysis of Oil Distribution and Reduction of Axial Force due to Oil Supply in a Multi-Plate Clutch. Tribology in Industry 44. Issue: 1, S. 268–282 (2022).

[Gro19b] Groetsch, D.; Niedenthal, R.; Voelkel, K.; Pflaum, H.; Stahl, K.: Efficient CFD Simulation Method for Calculation of Drag Torque in Wet Multi-plate Clutches in Comparison to Test Rig Results. Proceedings of the 18th International CTI Symposium 2019 Automotive Drivetrains I Intelligent I Electrified, Berlin. CTI (2019).

[Gro20] Groetsch, D.; Niedenthal, R.; Voelkel, K.; Pflaum, H.; Stahl, K.: Volume of Fluid vs. Cavitation CFD-Models to Calculate Drag Torque in Multi-Plate Clutches. WCX SAE World Congress Experience SAE Technical Paper Series, Detroit (2020).

[Gro21c] Groetsch, D.; Pflaum, H.; Stahl, K.: FVA-Nr. 413 V - Heft 1427 - Abschlussbericht Echtzeit-Temperaturberechnung Lamellenkupplungen - Echtzeit-Temperaturberechnung und Temperaturprädiktion nasslaufender Lamellenkupplungen im Betrieb. Forschungsvereinigung Antriebstechnik e.V., Frankfurt/Main (2021).

[Grü13] Grünzweig, C.; Wagner, M.; Ruf, J.; Herlmer, D.: Visualisierung der Ölverteilung in einer nasslaufenden Mehrscheibenkupplung. ATZ - Automobiltechnische Zeitschrift 2013. Issue: 3, 224-230 (2013).

[Häg16] Häggström, D.; Nyman, P.; Sellgren, U.; Björklund, S.: Predicting friction in synchronizer systems. Tribology International 97, S. 89–96 (2016).

[Häm95] Hämmerl, B.: Lebensdauer-und Temperaturverhalten ölgekühlter Lamellenkupplungen bei Lastkollektivbeanspruchung, Dissertation, Technische Universität München (1995).

[Hau07] Hauser, C.: Einfluss der Ölalterung auf Reibcharakteristik und Reibschwingverhalten von Lamellenkupplungen, Dissertation, Technische Universität München (2007).

[Hen14] Hensel, M.: Thermische Beanspruchbarkeit und Lebensdauerverhalten von nasslaufenden Lamellenkupplungen, Dissertation, Technische Universität München (2014).

[Hil22] Hildebrand, L.; Dangl, F.; Sedlmair, M.; Lohner, T.; Stahl, K.: CFD analysis on the oil flow of a gear stage with guide plate. Forschung im Ingenieurwesen - Engineering Research 86. Issue: 3, S. 395–408 (2022).

[Hoe01] Hoerbiger Antriebstechnik GmbH: Lamellen für Lastschaltgetriebe, Bremsen und Achsen - Hoerbiger Lamellenhandbuch. Hoerbiger Antriebstechnik GmbH, Schongau, 1. Aufl. (2001).

[Hol99] Holgerson, M.; Lundberg, J.: Engagement behaviour of a paper-based wet clutch Part 1: Influence of drive torque. Proceedings of the Institution of Mechanical Engineers, Part D: Journal of Automobile Engineering 213. Issue: 4, S. 341–348 (1999).

[Hu09] Hu, J.: Drag Torque Prediction Model for the Wet Clutches. Chinese Journal of Mechanical Engineering 22. Issue: 02, S. 238–243 (2009).

[Ing10a] Ingram, M.; Noles, J.; Watts, R.; Harris, S.; Spikes, H. A.: Frictional Properties of Automatic Transmission Fluids: Part II—Origins of Friction–Sliding Speed Behavior. Tribology Transactions 54. Issue: 1, S. 154–167 (2010).

[Ing10b] Ingram, M.; Noles, J.; Watts, R.; Harris, S.; Spikes, H. A.: Frictional Properties of Automatic Transmission Fluids: Part I—Measurement of Friction–Sliding Speed Behavior. Tribology Transactions 54. Issue: 1, S. 145–153 (2010).

[Iqb13] Iqbal, S.; Al-Bender, F.; Pluymers, B.; Desmet, W.: Mathematical Model and Experimental Evaluation of Drag Torque in Disengaged Wet Clutches. ISRN Tribology 2013. Issue: 12, S. 1–16 (2013).

[Iqb14] Iqbal, S.; Al-Bender, F.; Pluymers, B.; Desmet, W.: Model for Predicting Drag Torque in Open Multi-Disks Wet Clutches. Journal of Fluids Engineering 136. Issue: 2, S. 1–11 (2014).

[Iva09] Ivanović, V.; Herold, Z.; Deur, J.; Hancock, M.; Assadian, F.: Experimental characterization of wet clutch friction behaviors including thermal dynamics. SAE International Journal of Engines 2. Issue: 1, S. 1211–1220 (2009).

[Jam11] Jammulamadaka, A. K.; Gaokar, P.: Spin Loss Computation for Open Clutch Using CFD. SAE International Journal of Engines 4. Issue: 1, S. 1536–1544 (2011).

[Jan21] Jancik, M.: Experimentelle Untersuchungen zum thermischen Verhalten nasslaufender Lamellenkupplungen, Bachelorarbeit, Lehrstuhl für Maschinenelemente, Technische Universität München (2021).

[Jan99] Jang, J. Y.; Khonsari, M. M.: Thermal Characteristics of a Wet Clutch. Journal of Tribology 121. Issue: 3, S. 610–617 (1999).

[Jan11] Jang, J. Y.; Khonsari, M. M.; Maki, R.: Three-Dimensional Thermohydrodynamic Analysis of a Wet Clutch With Consideration of Grooved Friction Surfaces. Journal of Tribology 133. Issue: 1, S. 1–12 (2011).

[Jen08] Jen, T.-C.; Nemecek, D. J.: Thermal analysis of a wet-disk clutch subjected to a constant energy engagement. International Journal of Heat and Mass Transfer 51. Issue: 7-8, S. 1757–1769 (2008).

[Kar11] Karamavruc, A.; Shi, Z.; Gunther, D.: Determination of Empirical Heat Transfer Coefficients via CFD to Predict the Interface Temperature of Continuously Slipping Clutches. SAE 2011 World Congress & Exhibition SAE Technical Paper Series, Detroit (2011).

[Kat19] Katsukawa, M.: Effects of the Physical Properties of Resins on Friction Performance. WCX SAE World Congress Experience, SAE Technical Paper Series, Detroit (2019).

[Kea97] Kearsey, A.; Wagner, D.: Carbon Fiber for Wet Friction Applications. SAE Technical Paper 972754, S. 1–22 (1997).

[Kim18] Kim, S. C.; Shim, S. B.: Modeling of heat transfer for a wet multi-plate clutch based on empirical data. Proceedings of the Institution of Mechanical Engineers, Part D: Journal of Automobile Engineering 232. Issue: 12, S. 1634–1647 (2018).

[Kit03] Kitabayashi, H.; Li, C. Y.; Hiraki, H.: Analysis of the Various Factors Affecting Drag Torque in Multiple-Plate Wet Clutches. 2003 JSAE/SAE International Spring Fuels and Lubricants Meeting SAE Technical Paper Series, Yokohama (2003).

[Lam06] Lam, R. C.; Chavdar, B.; Newcomb, T.: New Generation Friction Materials and Technologies. SAE 2006 World Congress & Exhibition SAE Technical Paper Series, Detroit (2006).

[Lay11] Layher, M.: Einfluss der Schmierstoffadditivierung auf das Reibungsverhalten nasslaufender Reibschaltelemente, Dissertation, Technische Universität München (2011).

[Le 17] Le Li; Li, H.; Wang, L.: Numerical analysis of dynamic characteristics of wet friction temperature fields. Advances in Mechanical Engineering 9. Issue: 12, 1-14 (2017).

[Lei12] Lei, Y. L.; Wen, J. T.; Li, X. Z.; Yang, C.: A Numerical Study on the Influence of Grooves on Heat Transfer Performance of Wet Clutch. Applied Mechanics and Materials 249-250, S. 517–522 (2012).

[Lin18] Lin, T.; Tan, Z.; He, Z.; Cao, H.; Lv, H.: Analysis of influencing factors on transient temperature field of wet clutch friction plate used in marine gearbox. Industrial Lubrication and Tribology 70. Issue: 2, S. 241–249 (2018).

[Lin98] Linden, J. L.; Doi, J.; Furumoto, M.; Hoshikawa, N.; King, T.; Kurashina, H.; Murakami, Y.; Sprys, J. W.; Ueda, F.: A Comparison of Methods for Evaluating Automatic Transmission Fluid Effects on Friction Torque Capacity - A Study by the International Lubricant Standardization and Approval Committee (ILSAC) ATF Subcommittee. International Fall Fuels and Lubricants Meeting and Exposition SAE Technical Paper Series, San Francisco (1998).

[Lin17] Lingesten, N.; Marklund, P.; Höglund, E.: The influence of repeated high-energy engagements on the permeability of a paper-based wet clutch friction material. Proceedings of the Institution of Mechanical Engineers, Part J: Journal of Engineering Tribology 231. Issue: 12, S. 1574–1582 (2017).

[Liu18] Liu, H.; Jurkschat, T.; Lohner, T.; Stahl, K.: Detailed Investigations on the Oil Flow in Dip-Lubricated Gearboxes by the Finite Volume CFD Method. Lubricants 6. Issue: 2, S. 47–59 (2018).

[Liu21] Liu, J.-P.; Kolden, H. Ø.; Krovi, H. K.; Loureiro, N. F.; Trivisa, K.; Childs, A. M.: Efficient quantum algorithm for dissipative nonlinear differential equations. Proceedings of the National Academy of Sciences of the United States of America 118. Issue: 35, S. 1–36 (2021).

[Liu12] Liu, X.; Cheng, X. S.; Li, Y.; Gu, Q.; Wang, Y. S.: Study on the Temperature Filed of Wet Dual Clutch Transmission during Starting Process. Applied Mechanics and Materials 187, S. 95–102 (2012).

[Llo20] Lloyd, S.; Palma, G. de; Gokler, C.; Kiani, B.; Liu, Z.-W.; Marvian, M.; Tennie, F.; Palmer, T.: Quantum algorithm for nonlinear differential equations (2020).

[Loh16] Lohner, T.; Ziegltrum, A.; Stemplinger, J.-P.; Stahl, K.: Engineering Software Solution for Thermal Elastohydrodynamic Lubrication Using Multiphysics Software. Advances in Tribology 2016, S. 1–13 (2016).

[Ma19] Ma, B.; Yu, L.; Chen, M.; Li, H. Y.; Zheng, L. J.: Numerical and experimental studies on the thermal characteristics of the clutch hydraulic system with provision for oil flow. Industrial Lubrication and Tribology 71. Issue: 6, S. 733–740 (2019).

[Mah15a] Mahmud, S.; Pahlovy, S. A.: Investigation on Torque Jump Up and Vibration at High Rotation Speed of a Wet Clutch. SAE 2015 Noise and Vibration Conference and Exhibition SAE Technical Paper Series, Grand Rapids (2015).

[Mah15b] Mahmud, S. F.; Pahlovy, S. A.; Kubota, M.; Ogawa, M.; Takakura, N.: Multi-Phase Simulation for Predicting Better Groove Pattern of the Clutch Disk for Low Drag Torque. JSAE/SAE 2015 International Powertrains, Fuels & Lubricants Meeting SAE Technical Paper Series, Kyoto (2015).

[Mah16] Mahmud, S. F.; Pahlovy, S. A.; Kubota, M.; Ogawa, M.; Takakura, N.: Multi-Phase Simulation for Studying the Effect of Different Groove Profiles on the Drag Torque

Characteristics of Transmission Wet Clutch. SAE 2016 World Congress and Exhibition SAE Technical Paper Series, Detroit (2016).

[Mah17] Mahmud, S. F.; Pahlovy, S. A.; Kubota, M.; Ogawa, M.; Takakura, N.: A Simulation Model for Predicting High Speed Torque Jump Up Phenomena of Disengaged Transmission Wet Clutch. WCX 17: SAE World Congress Experience SAE Technical Paper Series, Detroit (2017).

[Mai06] Maier, U.; Huhnke, D.: Temperaturmesstechnik. Oldenbourg Industrieverlag, München, 1. Aufl. (2006).

[Mäk05a] Mäki, R.: Wet Clutch Tribology - Friction Characteristics in Limited Slip Differentials, Dissertation, Luleå University of Technology (2005).

[Mäk05b] Mäki, R.; Nyman, P.; Olsson, R.; Ganemi, B.: Measurement and Characterization of Anti-shudder Properties in Wet Clutch Applications. SAE Technical Paper 2005-01-0878, S. 1–12 (2005).

[Man02] Mansouri, M.; Khonsari, M. M.; Holgerson, M. H.; Aung, W.: Application of analysis of variance to wet clutch engagement. Proceedings of the Institution of Mechanical Engineers, Part J: Journal of Engineering Tribology 216. Issue: 3, S. 117–125 (2002).

[Mar09] Marklund, P.; Sahlin, F.; Larsson, R.: Modelling and simulation of thermal effects in wet clutches operating under boundary lubrication conditions. Proceedings of the Institution of Mechanical Engineers, Part J: Journal of Engineering Tribology 223. Issue: 8, S. 1129–1141 (2009).

[Mar08] Marklund, P.; Larsson, R.: Wet clutch friction characteristics obtained from simplified pin on disc test. Tribology International 41. Issue: 9-10, S. 824–830 (2008).

[Mar07] Marklund, P.; Mäki, R.; Larsson, R.; Höglund, E.; Khonsari, M. M.; Jang, J.: Thermal influence on torque transfer of wet clutches in limited slip differential applications. Tribology International 40. Issue: 5, S. 876–884 (2007).

[Mat93] Matsumoto, T.: A Study of the Influence of Porosity and Resiliency of a Paper-Based Friction Material on the Friction Characteristics and Heat Resistance of the Material. SAE Technical Paper 932924, S. 1–9 (1993).

[Mei17] Meingaßner, G. J.: Methodik zur Untersuchung des Reibungsverhaltens nasslaufender Lamellenkupplungen bei Langsamlauf- und Mikroschlupf, Dissertation, Technische Universität München (2017).

[Mei15] Meingaßner, G. J.; Pflaum, H.; Stahl, K.: Test-Rig Based Evaluation of Performance Data of Wet Disk Clutches. Proceedings of the 14th International CTI Symposium (2015).

[Miy09] Miyagawa, M.; Ogawa, M.; Okano, Y.; Hara, H.; Sasaki, S.; Okui, K.: Numerical Simulation of Temperature and Torque Curve of Multidisk Wet Clutch with Radial and Circumferential Grooves. Tribology Online 4. Issue: 1, S. 17–21 (2009).

[Mot21] Motzet, R.: Analyse der Druck- und Ölverteilung in einer geschlossenen nasslaufenden Lamellenkupplung mittels CFD-Simulationen, Masterarbeit, Lehrstuhl für Maschinenelemente, Technische Universität München (2021).

[Müh18] Mühlenstrodt, K.; Voelkel, K.; Lipinsky, D.; Stockinger, U.; Pflaum, H.; Stahl, K.: Use of Time of Flight Secondary Ion Mass Spectrometry (ToF-SIMS) for Examination of Tribological Layers Formed from Gear Oil Additives Under Tribological Load. Getlub - Tribologie- und Schmierstoffkongress, Würzburg (2018).

[Mur00] Murakami, Y.; Linden, J. L.; Flaherty, J. E.; Sprys, J. W.; King, T. E.; Kurashina, H.; Furumoto, M.; Iwamoto, S.; Kagawa, M.; Ueda, F.: Anti-Shudder Property of Automatic

Transmission Fluids - A Study by the International Lubricants Standardization and Approval Committee (ILSAC) ATF Subcommittee. CEC/SAE Spring Fuels & Lubricants Meeting & Exposition SAE Technical Paper Series, Paris (2000).

[Nau19] Naunheimer, H.; Bertsche, B.; Ryborz, J.; Novak, W.; Fietkau, P.: Fahrzeuggetriebe - Grundlagen, Auswahl, Auslegung und Konstruktion. Springer Vieweg, Berlin, Heidelberg, 3. Auflage (2019).

[Neu19] Neupert, T.; Bartel, D.: High-resolution 3D CFD multiphase simulation of the flow and the drag torque of wet clutch discs considering free surfaces. Tribology International 129, S. 283–296 (2019).

[Neu21] Neupert, T.: Strömungsuntersuchungen an geöffneten nasslaufenden Kupplungslamellen, Dissertation, Otto-von-Guericke-Universität Magdeburg (2021).

[Neu17] Neupert, T.; Bartel, D.: Einfluss des Nutdesigns von nasslaufenden Kupplungslamellen auf das Strömungsverhalten im Lüftspalt. Kupplungen und Kupplungssysteme in Antrieben VDI-Berichte: 2309, Karlsruhe (2017).

[Nie83] Niemann, G.: Maschinenelemente - Band 3: Schraubrad-, Kegelrad-, Schnecken-, Ketten-, Riemen-, Reibradgetriebe, Kupplungen, Bremsen, Freiläufe. Springer, Berlin, Heidelberg, Zweite, völlig neu bearbeitete Auflage (1983).

[Nie03] Niemann, G.; Winter, H.: Getriebe allgemein, Zahnradgetriebe - Grundlagen, Stirnradgetriebe. Springer, Berlin, 2., völlig neubearb. Aufl., 2. berichtigter Nachdr., korrigierter Nachdr (2003).

[Nym06] Nyman, P.; Mäki, R.; Olsson, R.; Ganemi, B.: Influence of surface topography on friction characteristics in wet clutch applications. Wear 261. Issue: 1, S. 46–52 (2006).

[Oer00] Oerleke, C.: Einflußgrößen auf die Schleppmomente schnelllaufender Lamellenkupplungen in Automatgetrieben, Dissertation, Universität der Bundeswehr Hamburg (2000).

[Oht94] Ohtani, H.; Hartley, R. J.; Stinnett, D. W.: Prediction of anti-shudder properties of automatic transmission fluids using a modified SAE No. 2 machine. SAE transactions. Issue: 103, S. 456–467 (1994).

[Ost01] Ost, W.; Baets, P. de; Degrieck, J.: The tribological behaviour of paper friction plates for wet clutch application investigated on SAE#II and pin-on-disk test rigs. Wear 249, S. 361–371 (2001).

[Pah14] Pahlovy, S. A.; Mahmud, S. F.; Kubota, M.; Ogawa, M.; Takakura, N.: Multiphase Drag Modeling for Prediction of the Drag Torque Characteristics in Disengaged Wet Clutches. SAE International Journal of Commercial Vehicles 7. Issue: 2, S. 441–447 (2014).

[Pah16a] Pahlovy, S. A.; Mahmud, S. F.; Kubota, M.; Ogawa, M.; Takakura, N.: Improvement of transmission efficiency by reducing the drag torque in disengaged wet clutch. Development of a model for calculating drag torque or spin loss of disengaged wet clutch of transmission. Getriebe in Fahrzeugen Triebstrang, Integration, Elektrifizierung mit Fachauchstellung VDI-Berichte: 2276, Friedrichshafen (2016).

[Pah16b] Pahlovy, S. A.; Mahmud, S. F.; Kubota, M.; Ogawa, M.; Takakura, N.: New Development of a Gas Cavitation Model for Evaluation of Drag Torque Characteristics in Disengaged Wet Clutches. SAE International Journal of Engines 9. Issue: 3, S. 1910–1915 (2016).

[Pah17] Pahlovy, S. A.; Mahmud, S. F.; Kubota, M.; Ogawa, M.; Takakura, N.: Development of an Analytical Model for Prediction of Drag Torque Characteristics of Disengaged Wet

Clutches in High Speed Region. WCX 17: SAE World Congress Experience SAE Technical Paper Series, Detroit (2017).

[Pan19] Pan, H.; Zhou, X.: Simulation Research on the Drag Torque of Disengaged Wet Clutches. 2019 IEEE 5th International Conference on Mechatronics System and Robots (ICMSR), Singapore (2019).

[Par19] Pardeshi, I.; Shih, T. I.-P.: A Computational Fluid Dynamics Methodology for Predicting Aeration in Wet Friction Clutches. Journal of Fluids Engineering 141. Issue: 12, S. 1536–1543 (2019).

[Par16] Park, S.-M.; Kim, M.-S.; Kim, J.-Y.; Lee, K.-S.: The Heating and Cooling Performance Analysis of Transmission Wet Clutch with Real Shape and Lubricant Condition. Proceedings of the 15th International CTI Symposium 2016, Berlin. CTI (2016).

[Pay91] Payvar, P.: Laminar heat transfer in the oil groove of a wet clutch. International Journal of Heat and Mass Transfer 34. Issue: 7, S. 1791–1798 (1991).

[Pay94] Payvar, P.; Lee, Y. N.; Minkowycz, W. J.: Simulation of heat transfer to flow in radial grooves of friction pairs. International Journal of Heat and Mass Transfer 37. Issue: 2, S. 313–319 (1994).

[Pen19] Peng, Z.; Yuan, S.: Mathematical Model of Drag Torque with Surface Tension in Single-Plate Wet Clutch. Chinese Journal of Mechanical Engineering 32. Issue: 1, S. 57–64 (2019).

[Pfl88] Pflaum, H.: Das Reibungsverhalten ölgeschmierter Kegelreibkupplungen in Synchronisationseinrichtungen von Kraftfahrzeug-Schaltgetrieben, Dissertation, Technische Universität München (1988).

[Pfl98] Pfleger, F.: Schalt- und Lebensdauerverhalten von Lamellenkupplungen, Dissertation, Technische Universität München (1998).

[Plo17] Plothe, A.; Graswald, C.; Grüning, A.; Erggelet, M.: Effizienzsteigerung bei modernen Antriebssystemen durch Kombination von Simulation und Versuch. Reibungsminimierung im Antriebsstrang 2016, Wiesbaden (2017).

[Poi22] Pointner-Gabriel, L.; Forleo, C.; Voelkel, K.; Pflaum, H.; Stahl, K.: Investigation of the Drag Losses of Wet Clutches at Dip Lubrication. WCX SAE World Congress Experience (2022).

[Pol09] Polifke, W.; Kopitz, J.: Wärmeübertragung - Grundlagen, analytische und numerische Methoden. Pearson Studium, München, 2., aktualisierte Aufl. (2009).

[Ran04] Rank, R.; Kearsey, A.: Carbon Based friction materials for automotive applications. 14th International Colloquium Tribology, Stuttgart/Ostfildern (2004).

[Rao12] Rao, G.: Modellierung und Simulation des Systemverhaltens nasslaufender Lamellenkupplungen, Dissertation, Technische Universität Dresden (2012).

[Rau19] Rauscher Markus: Entwicklung einer echtzeitfähigen Temperaturberechnung und -Prädiktion nasslaufender Lamellenkupplungen im Abgleich mit Prüfstandsversuchen, Masterarbeit, Lehrstuhl für Maschinenelemente, Technische Universität München (2019).

[Roh04] Rohm, A.; Reißer, W.: Thermische Festigkeit des Reibsystems nasslaufender (Doppel-)Kupplungen bei Extrembelastungen - Thermal stability of the friction system of (dual) wet clutches at extreme load conditions. Getriebe in Fahrzeugen 2004 VDI-Berichte: 1827, Friedrichshafen (2004).

[Rud11] Rudloff, M.; Bartel, D.; Deters, L.: Simulation der Strömung in nasslaufenden Lamellenkupplungen. Kupplungen und Kupplungssysteme in Antrieben, Wiesloch. VDI (2011).

[Sch19] Schermer, E.: Experimentelle Untersuchungen des thermischen Verhaltens nasslaufender Lamellenkupplungen, Bachelorarbeit, Lehrstuhl für Maschinenelemente, Technische Universität München (2019).

[Sch22a] Schermer, E.: Methode zur praxisnahen Visualisierung der Ölströmung in nasslaufenden Lamellenkupplungen, Masterarbeit, Lehrstuhl für Maschinenelemente, Technische Universität München (2022).

[Sch06] Schlichting, H.: Grenzschicht-Theorie - Mit 22 Tabellen. Springer-Verlag Berlin Heidelberg, Berlin, Heidelberg, 10., überarbeitete Auflage (2006).

[Sch22b] Schneider, T.; Dietsch, M.; Voelkel, K.; Pflaum, H.; Stahl, K.: Analysis of the Thermo-Mechanical Behavior of a Multi-Plate Clutch during Transient Operating Conditions Using the FE Method. Lubricants 10. Issue: 5, S. 76–98 (2022).

[Seo15] Seo, H.; Cha, S. W.; Lim, W.; Han, S.: Method for estimating temperature of 4WD coupling device wet clutches in severe operating condition. International Journal of Precision Engineering and Manufacturing 16. Issue: 1, S. 185–190 (2015).

[Seo11] Seo, H.; Zheng, C.; Lim, W.; Cha, S. W.; Han, S.: Temperature prediction model of wet clutch in coupling. 2011 IEEE Vehicle Power and Propulsion Conference (VPPC), Chicago (2011).

[Shu21] Shui, H.; Zhang, Y.; Yang, H.; Upadhyay, D.; Fujii, Y.: Machine Learning Approach for Constructing Wet Clutch Torque Transfer Function. SAE WCX Digital Summit SAE Technical Paper Series, Online (2021).

[Sie17] Siebertz, K.; van Bebber, D.; Hochkirchen, T.: Statistische Versuchsplanung - Design of Experiments (DoE). Springer Vieweg, Berlin, Heidelberg, 2. Auflage (2017).

[Sin02] Singhal, A. K.; Athavale, M. M.; Li, H.; Jiang, Y.: Mathematical Basis and Validation of the Full Cavitation Model. Journal of Fluids Engineering 124. Issue: 3, S. 617–624 (2002).

[Sta13] Stahl, K.; Pflaum, H.; Hensel, M.: Methods for performance evaluation of lubricants and friction materials in wet multiple disc clutches in axle brake applications. Getriebe in Fahrzeugen 2013 / Drivetrain for Vehicles 2013 - VDI-Berichte 2187, Friedrichshafen. VDI (2013).

[Ste62] Steinhilper, W.: Der zeitliche Temperaturverlauf in Reibungsbremsen und Reibungskupplungen beim Schaltvorgang, Dissertation, Technische Hochschule Karlsruhe (1962).

[Ste63a] Steinhilper, W.: Der zeitliche Temperaturverlauf in schnellgeschalteten Reibungskupplungen und -bremsen - Teil 1. Automobiltechnische Zeitschrift 65. Issue: 8, S. 223–229 (1963).

[Ste63b] Steinhilper, W.: Der zeitliche Temperaturverlauf in schnellgeschalteten Reibungskupplungen und -bremsen - Teil 2. Automobiltechnische Zeitschrift 65. Issue: 10, S. 326–329 (1963).

[Ste63c] Steinhilper, W.: Temperatuverlauf in Lamellenkupplungen beim Schaltvorgang. VDI-Tagung Wellenkupplungen VDI-Berichte: 73, Wiesbaden. VDI (1963).

[Ste64] Steinhilper, W.: Ermittlung des Temperaturverlaufs in Reibungsbremsen und -kupplungen mit Hilfe eines Analogieverfahrens. Automobiltechnische Zeitschrift 66. Issue: 8, S. 228–371 (1964).

[Sto21] Stockinger, U.; Groetsch, D.; Reiner, F.; Voelkel, K.; Pflaum, H.; Stahl, K.: Friction behavior of innovative carbon friction linings for wet multi-plate clutches. Forschung im Ingenieurwesen - Engineering Research 85. Issue: 1, S. 115–127 (2021).

[Sto19] Stockinger, U.; Mühlenstrodt, K.; Voelkel, K.; Pflaum, H.; Lipinsky, D.; Stahl, K.; Arlinghaus, H. F.: Analyse tribologischer Schichten mit der Flugzeit-Sekundärionenmassenspektrometrie (ToF-SIMS) – Additiveinflüsse auf das Reibungsverhalten nasslaufender Lamellenkupplungen. Forschung im Ingenieurwesen - Engineering Research 83. Issue: 2, S. 219–226 (2019).

[Sto18a] Stockinger, U.; Pflaum, H.; Stahl, K.: Zeiteffiziente Methodik zur Ermittlung des Reibungsverhaltens nasslaufender Lamellenkupplungen mit Carbon-Reibbelag. Forschung im Ingenieurwesen - Engineering Research 82. Issue: 1, S. 1–7 (2018).

[Sto18b] Stockinger, U.; Pflaum, H.; Stahl, K.: Friction screening tests for wet multi-plate clutches - Variation of lubricant and friction lining. Proceedings of Asia International Conference on Tribology, Kuching (2018).

[Str21] Strobl, P.; Pflaum, H.; Stahl, K.: FVA-Nr. 719 II - Heft 1431 - Abschlussbericht Langsamlauf-Mikroschlupf Lamellenkupplungen - Einflüsse des Reibsystems und der Beanspruchung auf das Reibungsverhalten von Lamellenkupplungen bei Langsamlauf- und Mikroschlupf. Forschungsvereinigung Antriebstechnik e.V., Frankfurt/Main (2021).

[Str22] Strobl, P.; Schermer, E.; Groetsch, D.; Pointner-Gabriel, L.; Voelkel, K.; Pflaum, H.; Stahl, K.: Identification and Validation of Linear Friction Models Using ANOVA and Stepwise Regression. Lubricants 10. Issue: 11, S. 286–302 (2022).

[Sud11] Sudarsanam, N.; Frey, D. D.: Using ensemble techniques to advance adaptive one-factor-at-a-time experimentation. Quality and Reliability Engineering International 27. Issue: 7, S. 947–957 (2011).

[Sun14] Sun, S.; Lei, Y. L.; Li, X. Z.: Simulations of Drag Torque in Multi-Plate Wet Clutch Affecting Synchronizers in a TC+AMT Transmission. SAE 2014 World Congress & Exhibition SAE Technical Paper Series, Detroit (2014).

[Tak11] Takagi, Y.: Effect of two-phase flow on drag torque in a wet clutch. Journal of Advanced Research in Physics 2. Issue: 2, 1-5 (2011).

[Ter18a] Terzi, S.; Manhartsgruber, B.; Milani, M.; Montorsi, L.: Optimization of the Lubrication Distribution in Multi Plate Wet-Clutches for HVT Transmissions: An Experimental - Numerical Approach. International Powertrains, Fuels & Lubricants Meeting SAE Technical Paper Series, Heidelberg (2018).

[Ter18b] Terzi, S.; Milani, M.; Montorsi, L.; Manhartsgruber, B.: Experimental and numerical analysis of the multiphase flow distribution in multi plate wetclutches for HVT transmissions under actual operating conditions. 2018 Global Fluid Power Society PhD Symposium (GFPS), Samara (2018).

[Voe17] Voelkel, K.; Pflaum, H.; Stahl, K.: Thermal behavior and cooling conditions of wet multi-plate clutches in modern applications. Proceedings of the STLE 72th Annual Meeting & Exhibition (2017).

[Voe18] Voelkel, K.; Wohlleber, F.; Pflaum, H.; Stahl, K.: Kühlverhalten nasslaufender Lamellenkupplungen in neuen Anwendungen - Cooling performance of wet multi-plate disk clutches in modern applications. Forschung im Ingenieurwesen - Engineering Research 82. Issue: 3, S. 197–203 (2018).

[Voe20] Voelkel, K.: Charakterisierung des Einlaufverhaltens nasslaufender Lamellenkupplungen, Dissertation, Technische Universität München (2020).

[Voe16a] Voelkel, K.; Pflaum, H.; Stahl, K.: Das thermische Verhalten nasslaufender Lamellenkupplungen - Simulation mit dem FVA-Programm KUPSIM. Getlub - Tribologie- und Schmierstoffkongress, Würzburg (2016).

[Voe16b] Voelkel, K.; Pflaum, H.; Stahl, K.: FVA-Nr.150/VII - Heft 1204 - KUPSIM 3.0 Abschlussbericht - Erweiterung der Simulationsmethodik zur Berechnung des instationären Temperaturverhaltens nasslaufender Lamellenkupplungen. Forschungsvereinigung Antriebstechnik e.V., Frankfurt/Main (2016).

[Voe19] Voelkel, K.; Pflaum, H.; Stahl, K.: Einflüsse der Stahllamelle auf das Einlaufverhalten von Lamellenkupplungen. Forschung im Ingenieurwesen - Engineering Research 83. Issue: 2, S. 185–197 (2019).

[Wan18] Wang, Y.; Guo, C.; Li, Y.; Li, G.: Modelling the influence of velocity on wet friction-element friction in clutches. Industrial Lubrication and Tribology 70. Issue: 1, S. 42–50 (2018).

[Wäs14] Wäsche, R.; Woydt, M.: Stribeck Curve. Mang, T. Encyclopedia of Lubricants and Lubrication, Berlin, Heidelberg (2014).

[Web10] Weber, N.; Skubacz, T.; Poll, G.; Elfrath, T.: Fluorescence-based Investigations into the Contact of Wet-Disc Clutches. Optical investigations into the flat friction contact of multi-disc clutches. Getriebe in Fahrzeugen 2010 VDI-Berichte: 2081, Friedrichshafen (2010).

[Wei12] Weißbach, W.: Werkstoffkunde - Strukturen, Eigenschaften, Prüfung ; mit 248 Tabellen. Vieweg + Teubner, Wiesbaden, 18., überarb. Aufl. (2012).

[Win85] Winkelmann, S.; Harmuth, H.: Schaltbare Reibkupplungen - Grundlagen, Eigenschaften, Konstruktionen. Springer, Berlin, 1. Aufl. (1985).

[Win08] Winkler, J.: Tribologischer Schichtaufbau bei Synchronisierungen und sein Einfluss auf Reibung und Verschleiß, Dissertation, Technische Universität München (2008).

[Wit13] Wittel, H.; Muhs, D.; Jannasch, D.; Voßiek, J.: Maschinenelemente - Normung, Berechnung, Gestaltung. Springer Vieweg, Wiesbaden, 21. Aufl. (2013).

[Woh12] Wohlleber, F.: Thermischer Haushalt nasslaufender Lamellenkupplungen, Dissertation, Technische Universität München (2012).

[Woh09] Wohlleber, F.; Pflaum, H.; Höhn, B.-R.: FVA-Nr. 150 VI - Heft 899 - KUPSIM 2.2 - Programmerweiterung zur thermischen Nachrechnung von Lamellenkupplungen und Integration des Programms in die FVA-Workbench. Forschungsvereinigung Antriebstechnik e.V., Frankfurt/Main (2009).

[Woh11] Wohlleber, F.; Pflaum, H.; Höhn, B.-R.; Stahl, K.: FVA-Nr. 413 II+III - Heft 985 - Wärmeübergang Lamellenkupplung - Ermittlung von Wärmeübergangsverhalten und Schluckvermögen von Lamellenkupplungen. Forschungsvereinigung Antriebstechnik e.V., Frankfurt/Main (2011).

[Wu21] Wu, B.; Qin, D.; Hu, J.; Liu, Y.: Experimental Data Mining Research on Factors Influencing Friction Coefficient of Wet Clutch. Journal of Tribology 143. Issue: 12, S. 1–10 (2021).

[Wu19] Wu, J.; Ma, B.; Li, H.; Liu, J.: Creeping control strategy for Direct Shift Gearbox based on the investigation of temperature variation of the wet multi-plate clutch. Proceedings of the Institution of Mechanical Engineers, Part D: Journal of Automobile Engineering 233. Issue: 14, S. 3857–3870 (2019).

[Wu15] Wu, W.; Xiong, Z.; Hu, J.; Yuan, S.: Application of CFD to model oil–air flow in a grooved two-disc system. International Journal of Heat and Mass Transfer 91, S. 293–301 (2015).

[Xie10] Xie, F.; Hou, Y.: Transient temperature field of a friction pair in a HVD device of a belt conveyor. Mining Science and Technology (China) 20. Issue: 6, S. 904–907 (2010).

[Xie15] Xie, X.; Qu, D.; Liu, F.; Wang, Q.: Thermal-Structural Coupling Analysis of Wet Clutch Friction Discs Based on APDL. 2015 8th International Conference on Intelligent Computation Technology and Automation (ICICTA), Nanchang (2015).

[Yan95] Yang, Y.; Lam, R. C.; Chen, Y. F.; Yabe, H.: Modeling of Heat Transfer and Fluid Hydrodynamics for a Multidisc Wet Clutch. SAE International Congress & Exposition SAE Technical Paper Series, Detroit (1995).

[Yan98] Yang, Y.; Lam, R. C.; Fujii, T.: Prediction of Torque Response During the Engagement of Wet Friction Clutch. SAE International Congress & Exposition SAE Technical Paper Series, Detroit (1998).

[Yas18] Yashwanth, B. L.; Ngo, D.; Schroeder, D.; Hopson, B.; Wang, D. M.: Drag and Cooling Characteristics of Circular Pin-Fin Groove Pattern of a Multi-plate Clutch Pack Using CFD. WCX World Congress Experience SAE Technical Paper Series, Detroit (2018).

[Yos19] Yoshizumi, F.; Tani, H.; Sanda, S.: Simulation of the Friction Coefficient of Paper-Based Wet Clutch With Wavy Separators. Journal of Tribology 141. Issue: 1, S. 1–13 (2019).

[Yua11] Yuan, S.: Experimental Research and Mathematical Model of Drag Torque in Single-plate Wet Clutch. Chinese Journal of Mechanical Engineering 24. Issue: 01, S. 91–99 (2011).

[Yua10] Yuan, S.; Guo, K.; Hu, J.; Peng, Z.: Study on Aeration for Disengaged Wet Clutches Using a Two-Phase Flow Model. Journal of Fluids Engineering 132. Issue: 11, S. 1–6 (2010).

[Yua03] Yuan, Y.; Attibele, P.; Dong, Y.: CFD Simulation of the Flows Within Disengaged Wet Clutches of an Automatic Transmission. SAE 2003 World Congress & Exhibition SAE Technical Paper Series, Detroit (2003).

[Yua07] Yuan, Y.; Liu, E. A.; Hill, J.; Zou, Q.: An Improved Hydrodynamic Model for Open Wet Transmission Clutches. Journal of Fluids Engineering 129. Issue: 3, S. 333–337 (2007).

[Zha09] Zhang, J.-L.; Ma, B.; Zhang, Y.-F.; Li, H.: Simulation and Experimental Studies on the Temperature Field of a Wet Shift Clutch during One Engagement. 2009 International Conference on Computational Intelligence and Software Engineering, Wuhan (2009).

[Zha18] Zhao, E.; Ma, B.; Li, H.: The Tribological Characteristics of Cu-Based Friction Pairs in a Wet Multidisk Clutch Under Nonuniform Contact. Journal of Tribology 140. Issue: 1, 1-9 (2018).

[Zhi16] Zhigang, Z.; Xiaohui, S.; Dong, G.: Dynamic Temperature Rise Mechanism and Some Controlling Factors of Wet Clutch Engagement. Mathematical Problems in Engineering 2016. Issue: 2, S. 1–12 (2016).

[Zör17] Zörntlein, K.: Literaturrecherche und Auswertung zum Thema Simulation und Berechnung von nasslaufenden Lamellenkupplungen, Semesterarbeit, Lehrstuhl für Maschinenelemente, Technische Universität München (2017).

[Zou13] Zou, Q.; Rao, C.; Barber, G.; Zhou, B.; Wang, Y.: Investigation of surface characteristics and tribological behavior of clutch plate materials. Wear 302. Issue: 1-2, S. 1378–1383 (2013).

Websites and User Manuals

[Hts21] Htsteelmill: Mat.No. 1.0601, DIN C60, AISI 1060. URL: http://www.htsteelmill.com/mat-no-1-0601-din-c60-aisi-1060.html. Last Access 11.10.2021.

[Mat22a] MathWorks: MATLAB Documentation. URL: https://de.mathworks.com/help/matlab/. Last Access 24.09.2022.

[Mat22b] MathWorks: Simulink Documentation. URL: https://de.mathworks.com/help/simulink/. Last Access 24.09.2022.

[Pho22a] Photron Deutschland GmbH: FASTCAM Mini AX. URL: https://photron.com/de/fastcam-mini-ax/. Last Access 03.06.22.

[Pho22b] Photron Deutschland GmbH: PRODUCT DATASHEET Mini AX - FASTCAM series by Photron. URL: https://photron.com/wp-content/uploads/2021/12/Mini-AX-2021_LR.pdf. Last Access 0.30.6.22.

[Sim22] Simerics GmbH: Solutions - Simerics. URL: https://simerics.de/solutions/?lang=en. Last Access 24.09.2022.

[Sim20] Simerics Inc.: Simerics MP+ Manual v5.1. Simerics Inc., Seattle, 1. Aufl. (2020).

[Tam22] Tamron Europe GmbH: SP AF 28-75mm F/2.8 XR Di LD Aspherical [IF] MACRO. URL: https://www.tamron.eu/de/objektive/sp-af-28-75mm-f28-xr-di-ld-aspherical-if-macro/. Last Access 03.06.22.

[Vis22] Vision Devices GmbH: LED Strahler VD36. URL: https://www.visiondevices.de/overview/produkte/led-leuchte-vd7000-2/. Last Access 03.06.22.

Supervised Student Research Projects Relevant to This Thesis

The following student research projects, whose processing, evaluation, interpretation and presentation of results were carried out under the author's substantial scientific guidance, were carried out at the Institute of Machine Elements, Gear Research Center (FZG). Some of the results were incorporated into the work.

Schermer, E.: Methode zur praxisnahen Visualisierung der Ölströmung in nasslaufenden Lamellenkupplungen, Masterarbeit, Technische Universität München (2022).

Jancik, M.: Experimentelle Untersuchungen zum thermischen Verhalten nasslaufender Lamellenkupplungen, Bachelorarbeit, Technische Universität München (2021).

Motzet, R.: Analyse der Druck- und Ölverteilung in einer geschlossenen nasslaufenden Lamellenkupplung mittels CFD-Simulationen, Masterarbeit, Technische Universität München (2021).

Baumgartner, A.: Reibungsverhalten nasslaufender Lamellenkupplungen – Messunsicherheiten und Auswertemethoden, Masterarbeit, Technische Universität München (2020).

Rauscher Markus: Entwicklung einer echtzeitfähigen Temperaturberechnung und -Prädiktion nasslaufender Lamellenkupplungen im Abgleich mit Prüfstandsversuchen, Masterarbeit, Technische Universität München (2019).

Schermer, E.: Experimentelle Untersuchungen des thermischen Verhaltens nasslaufender Lamellenkupplungen, Bachelorarbeit, Technische Universität München (2019).

Zörntlein, K.: Literaturrecherche und Auswertung zum Thema Simulation und Berechnung von nasslaufenden Lamellenkupplungen, Semesterarbeit, Technische Universität München (2017).

Other Unpublished Work

The following papers, which were written in the years 2016 to 2022 at the Institute of Machine Elements, Gear Research Center (FZG), were partly included in this work:

Groetsch, D.; Pflaum, H.; Stahl, K.: FVA-Nr. 413 V - Heft - Abschlussbericht Echtzeit-Temperaturberechnung Lamellenkupplungen - Echtzeit-Temperaturberechnung und Temperaturprädiktion nasslaufender Lamellenkupplungen im Betrieb. Forschungsvereinigung Antriebstechnik e.V., Frankfurt/Main (2021).

Dissertationen der FZG

1	PERRET, H.	Übertragung konstanter Leistung durch stufenlos mechanische Regeltriebe. TH Braunschweig (1935).
2	BELLMANN, H.	Beiträge zur Prüfung von Bremsbelägen. TH Braunschweig (1939).
3	HIERSIG, H.M.	Der Zusammenhang von Gestaltung und Beanspruchung bei Schneckengetrieben mit Evolventenverzahnung. TH Braunschweig (1943).
4	HELBIG, F.	Walzenfestigkeit und Grübchenbildung von Zahnrad- und Wälzlagerwerkstoffen. TH Braunschweig (1943).
5	ARF, D.	Pendelrollenlager mit symmetrischen und unsymmetrischen Rollen. TH Braunschweig (1944).
6	OESMANN, W.	Entwicklung einer Stahlsand-Schalt- und Regelkupplung. TH Braunschweig (1945).
7	RUBO, E.	Ermittlung der Achsfehler-Empfindlichkeit verschiedener Zylinder-Schneckengetriebe mit Hilfe des Einlauf-Abschliffvolumens. TH Braunschweig (1948).
8	GLAUBITZ, H.	Drehmomentmessungen zum Wendevorgang bei Raupenfahrwerken. TH Braunschweig (1948).
9	TALKE, H.	Beiträge zur hydrodynamischen Schmiertheorie des ebenen Gleitschuhes auf ebener Fläche. TH Braunschweig (1948).
10	CRAMER, H.	Über die Reibung und Schmierung feinmechanischer Geräte. TH Braunschweig (1949).
11	THOMAS, W.	Reibscheiben-Regelgetriebe mit Linienberührung. TH Braunschweig (1949).
12	MAUSHAKE, W.	Theoretische Untersuchung von Schneckengetrieben mit Globoidschnecke und Stirnrad. TH Braunschweig (1950).
13	KRAUPNER, K.W.	Das plastische Verhalten umlaufender Stahlrollen bei Punktberührung. TH Braunschweig (1951).
14	BANASCHEK, K.	Die Gleitreibung geschmierter Flächen kleiner Schmiegung. Einfluß von Werkstoffpaarung, Krümmung, Oberfläche und Schmierstoff. TH Braunschweig (1951).
15	HEYER, E.	Versuche mit Zylinderschneckentrieben. Einfluß von Zahnform, Modul, Durchmesser und Schmierstoff auf Verlustleistung und Tragfähigkeit. TH München (1952).
16	HENTSCHEL, G.	Der Hochleistungswälztrieb. Entwicklungsstand und Entwicklungsmöglichkeiten. TH München (1952).
17	WINTER, H.	Tragfähigste Evolventengeradverzahnung. TH München (1954).
18	ROY, A.K.	Spannungsoptische Untersuchung eines schrägverzahnten Stirnrades. TH München (1957).

19	RETTIG, H.	Dynamische Zahnkraft. TH München (1957).
20	OHLENDORF, H.	Verlustleistung und Erwärmung von Stirnrädern. TH München (1958).
21	UNTERBERGER, M.	Geräuschuntersuchungen an geradverzahnten Zahnrädern. TH München (1958).
22	LOOMAN, J.	Das Abrichten von profilierten Schleifscheiben zum Schleifen von schrägverzahnten Stirnrädern. TH München (1959).
23	JARCHOW, F.	Versuche an Stirnrad-Globoidschneckentrieben. TH München (1960).
24	POPOVIC, L.	Einfluß von Zahnform und Bearbeitung auf die Zahnfußfestigkeit. TH München (1960).
25	EHRLENSPIEL, K.	Die Festkörperreibung von geschmierten und ungeschmierten Metallpaarungen mit Linienberührung. TH München (1962).
26	PITTROFF, H.	Riffelbildung infolge Stillstandserschütterungen bei Wälzlagern. TH München (1962).
27	SCHREIBER, H.	Zur Auswertung von Lebensdauerversuchen an Wälzlagern. TH München (1962).
28	ROTH, K.	Untersuchungen über die Eignung der Evolventenzahnform für eine allgemein verwendbare feinwerktechnische Normverzahnung. TH München (1963).
29	NARUSE, Ch.	Verschleiß, Tragfähigkeit und Verlustleistung bei Schraubenradgetrieben. TH München (1964).
30	GARTNER, F.	Die Mischreibung bei Linienberührung. TH München (1964).
31	ASSMANN, H.	Vergleichende Untersuchung von Getriebeölen im FZG-Stirnrad- und Esso-Hypoidprüfstand. TH München (1965).
32	REISTER, D.	Einseitiges Breitentragen bei Stirnrädern. TH München (1965).
33	KORRENN, H.	Gleitreibung in den Kontaktstellen zwischen den Wälzkörpern und den Laufbahnen der Ringe von Wälzlagern. TH München (1965).
34	HÖSEL, Th.	Geräuschuntersuchungen an schrägverzahnten Stirnrädern mit Evolventenverzahnung. TH München (1965).
35	LANGENBECK, K.	Die Verschleiß- und Freßgrenzlast der Hypoidgetriebe. TH München (1966).
36	MEMMEL, M.	Untersuchungen über die Tragfähigkeit und Gebrauchsdauer von Gelenklagern. TH München (1966).
37	BÖTSCH, H.	Der Einfluß der Oberflächenbearbeitung und -behandlung auf die Flankenfestigkeit von Stirnrädern aus Vergütungsstahl. TH München (1966).
38	LECHNER, G.	Die Freßlastgrenze bei Stirnrädern aus Stahl. TH München (1966).

39	LANGE, S.	Untersuchungen von Helicon- und Spiroidgetrieben mit abwickelbaren Schneckenflanken nach der hydrodynamischen und nach der Hertzschen Theorie. TH München (1967).
40	SCHWÄGERL, D.	Untersuchung von Helicon- und Spiroidgetrieben mit trapezförmigem Schneckenprofil nach der Hertzschen und nach der hydrodynamischen Theorie. TH München (1967).
41	MICHELS, K.	Schneckengetriebe mit Werkstoffpaarung Stahl/Grauguß. TH München (1968).
42	GACKSTETTER, G.	Verlustarme Verzahnung. TH München (1968).
43	GEUPEL, H.	Flüssigkeitsreibung bei Punktberührung. TH München (1969).
44	GREKOUSSIS, R.	Vergleichende Untersuchungen zur Freßtragfähigkeit von Hypoid- und Stirnrädern. TH München (1969).
45	BAETHGE, J.	Zahnfederhärte, Drehwegfehler und Geräusch bei Stirnrädern. TH München (1969).
46	SCHULZ, H.D.	Untersuchung über Tragfähigkeiten und Verlustleistung von Schneckengetrieben mit trapezförmigem Schneckenprofil und kegeliger Schnecke. TH München (1969).
47	STÖLZLE, K.	Leistungsübertragung in Planetengetrieben bei statischem und dynamischem Betrieb. Berechnung, Optimierung und Versuchsergebnisse. TH München (1970).
48	SEITZINGER, K.	Die Erwärmung einsatzgehärteter Zahnräder als Kennwert für ihre Freßtragfähigkeit. TU München (1971).
49	STÖSSEL, K.	Reibungszahlen unter elasto-hydrodynamischen Bedingungen. TU München (1971).
50	SCHMIDT, G.	Berechnung der Wälzpressung schrägverzahnter Stirnräder unter Berücksichtigung der Lastverteilung. TU München (1972).
51	HIRT, M.	Einfluß der Zahnfußausrundung auf Spannung und Festigkeit von Geradstirnrädern. TU München (1974).
52	WILKESMANN, H.	Berechnung von Schneckengetrieben mit unterschiedlichen Zahnprofilformen (Tragfähigkeits- und Verlustleistung für Hohlkreis-, Evolventen- und Geradlinienprofil). TU München (1974).
53	RICHTER, M.	Der Verzahnungswirkungsgrad und die Freßtragfähigkeit von Hypoid- und Schraubenradgetrieben - Versuchsergebnisse und Berechnungsmethoden. TU München (1976).
54	RÖSCH, H.	Untersuchungen zur Wälzfestigkeit von Rollen - Einfluß von Werkstoff, Wärmebehandlung und Schlupf. TU München (1976).
55	GAGGERMEIER, H.	Untersuchungen zur Reibkraftübertragung in Regel-Reibradgetrieben im Bereich elasto-hydrodynamischer Schmierung. TU München (1977).

56	KÄSER, W.	Beitrag zur Grübchenbildung an gehärteten Zahnrädern. Einfluß von Härtetiefe und Schmierstoff auf die Flankentragfähigkeit. TU München (1977).
57	KNABEL, W.	Geräusche und Schwingungen an Stirnradgetrieben. Untersuchungen geometrischer Einflüsse bei hohen Drehzahlen und Belastungen. TU München (1977).
58	WIRTH, X.	Über den Einfluß von Schleifkerben auf die Zahnfußtragfähigkeit und das Schädigungsverhalten oberflächengehärteter Zahnräder. TU München (1977).
59	HUBER, G.	Zylinderschneckengetriebe, ein Beitrag zur Berechnung von Grübchen- und Gleitverschleiß und Angaben zum Wirkungsgradverhalten aus Versuchen. TU München (1978).
60	BROSSMANN, U.	Über den Einfluß der Zahnfußausrundung und des Schrägungswinkels auf Beanspruchung und Festigkeit schrägverzahnter Stirnräder. TU München (1979).
61	PLEWE, H.-J.	Untersuchungen über den Abriebverschleiß von geschmierten, langsam laufenden Zahnrädern. TU München (1980).
62	FRESEN, G.	Untersuchungen über die Tragfähigkeit von Hypoid- und Kegelradgetrieben (Grübchen, Ridging, Rippling, Graufleckigkeit und Zahnbruch). TU München (1981).
63	OSTER, P.	Beanspruchung der Zahnflanken unter Bedingungen der Elastohydrodynamik. TU München (1982).
64	HORNUNG, K.	Zahnräder aus Bainitischem Gusseisen mit Kugelgraphit. TU München (1983).
65	WEISS, T.	Zum Festigkeits- und Verzugsverhalten von randschichtgehärteten Zahnrädern. TU München (1983).
66	VOJACEK, H.	Das Reibungsverhalten von Fluiden unter elastohydrodynamischen Bedingungen. Einfluß der chem. Struktur des Fluides, der Werkstoffe und der Makro- und Mikrogeometrie der Gleit/Wälzkörper. TU München (1984).
67	SCHÖNNENBECK, G.	Einfluß der Schmierstoffe auf die Zahnflankenermüdung (Graufleckigkeit und Grübchenbildung) hauptsächlich im Umfangsgeschwindigkeitsbereich 1...9 m/s. TU München (1984).
68	WIENER, H.	Untersuchung der Rollenkinematik im Axial-Pendelrollenlager. TU München (1984).
69	MATHIAK, D.	Untersuchungen über Flankentragfähigkeit, Zahnfußtragfähigkeit und Wirkungsgrad von Zylinderschneckengetrieben. TU München (1984).
70	STRASSER, H.	Einflüsse von Verzahnungsgeometrie, Werkstoff und Wärmebehandlung auf die Zahnfußtragfähigkeit. TU München (1984).

71	JOACHIM, F.-J.	Untersuchungen zur Grübchenbildung an vergüteten und normalisierten Zahnrädern (Einfluß von Werkstoffpaarung, Oberflächen- und Eigenspannungszustand). TU München 1984.
72	GERBER, H.	Innere dynamische Zusatzkräfte bei Stirnradgetrieben - Modellbildung, innere Anregung und Dämpfung. TU München (1984).
73	SIMON, M.	Messung von elasto-hydrodynamischen Parametern und ihre Auswirkung auf die Grübchentragfähigkeit vergüteter Scheiben und Zahnräder. TU München (1984).
74	SCHMIDT, W.	Untersuchungen zur Grübchen- und zur Zahnfußtragfähigkeit geradverzahnter evolventischer Innenstirnräder. TU München (1984).
75	FUNCK, G.	Wärmeabführung bei Getrieben unter quasistationären Betriebsbedingungen. TU München (1985).
76	PAUL, M.	Einfluß von Balligkeit und Lageabweichungen auf die Zahnfußbeanspruchung spiralverzahnter Kegelräder. TU München (1986).
77	HOPPE, F.	Das Abschalt- und Betriebsverhalten von mechanischen Sicherheitskupplungen. TU München (1986).
78	MICHAELIS, K.	Die Integraltemperatur zur Beurteilung der Freßtragfähigkeit von Stirnradgetrieben. TU München (1987).
79	WECH, L.	Untersuchungen zum Wirkungsgrad von Kegelrad- und Hypoidgetrieben. TU München (1987).
80	KNAUER, G.	Zur Grübchentragfähigkeit einsatzgehärteter Zahnräder - Einfluß von Werkstoff, Schmierstoff und Betriebstemperatur. TU München (1988).
81	PLACZEK, T.	Lastverteilung und Flankenkorrektur in gerad- und schrägverzahnten Stirnradstufen. TU München (1988).
82	PFLAUM, H.	Das Reibungsverhalten ölgeschmierter Kegelreibkupplungen in Synchronisationseinrichtungen von Kraftfahrzeug-Schaltgetrieben. TU München (1988).
83	BRINCK, P.	Zahnfußtragfähigkeit oberflächengehärteter Stirnräder bei Lastrichtungsumkehr. TU München (1989).
84		entfallen
85	NEUPERT, K.	Verschleißtragfähigkeit und Wirkungsgrad von Zylinder-Schneckengetrieben. TU München (1990).
86	PREXLER, F.	Einfluß der Wälzflächenrauheit auf die Grübchenbildung vergüteter Scheiben im EHD-Kontakt. TU München (1990).
87	SCHALLER, K.-V.	Betriebsfestigkeitsuntersuchungen zur Grübchenbildung an einsatzgehärteten Stirnradflanken. TU München (1990).
88	COLLENBERG, H.-F.	Untersuchungen zur Freßtragfähigkeit schnellaufender Stirnradgetriebe. TU München (1991).

89	MÜLLER, R.	Schwingungs- und Geräuschanregung bei Stirnradgetrieben. TU München (1991).
90	ANZINGER, M.	Werkstoff- und Fertigungseinflüsse auf die Zahnfußtragfähigkeit, insbesondere im hohen Zeitfestigkeitsgebiet. TU München (1991).
91	KAGERER, E.	Messung von elastohydrodynamischen Parametern im hochbelasteten Scheiben- und Zahnkontakt. TU München (1991).
92	HASLINGER, K.	Untersuchungen zur Grübchentragfähigkeit profilkorrigierter Zahnräder. TU München (1991).
93	VOLLHÜTER, F.	Einfluß der Achsversetzung auf die Grübchen- und Zahnfußtragfähigkeit von spiralverzahnten Kegelrädern. TU München (1992).
94	PINNEKAMP, B.	Das Schaltverhalten von PKW-Getriebesynchronisierungen. TU München (1992).
95	SCHUBERT, M.	Einfluß der Befestigungsart und Radkranzdicke auf die Zahntragfähigkeit von Innenstirnrädern. TU München (1993).
96	STEINGRÖVER, K.	Untersuchung zu Verschleiß, Verlustgrad und Fressen bei Zylinder-Schneckengetrieben. TU München (1993).
97	ELSTORPFF, M.-G.	Einflüsse auf die Grübchentragfähigkeit einsatzgehärteter Zahnräder bis in das höchste Zeitfestigkeitsgebiet. TU München (1993).
98	EMMERT, S.	Untersuchungen zur Zahnflankenermüdung (Graufleckigkeit, Grübchenbildung) schnellaufender Stirnradgetriebe. TU München (1994).
99	SUCHANDT, Th.	Betriebsfestigkeitsuntersuchungen zur Zahnfußtragfähigkeit einsatzgehärteter Zahnräder und zur Bruchfestigkeit vergüteter Laschenketten. TU München (1994).
100	HÄMMERL, B.	Lebensdauer- und Temperaturverhalten ölgekühlter Lamellenkupplungen bei Lastkollektivbeanspruchung. TU München (1994).
101	WEISS, R.	Einfluß der Ölalterung auf die Zahnflankentragfähigkeit. TU München (1994).
102	SCHLENK, L.	Untersuchungen zur Freßtragfähigkeit von Großzahnrädern. TU München (1995).
103	MANN, U.	Schmierfilmbildung in elastohydrodynamischen Kontakten, Einfluß verschiedener Grundöle und Viskositäts-Index-Verbesserer. TU München (1995).
104	RUDZEWSKI, S.	Systemtechnische Verknüpfung eingeführter Getriebeberechnungsprogramme. TU München (1995).
105	RANK, R.	Untersuchungen zur Lebensdauerprüfung von Synchronisierungen. TU München (1995).

106	EBERSPÄCHER, C.	Reihenfolgeeffekte bei der Grübchen-Betriebsfestigkeit einsatzgehärteter Zahnräder. TU München (1995).
107	RANK, B.	Untersuchungen zur Grübchenbildung bei Zylinder-Schneckengetrieben. TU München (1996).
108	SATTELBERGER, K.	Schwingungs- und Geräuschanregung bei ein- und mehrstufigen Stirnradgetrieben. TU München (1997).
109	HIRSCHMANN, V.	Tragfähigkeitsuntersuchungen an stufenlosen Umschlingungsgetrieben. TU München (1997).
110	THOMAS, J.	Flankentragfähigkeit und Laufverhalten von hartfeinbearbeiteten Kegelrädern. TU München (1998).
111	WIKIDAL, F.	Berechnung der Flankenpressung gerad- und schrägverzahnter Stirnräder für last- und fertigungsbedingte Abweichungen. TU München (1998).
112	PERPONCHER, V., CH.	Einflüsse von Reibflächentopographie und Beanspruchungen auf das Reibungs- und Verschleißverhalten von Synchronisierungen. TU München (1998).
113	SCHEDL, U.	Einfluß des Schmierstoffs auf die Grübchenlebensdauer einsatzgehärteter Zahnräder. TU München (1998).
114	VOLLMER, T.	Methodik zur Entwicklung einer Fahrstrategie für Fahrzeuge, ausgeführt am Beispiel des Autarken Hybrids. TU München (1998).
115	HEITMANN, A.	Entwicklung des i²-Getriebes für den Autarken Hybrid-Antriebsstrang. TU München (1998).
116	PFLEGER, F.	Schalt- und Lebensdauerverhalten von Lamellenkupplungen. TU München (1998).
117	KERSCHL, S.	Der Autarke Hybrid - Optimierung des Antriebsstrangs hinsichtlich Energieverbrauch und Bestimmung des Einsparpotentials. TU München (1998).
118	DÖBEREINER, R.	Tragfähigkeit von Hochverzahnungen geringer Schwingungsanregung. TU München (1998).
119	WEIGAND, U.	Werkstoff- und Wärmebehandlungseinflüsse auf die Zahnfußtragfähigkeit. TU München (1999).
120	SCHRADE, U.	Einfluß von Verzahnungsgeometrie und Betriebsbedingungen auf die Graufleckentragfähigkeit von Zahnradgetrieben. TU München (2000).
121	KÖLL, J.	Konstruktion des Getriebes für ein Pkw-Hybridantriebssystem. TU München (2000).
122	FÖRSTER, W.	Der Lastschaltvorgang beim stufenlosen i²-Getriebe des Autarken Hybrid-Antriebsstrangs. TU München (1999).
123	LANGE, N.	Hoch fresstragfähige Schneckengetriebe mit Rädern aus Sphaeroguß. TU München (2000).
124	LUTZ, M.	Methoden zur rechnerischen Ermittlung und Optimierung von Tragbildern an Schneckengetrieben. TU München (2000).

125	KOPATSCH, F.	Wirksamkeit von Viskositätsindex-Verbesserern im EHD-Zahnradkontakt. TU München (2000).
126	BAYERDÖRFER, I.	Einfluß von betriebsbedingten Schmierstoffveränderungen auf die Flankentragfähigkeit einsatzgehärteter Stirnräder. TU München (2000).
126e	DOMIAN, H.-J.	Systematische Synthese von Getriebestrukturen der Vorgelegebauart. TU München 2001.
127	TOBIE, T.	Zur Grübchen- und Zahnfußtragfähigkeit einsatzgehärteter Zahnräder. TU München (2001).
128	STAHL, K.	Grübchentragfähigkeit einsatzgehärteter Gerad- und Schrägverzahnungen unter besonderer Berücksichtigung der Pressungsverteilung. TU München (2001).
129	NEUMÜLLER, M.	Einfluß der Ölalterung auf Reibungs- und Verschleißverhalten von Synchronisierungen. TU München (2001).
130	MOSBACH, C.	Das Reibungs- und Reibschwing-Verhalten nasslaufender Lamellenkupplungen. TU München (2002).
131	DYLA, A.	Modell einer durchgängig rechnerbasierten Produktentwicklung. TU München (2002).
132	GRASWALD, C.	Reibung im elastohydrodynamischen Kontakt von Reibradgetrieben. TU München (2002).
133	GEISER, H..	Grundlagen zur Beurteilung des Schwingungsverhaltens von Stirnrädern. TU München (2002).
134	SCHINAGL, S.	Zahnfußtragfähigkeit schrägverzahnter Stirnräder unter Berücksichtigung der Lastverteilung. TU München (2002).
135	DOLESCHEL, A.	Wirkungsgradberechnung von Zahnradgetrieben in Abhängigkeit vom Schmierstoff. TU München (2003).
136	ANNAST, R.	Kegelrad-Flankenbruch. TU München (2003)
137	SÜSSMUTH, J.-F.	Eignungsbeurteilung von Schmierstoffen für stufenlose Umschlingungsgetriebe. TU München (2003).
138	MATTEN, D.	Methode zur Entwicklung ingenieurwissenschaftlicher Berechnungsprogramme. TU München (2003).
139	GEIER, N.	Untersuchung des Reibungs- und Verschleißverhaltens nasslaufender Kupplungen in Abhängigkeit ihrer Reibflächentopographie. TU München (2003).
140	HERTTER, T.	Rechnerischer Festigkeitsnachweis der Ermüdungstragfähigkeit vergüteter und einsatzgehärteter Stirnräder. TU München (2003).
141	KRIEGER, H.	Alterung von Schmierstoffen im Zahnradprüfstand und in Praxisgetrieben. TU München (2004).
142	STEUTZGER, M.	Einfluß der Baugröße auf die Zahnfußtragfähigkeit einsatzgehärteter Stirnräder. TU München (2004).
143	SCHMIDBAUER, T.	Aufbau und Erprobung des Autarken Hybrid-Antriebsstrangs im Versuchsfahrzeug. TU München (2004).

144	LIU, W.	Einfluss verschiedener Fertigungsverfahren auf die Graufleckentragfähigkeit von Zahnradgetrieben. TU München (2004).
145	FEHLING, R.	Höhere Tragfähigkeit bei Zahnradflanken durch eine nichtevolventische Profilmodifikation. TU München (2004).
146	GUTTENBERG, P.	Der autarke Hybrid am Prüfstand - Funktion, Kraftstoffverbrauch und energetische Analyse. TU München (2004).
147	WIMMER, T.	Einflüsse auf das Lastübernahmeverhalten von nasslaufenden Lamellenkupplungen. TU München (2004).
148	RADEV, T.	Einfluss des Schmierstoffes auf die Grübchentragfähigkeit einsatzgehärteter Zahnräder - Entwicklung des Praxisnahen Pittingtests. TU München (2005).
149	KRASTEV, I.	Optimierung des Lastschaltvorgangs im i²-Getriebe. TU München (2005).
150	HEILEMANN, J.	Tragfähigkeit und Wirkungsgrad bei unterschiedlichen Schnecken-Zahnflankenformen unter Berücksichtigung der Oberflächenhärte und Härtetiefe. TU München (2005).
151	HEIZENRÖTHER, M.	Das Stirnraddifferenzial mit Innenverzahnung im Vergleich zum Kegelraddifferenzial inklusive einer Sperrwertanalyse. TU München (2005).
152	WIMMER, A.	Lastverluste von Stirnradverzahnungen - Konstruktive Einflüsse, Wirkungsgradmaximierung, Tribologie. TU München (2006).
153	BRUCKMEIER, S.	Flankenbruch bei Stirnradgetrieben. TU München (2006).
154	HAUSER, C.	Einfluss der Ölalterung auf Reibcharakteristik und Reibschwingverhalten von Lamellenkupplungen. TU München (2007).
155	GROSSL, A.	Einfluss von PVD-Beschichtungen auf die Flanken- und Fußtragfähigkeit einsatzgehärteter Stirnräder. TU München (2007).
156	STEINBERGER, G.	Optimale Grübchentragfähigkeit von Schrägverzahnungen. TU München (2007).
157	JAROS, M.	Integration des STEP-Produktmodells in den Getriebeentwicklungsprozess. TU München (2007).
158	RADEV, S.	Einfluss von Flankenkorrekturen auf das Anregungsverhalten gerad- und schrägverzahnter Stirnradpaarungen. TU München (2007).
159	BRAYKOFF, C.	Tragfähigkeit kleinmoduliger Zahnräder. TU München (2007).
160	STANGL, M.	Methodik zur kinematischen und kinetischen Berechnung mehrwelliger Planeten-Koppelgetriebe. TU München (2007).

161	STENICO, A.	Werkstoffmechanische Untersuchungen zur Zahnfußtragfähigkeit einsatzgehärteter Zahnräder. TU München (2007).
162	SCHWIENBACHER, S.	Einfluss von Schleifbrand auf die Flankentragfähigkeit einsatzgehärteter Zahnräder. TU München (2008).
163	WINKLER, J.	Tribologischer Schichtaufbau bei Synchronisierungen und sein Einfluss auf Reibung und Verschleiß. TU München (2008).
164	WIRTH, C.	Zur Tragfähigkeit von Kegelrad- und Hypoidgetrieben. TU München (2008).
165	KREIL, O.	Einfluss der Oberflächenstruktur auf Druckverteilung und Schmierfilmdicke im EHD-Kontakt. TU München (2009).
166	OTTO, H.-P.	Flank load carrying capacity and power loss reduction by minimised lubrication. TU München (2009).
167	OTTO, M.	Lastverteilung und Zahnradtragfähigkeit von schrägverzahnten Stirnrädern. TU München (2009).
168	TOMIC, D.	Zum Verschleiß von Kegelreibkupplungen - Einflüsse von Belastung und Schmierstoff auf Reibschichteigenschaften. TU München (2009).
169	WEISEL, C.	Schneckengetriebe mit lokal begrenztem Tragbild. TU München (2009).
170	WEITL, R.	Zur Tragfähigkeitsberechnung von Wälzlagern und Stirnrädern. TU München (2010).
171	MULZER, F.	Systematik hochübersetzender koaxialer Getriebe. TU München (2010).
172	SCHUDY, J.	Untersuchungen zur Flankentragfähigkeit von Außen- und Innenverzahnungen. TU München (2010).
173	BRETL, N.	Einflüsse auf die Zahnfußtragfähigkeit einsatzgehärteter Zahnräder im Bereich hoher Lastspielzahlen. TU München (2010).
174	GRIGGEL, T.	Einfluss der Fertigungsqualität auf die Schwingungsanregung von Stirnrädern. TU München (2010).
175	LAYHER, M.	Einfluss der Schmierstoffadditivierung auf das Reibungsverhalten nasslaufender Reibschaltelemente. TU München (2011).
176	HOCHMANN, M.	Zahnradtragfähigkeit bei Schmierung mit Getriebefließfetten. TU München (2011).
177	DETZEL, J.	Tribologische Untersuchungen an Achsgetrieben zur Verbesserung des Wirkungsgrads. TU München (2011).
178	ZIEGLER, A.	Zur verkürzten Systemlebensdauerprüfung von Zahnradgetrieben. TU München (2011).
179	THOMA, F.	Lastübertragung im verformten System Lager-Welle-Zahnrad. TU München (2012).

180	FRÜHE, T.	Berechnung und Minimierung der Zahnfußspannung von Standard- und LowLos-Verzahnungen. TU München (2012).
181	WITZIG, J.	Flankenbruch - Eine Grenze der Zahnradtragfähigkeit in der Werkstofftiefe. TU München (2012).
182	KLEIN, M.	Zur Fresstragfähigkeit von Kegelrad- und Hypoidgetrieben. TU München (2012).
183	KURTH, F.	Efficiency Determination and Synthesis of Complex-Compound Planetary Gear Transmissions. TU München (2012).
184	WOHLLEBER, F.	Thermischer Haushalt nasslaufender Lamellenkupplungen. TU München (2012).
185	HEIDER, M.	Schwingungsverhalten von Zahnradgetrieben. TU München (2012).
186	MONZ, A.	Tragfähigkeit und Wirkungsgrad von Schneckengetrieben bei Schmierung mit konsistenten Getriebefetten. TU München (2012).
187	WIRTH, M.	Schleppmomente in Synchronisierungen von Fahrzeuggetrieben. TU München (2012).
188	BANSEMIR, G.	Konstruktionsleitsystem für den durchgängig rechnerbasierten Zahnradgetriebeentwurf. TU München (2012).
189	HERGESELL, M.	Grauflecken- und Grübchenbildung an einsatzgehärteten Zahnrädern mittlerer und kleiner Baugröße. TU München (2013).
190	KOLLER, P.	Steigerung der Zahnflankentragfähigkeit durch Optimierung von Eigenspannungs- und Oberflächenzustand. TU München (2013).
191	SCHLEICH, T.	Temperatur- und Verlustleistungsverhalten von Wälzlagern in Getrieben. TU München (2013).
192	STEMPLINGER, J.-P.	Tragfähigkeit und Wirkungsgrad von Stirnradgetrieben bei Schmierung mit hochviskosen Fluiden und Fetten NLGI 0,1 und 2. TU München (2013).
193	FÜRSTENBERGER, M.	Betriebsverhalten verlustoptimierter Kunststoffzahnräder. TU München (2013).
194	HOMBAUER, M.	Grauflecken an Kegelrad- und Hypoidverzahnungen und deren Einfluss auf die Grübchentragfähigkeit. TU München (2013).
195	MAYER, J.	Einfluss der Oberfläche und des Schmierstoffs auf das Reibungsverhalten im EHD-Kontakt. TU München (2013).
196	BAUHOFFER, H.	Kontakt- und Laufverhalten von Kronenrädern unter Montageabweichungen. TU München (2014).
197	LECHNER, C.	Energiebilanzierung des CVT-Hybrid. TU München (2014).
198	HINTERSTOISSER, M.	Zur Optimierung des Wirkungsgrades von Stirnradgetrieben TU München (2014).

199	LOMBARDO, S.	Einfluss von verschiedenen Carbonitrierverfahren auf die Zahnfuß- sowie Zahnflankentragfähigkeit von Stirnrädern. TU München (2014).
200	IDLER, S.	Die Fresstragfähigkeit stufenloser Umschlingungsgetriebe. TU München (2014).
201	LANGHEINRICH, A.	Geometrie, Beanspruchung und Verformung asymmetrischer Stirnradverzahnungen. TU München (2014).
202	MATT, P.	Einfluss der Stirnkanten auf die Tragfähigkeit von Verzahnungen. TU München (2014).
203	HENSEL, M.	Thermische Beanspruchbarkeit und Lebensdauerverhalten von nasslaufenden Lamellenkupplungen. TU München (2014).
204	GEIGER, J.	Wirkungsgrad und Wärmehaushalt von Zahnradgetrieben bei instationären Betriebszuständen. TU München (2015).
205	SIGMUND, W.	Untersuchung und Simulation des Verschleißverhaltens von Schneckengetrieben mit unvollständigem Tragbild. TU München (2015).
206	PARLOW, J.	Erweiterter Verzahnungsentwurf im Anforderungs- und Gesamtsystemkontext. TU München (2016).
207	NEUBAUER, B.	Lastverteilung und Anregungsverhalten in Planetengetriebesystemen. TU München (2016).
208	NITSCH, C.	Dynamisches Betriebsverhalten von Werkstoffverbundzahnrädern. TU München (2016).
209	BIHR, J.	Untersuchung des Schwingungsverhaltens von mehrstufigen Stirnradgetrieben unter besonderer Berücksichtigung des Welle-Lager-Systems. TU München (2016).
210	SCHURER, S.	Einfluss nichtmetallischer Einschlüsse in hochreinen Werkstoffen auf die Zahnfußtragfähigkeit. TU München (2016).
211	KADACH, D.	Stillstandsmarkierungen an Zahnrädern und deren Auswirkungen auf die Flankentragfähigkeit. TU München (2016).
212	FELBERMAIER, M.	Untersuchungen zur Graufleckenbildung und deren Einfluss auf die Grübchentragfähigkeit einsatzgehärteter Stirnräder. TU München (2016).
213	ACUNER, R.	Synchronisierungen mit Carbon-Reibwerkstoffen unter hohen und extremen Beanspruchungen. TU München (2016).
214	LOHNER, T.	Berechnung von TEHD Kontakten und Einlaufverhalten von Verzahnungen. TU München (2016).
215	ZIMMER, M.	Berechnung und Optimierung von Geometrie und Eingriffsverhalten von Verzahnungen beliebiger Achslage. TU München (2017).
216	GWINNER, P.	Auslegung schwingungsarmer Stirnradverzahnungen für den automobilen Einsatz in hochdrehenden, elektrisch angetriebenen Achsgetrieben. TU München (2017).

217	SCHULTHEISS, H.	Zum Verschleißverhalten einsatzgehärteter Zahnradpaarungen in Abhängigkeit des Schmierungsmechanismus bei Fettschmierung. TU München (2017).
218	MOSER, K.	Methode zur Untersuchung des Betriebsverhaltens stufenloser Umschlingungsgetriebe. TU München (2017).
219	STREBEL, M.	Spontanschäden an nasslaufenden Lamellenkupplungen. TU München (2017).
220	BAAR, M.	Kennwerte zur Tragfähigkeit kleinmoduliger Kronenradverzahnungen unterschiedlicher Werkstoffpaarung. TU München (2017).
221	WICKBORN, C.	Erweiterung der Flankentragfähigkeitsberechnung von Stirnrädern in der Werkstofftiefe. TU München (2017).
222	MEINGASSNER, G.	Methodik zur Untersuchung des Reibungsverhaltens nasslaufender Lamellenkupplungen bei Langsamlauf- und Mikroschlupf. TU München (2017).
223	ZORNEK, B.	Untersuchungen zur Flankentragfähigkeit vergüteter und nitrierter Innen- und Außenverzahnungen. TU München (2018).
224	DOBLER, F.	Einflüsse auf die Tragfähigkeit induktiv umlaufgehärteter Stirnräder. TU München (2018).
225	DAFFNER, M.	Validierung von Verformungsberechnungen im System Zahnrad-Welle-Lager-Gehäuse. TU München (2018).
226	HEIN, M.	Zur ganzheitlichen betriebsfesten Auslegung und Prüfung von Getriebezahnrädern. TU München (2018).
227	HASEL, C.	Zur Zahnfußtragfähigkeit von Kunststoffzahnrädern. TU München, (2018)
228	KOHN, B.	Topologische Flankenkorrektur zur Anregungsoptimierung von Stirnradgetrieben. TU München (2019).
229	BOIADJIEV, I.	Schadensentwicklung und Tragfähigkeit carbonitrierter Kegelradverzahnungen. TU München (2019).
230	MAUTNER, E.	Grübchentragfähigkeit von Schneckengetrieben großer Baugröße mit unvollständigem Tragbild. TU München (2019).
231	ENGELHARDT, C.	Einfluss von Wasser in Getriebeölen auf die Zahnflankentragfähigkeit einsatzgehärteter Stirnräder. TU Mün-chen (2019).
232	VÖLKEL, K.	Charakterisierung des Einlaufverhaltens nasslaufender Lamellenkupplungen. TU München (2020).
233	BANSEMIR, S.	Bewertung von Berechnungstiefe und Aussagegüte bei der Stirnradgetriebeberechnung. TU München (2020).
234	UTAKAPAN, T.	Schwingungsverhalten mehrstufiger Getriebe. TU München (2020).
235	KÖNIG, J.	Steigerung der Zahnflankentragfähigkeit durch optimierte Fertigung und Schmierung. TU München (2020).

236	JURKSCHART, T.	Erweiterte Bestimmung lastabhängiger Verluste von Stirnradgetrieben. TU München (2020).
237	EBNER, M.	Selbstschmierung hochbelasteter Zahnkontakte mit schmierstoffgetränkten porösen Eisenwerkstoffen. TU München (2021).
238	REIMANN, T.	Einfluss der Treibrichtung auf die Flankentragfähigkeit von Stirnrad-, Kegelrad-, und Hypoidgetrieben. TU München (2021).
239	DOBLER, A.	Verschleiß als Lebensdauergrenze für Zahnräder. TU München (2021).
240	DAI, R.	Change-Management-fokussierte Einführung eines „Ganzheitlichen Produktionssystems“ in Klein- und Kleinstunternehmen. TU München (2021)
241	NORGAUER, P.	Verschleißverhalten von modernen Schneckenverzahnungen. TU München (2021).
242	GÜNTNER, C.	Zum Einfluss der Härtbarkeit auf die Zahnfußtragfähigkeit einsatzgehärteter Stirnräder größerer Baugröße. TU München (2021)
243	WEIGL, A.	Reibungsreduzierung durch DLC-Beschichtungen. TU München (2021)
244	ILLENBERGER, C.	Zahnflankentragfähigkeit ölgeschmierter Kunststoffverzahnungen. TU München (2021)
245	FROMBERGER, M.	Beschleunigung und Drehwegabweichung zur Erkennung von Grübchenschäden. TU München (2021)
246	PELLKOFER, J.	Zum Verzahnungswirkungsgrad von Kegelradgetrieben. TU München (2021)
247	SAGRALOFF, N.	Zuverlässige Beurteilung der Zahnrad-Graufleckentragfähigkeit von Getriebeölen. TU München (2022)
248	PAUCKER, T.	Berechnung der örtlichen Zahnfußtragfähigkeit von Stirnradverzahnungen. TU München (2022)
249	FUCHS, D.	Einfluss mikroskopischer Fehlstellen auf die Zahnfußtragfähigkeit. TU München 2023
250	TRÜBSWETTER, M.	Geometrie des Wälzschälens. TU München 2023
251	YILMAZ, M.	Getriebeschmierung mit wasserhaltigen Polyglykolen. TU München 2023
252	KRATZER, D.	Zum Einfluss oberflächennaher Eigenschaften auf die Zahnradtragfähigkeit. TU München 2023
253	GÖTZ, J.	Anregungs- und Schwingungsverhalten von Planetengetrieben. TU München 2023
254	WEINBERGER, U.	Anregungsverhalten doppelschrägverzahnter Planetenradgetriebe - Einfluss des Apex-Punktes. TU München 2023

255	MILETI, M.	Performance Optimization of a Coupled Cone and Dog Clutch for Automotive Application. TU München 2023
256	STOCKINGER, U.	Untersuchung der Leistungsfähigkeit von Einfach- und Mehrfachkonus-Synchronisierungen. TU München 2023
257	SCHWARZ, A.	Thermische Analyse von elastohydrodynamischen Kontakten. TU München 2023
258	GRÖTSCH, D.	Thermal Behavior of Wet Clutches in Industrial Applications. TU München 2023